# MODELLING EQUILIBRIUM BEACH PROFILES

by

Christopher G. Creed

**Research Report No. CACR-93-01**

Sponsored by
Department of Natural Resources and Environemental Control
State of Delaware

January, 1993

# TABLE OF CONTENTS

## LIST OF FIGURES

## LIST OF TABLES

# ABSTRACT

A quantitative understanding of the steady state condition of a beach is an important aspect of predicting the shape of nearshore bathymetry due to changes in the wave climate. In this thesis, a numerical model will be developed to simulate the presence of longshore bar formations in an equilibrium beach profile. The method will utilize the work of Roelvink and Stive (1989), who modelled cross-shore flow mechanisms that produced longshore bars.

A no-net sediment movement condition across the surf zone is applied to the cross-shore energetics sediment transport formulation of Bailard (1982), resulting in an equilibrium beach slope equation. The proposed flow models of Roelvink and Stive (1989) will be used as approximate representations of the nearshore hydrodynamics and will be applied directly as the representative flow field across the equilibrium beach profile. Combining the bottom slope equation with the energy and the momentum balances, the system of equations is numerically integrated as an initial value problem across the surf zone, calculating the local values of the wave and current fields that drive variations in bottom slope. The results are solutions for depth, root-mean squared wave height, and mean water surface elevation across the equilibrium profile.

This model provides a solution for the equilibrium beach profile resulting from a no-net sediment transport condition. A breakpoint longshore bar exists in the equilibrium beach profile due to a change in the near-bottom steady current from onshore to offshore as wave breaking begins. The results are qualitatively compared to the experimental tank data of Roelvink and Stive (1989), where a longshore bar was generated with an exaggerated undertow mechanism, and to time averaged profile measurements

at the U.S. Army Corps of Engineers Field Research Facility. In a qualitative sense, for a broad range of incident wave conditions with relative small wave steepness values, the model predicts the trend for bar migration as the wave climate changes varies in a mild erosional state. However, the model cannot be used to predict quantitatively the equilibrium beach profile for an arbitrary set of wave conditions.

# Chapter 1

# INTRODUCTION

Coastal engineers require accurate methods to determine the shape of the nearshore bathymetry under given wave conditions. The dèsign of beach fills and coastal structures requires methods to predict how a beach will respond to changes in wave climate, especially during storm events, and nearshore current conditions. The ability to make such predictions proves beneficial in engineering applications when estimates for volume changes of a beach during climatic and seasonal changes provide low cost solutions to beach stablization and management. Most shore response models are time-varying predictors that model the change in the nearshore bathymetry in response to changes in wave climate. These types of models demand many computations and large amounts of computer time that can prove costly for most engineering applications. However, the ability to predict accurately the steady state shape of a beach for an arbitrary set of wave conditions proves to be a low cost solution to nearshore management.

To date, the most accepted means to quantify the steady state shape of a beach, or the *equilibrium beach profile*, is the $h(x) = Ax^{2/3}$ model presented by Dean (1977). This model has proven useful for a number of engineering applications but lacks versatility due to inherent assumptions related to the wave field and wave breaking. Recent advances have led to models that better quantify the physics of the nearshore wave environment through more complete breaking models. These models include the work of Larson (1989), who establishes an equilibrium beach profile model by utilizing the monochromatic breaking model of Dally *et al.* (1985). Further work by Kaihatu (1990) and Dalrymple (1992) apply the spectral breaking models of Thornton and Guza (1983)

to quantify the equilibrium beach profile caused by a random wave field. These models provide more realistic assumptions of the processes in the nearshore region, but still offer only a monotonic description of the beach shape and cannot generate or identify the presence of longshore bars, which are frequently observed to exist in natural stable beach shapes.

In this thesis, a numerical model is developed to simulate the presence of longshore bar formations in an equilibrium beach profile using a random representation of the wave field. The flow models proposed by Roelvink and Stive (1989), hereafter referred to as R&S, are adopted as representations of the dominant nearshore flow mechanisms that govern sediment transport across the beach. The replication of the models for wave asymmetry-induced onshore flow and the momentum decay-induced mean return flow will be calibrated with the 1:40 plane beach data of R&S.

To determine the equilibrium beach profile resulting from the wave and current fields across the surf zone, an equilibrium bottom slope equation will be derived by applying a no-net sediment transport condition to Bailard's (1982) energetics total load sediment transport formulation. The no-net sediment transport condition requires a local time-averaged sediment transport to be zero for all locations across the nearshore region. This condition artificially imposes a local balance between the bedload and suspended load at each location across the equilibrium profile.

A system of three ordinary differential equations governing nearshore wave, current and sediment transport interaction is used to solve for the equilibrium beach profile. The aforementioned bottom slope equation is combined with the energy and the momentum balances to establish a system of ordinary differential equations coupled through $H_{\text{rms}}$ wave height, mean water surface elevation, $\overline{\eta}$, and bottom depth, $d$. The system of equations is solved numerically as an initial value problem using a fourth order Runge-Kutta scheme, where all three equations are solved simultaneously. The model provides

solutions for the equilibrium conditions of $H_{rms}$ wave height, mean water surface elevation and bottom depth. For variations in the wave and sediment characteristics, the system of equations will provide unique solutions for each combination of conditions.

Solutions to the system of equations will be compared to wave tank profile data of R&S and to a time-averaged profile at the U.S. Army Corps of Engineers Field Research Facility to determine possible applications of the model for predicting stable beach shapes with predominant longshore bar features. Further, analysis of the model's response to variation in offshore wave climate will be conducted to determine whether trends in the model's response replicate observations in nature.

# Chapter 2

# BACKGROUND AND PROBLEM STATEMENT

This thesis is concerned with applying highly accurate numerical descriptions of the nearshore wave and current climate to predict the equilibrium shape of the nearshore bathymetry through what is defined as a kinematic approach, also known as an *energetics* approach. Historically, the equilibrium beach profile has been described by dynamic and empirical methods. Section 2.1 will review methods based on the dynamic approach as described by Dean (1977), where the general form of the beach shape results from a balance between the *constructive* and *destructive* forces in the surf zone. Section 2.2 will discuss early attempts at energetics approaches, where simple approximations to nearshore processes have led to less than desirable descriptions of the nearshore slopes.

## 2.1 Dynamic Approach

### 2.1.1 Monochromatic Methods

Qualitative models for equilibrium beach profiles date back to Bruun (1954) who hypothesized that the general shape of a beach in the cross-shore direction is concave upwards, decreasing in depth from offshore to onshore. Dean (1977) quantified this hypothesis with an analytical model that represents the stable shape of a beach or what has been termed the *equilibrium beach profile*. Dean's equilibrium condition requires that a given sediment size must be able to withstand a given level of energy dissipation per unit volume induced by wave breaking. To apply this hypothesis, Dean related the change in wave energy flux, which is the change in the rate at which energy is transferred

by the waves per unit volume, to a constant rate of wave energy dissipation, $D_*$, for which the sediment is stable. The resulting expression is

$$\frac{\partial EC_g}{\partial x} = -hD_*, \tag{2.1}$$

where $EC_g$ is the wave energy flux.

For simplicity, Dean developed the model based on linear shallow water wave theory where the linear shallow water wave energy flux is

$$EC_g = \frac{1}{8}\rho g H^2 \sqrt{gh}, \tag{2.2}$$

where $E$ is the linear wave energy,

$$E = \frac{1}{8}\rho g H^2, \tag{2.3}$$

and $C_g$ is the shallow water group celerity,

$$C_g = \sqrt{gh} \tag{2.4}$$

The wave height is defined as $H$, $h$ is the water depth, $\rho$ is the fluid density, and $g$ is the gravitational acceleration.

Introducing a spilling breaker assumption, $H = \kappa h$, where $\kappa$ is taken as $O(1)$, eqn. 2.1 is written explicitly in terms of the water depth, $h$, as

$$\frac{\partial\left(\frac{1}{8}\rho g \kappa^2 \sqrt{gh}\right)}{\partial x} = -hD_* \tag{2.5}$$

where $h$ is the only variable in $x$.

The equilibrium shape of the beach is determined by defining the shoreline as the location of zero water depth and integrating eqn. 2.5 in $x$, where $x$ is the shore normal direction defined as positive offshore. The resulting expression for the equilibrium profile is

$$h(x) = Ax^{2/3} \tag{2.6}$$

where

$$A = (\frac{24D_*}{5\rho g\sqrt{g}\kappa^2})^{2/3} \tag{2.7}$$

The equilibrium beach takes a shape that is a balance between the destructive forces induced by the wave energy dissipation and the ability of the sediment to resist those destructive forces.

One aspect of interest with this model is an accurate representation and calibration of the dissipation term $D_*$, which is assumed to be constant across the surf zone. Moore (1982) related $A$, and thus $D_*$, to surf zone sediment grain size by applying a least squares fit between the $Ax^{2/3}$ model and measured profile data where average sediment grain size is known and assumed constant over the entire surf zone. Moore presented tables that directly relate values of $D_*$ to sediment size, allowing the $Ax^{2/3}$ to predict the shape of the equilibrium beach profile at a specific site given local sediment size characteristics. This model has proven to be very useful in predicting the general shape of beach profiles In fact, Dean (1977) showed that profiles along the East and Gulf coasts of the United States can be generally defined as having $Ax^{2/3}$ shapes, where, again, $A$ is adjusted according to local sediment conditions.

However, this model is limited in its validity by its basic assumptions: (1) wave breaking is modelled according to the spilling breaker assumption, $H = \kappa h$, (2) the

wave field is linear and monochromatic, and (3) a fixed breakpoint is used. Further, the model yields an infinite slope at the still waterline where the depth approaches zero and cannot predict the presence of sand bars which were found by Dean (1977) to be common features in some stable beach shapes.

Modifications to this method have been presented by recent authors, (*e.g.*, Larson 1989, Bodge 1991.) Larson modified Dean's method by replacing the spilling breaker assumption with the more comprehensive breaking model of Dally *et al.* (1985). This breaking model is based on the argument that the rate of energy flux decay is proportional to the amount of excess energy flux in the wave form and is expressed mathematically as

$$\frac{\partial EC_g}{\partial x} = -\epsilon_b = -\frac{K}{h}\left[(EC_g) - (EC_g)_s\right] \tag{2.8}$$

where $K$ is an empirical constant equal to 0.17, $EC_g$ is the energy flux of the wave and $(EC_g)_s$ is the stable energy flux of the wave. The excess of energy flux is described as the difference between the actual energy flux and the stable energy flux where the stable energy flux is defined as the energy flux, associated with the height of a broken wave propagating across a flat bottom. The stable wave height is found to be approximately $H = \gamma h$, where $\gamma$ is about 0.4.

To determine the wave height across the equilibrium beach profile, Larson approximated the dissipation assuming linear shallow water wave theory and equated the dissipation term to Dean's equilibrium concept of constant dissipation per unit volume

$$h\mathcal{D}_* = \epsilon_b \tag{2.9}$$

where the dissipation term is approximated as

$$\epsilon_b = \frac{K}{h}\left(\frac{1}{8}\rho g\sqrt{gh}(H^2 - \gamma^2 h^2)\right) \tag{2.10}$$

Solving for $H$, Larson obtained

$$H = \sqrt{\frac{8h^2 D_*}{\rho g\sqrt{gh}K} + \gamma^2 h^2}, \tag{2.11}$$

which provides the wave height across the equilibrium profile as a function of the profile depth, $h$.

To proceed, this expression for wave height is substituted into the energy flux expression (eqn. 2.2), and subsequently into the energy balance (eqn. 2.1). After some manipulation and integration in $x$ this leads to

$$2\frac{h}{K} + \frac{5}{24}\rho g^{3/2}\left(\frac{\gamma^2 h^{3/2}}{D_*}\right) = x \tag{2.12}$$

This equation, relating the equilibrium water depth to the distance offshore, is best solved for the distance $x$ in terms of $h$. This relationship differs from Dean's in that the profile now includes a linear term which removes the infinite slope at the shoreline.

The monochromatic methods present simple, very usable representations of the general shape of cross-shore bathymetry. With knowledge of sediment size at a given site, Dean (1991) has shown his model to be a valuable tool in estimating beach response to sea level rise and added beach fill material. However, the models are based on extremely idealized conditions and simple additions to these formulations may be valuable for better descriptions of the nearshore bathymetry.

### 2.1.2 Spectral Methods

Recently, the work of Larson was extended to account for the dissipation in a random wave field. Kaihatu (1990) adopted the random wave breaking model of Thornton and Guza (1983) as the dissipation term in the energy balance presented by Larson (eqn. 2.8). Thornton and Guza had presented two dissipation terms based on the probability density of breaking wave heights across the surf zone. The two terms are categorized as simple and complete expressions for wave height decay. Kaihatu adopted the simple expression,

$$\epsilon_b = \frac{3\sqrt{\pi}}{16}\rho g \frac{B^3 \bar{f}}{\gamma^4 h^5} H_{\rm rms}^7, \tag{2.13}$$

which is a reduced version of the complete expression. This can be solved analytically across a planar beach for the root-mean-squared wave height, $H_{\rm rms}$.

Following Larson, the dissipation term was equated to Dean's constant dissipation per unit volume (eqn. 2.9), and an expression for $H_{\rm rms}$ wave height was obtained in terms of the cross-shore depth as

$$H_{\rm rms} = \left(\frac{\gamma^2 D_*}{A'}\right)^{1/7} h^{6/7} \tag{2.14}$$

where the constant $A'$ has been introduced for convenience and is defined as

$$A' = \frac{3\sqrt{\pi}\rho g B^3 \bar{f}}{16\gamma^2} \tag{2.15}$$

where $\bar{f}$ is the mean frequency of the wave field, $B$ is the fraction of white water on the breaker face, and $\gamma$ is a constant taken to be 0.42.

Substituting this relationship for $H_{rms}$ wave height into the energy flux expression (eqn. 2.2), and subsequently into the energy balance (eqn. 2.1), the resulting expression was integrated with respect to the offshore distance $x$, using the initial condition $h(x) = 0$ at $x = 0$. The resulting expression for depth across the profile is

$$h(x) = \beta\, x^{14/17} \tag{2.16}$$

where the dimensional coefficient $\beta$ is given by

$$\beta = \left(\frac{136 D_*}{31 \rho g^{3/2}} \left(\frac{A'}{\gamma^2 D_*}\right)^{2/7}\right)^{14/17} \tag{2.17}$$

where all terms are previously defined.

This result provides an analytical solution for the equilibrium beach profile under attack by a random wave field and the corresponding $H_{rms}$ wave height across the profile. There are similar characteristics between the $\beta x^{14/17}$ solution and Dean's $Ax^{2/3}$, which include a monotonic decrease in water depth from offshore to onshore, an infinite beach slope at the still water level, and a constant dissipation term $D_*$. The $D_*$, although well calibrated for Dean's model, may be different for the case of random wave dissipation. Kriebel (1992) has suggested that the value of $D_*$ be related to probability distribution of the breaking waves through an effective value of $D_*$, say $D'_*$.

Dalrymple (1992) derived the solution for the equilibrium beach profile using the complete dissipation term of Thornton and Guza,

$$\epsilon_b = \frac{3\sqrt{\pi}}{16} \rho g \frac{B^3 \bar{f}}{\gamma^2 h^3} H_{rms}^5 \left[1 - \frac{1}{(1 + (H_{rms}/\gamma h)^2)^{5/2}}\right] \tag{2.18}$$

Dalrymple followed the method of Larson and Kaihatu, and presents the solution of the $H_{rms}$ wave height across the surf zone as

$$h\mathcal{D}_* = \frac{A' H_{rms}^5}{h^3}\left[1 - \frac{1}{(1+(H_{rms}/\gamma h)^2)^{5/2}}\right], \tag{2.19}$$

where $A'$, $B$, $\bar{f}$, and $\gamma$ are defined above. From this expression the $H_{rms}$ wave height must be solved for by iteration.

Because the expression for wave height cannot be solved analytically, a generalized bottom slope equation is required. From the energy balance (eqn. 2.1), the expression for bottom slope can be expressed in terms of the bottom depth, $h$, and the $H_{rms}$ wave height as

$$\frac{dh}{dx} = \frac{8h\mathcal{D}_*}{\rho g\sqrt{gh}H_{rms}\left(2\frac{dH_{rms}}{dh} + \frac{H_{rms}}{2h}\right)} \tag{2.20}$$

The equilibrium depth across the surf zone can be found by numerical integration of eqn. 2.20. When integrated, this solution does not differ drastically from the results of Kaihatu (figure 2.1), but this formulation does allow for more elaborate dissipation terms or bottom slope formulations to be added to the numerical scheme. As shown in figure 2.1, with calibration of $B$ and $D_*$ the models can be used to represent the equilibrium beach profile and the associated $H_{rms}$ wave height across the surf zone. The fit to data for both the profile depths and the $H_{rms}$ wave heights is remarkably good considering the assumptions and approximations in the formulations.

## 2.2 Kinematic Approach

A second type of equilibrium beach profile method is described as a kinematic approach where more fundamental physics are taken into account to describe the stable shape of the beach. To apply this method, a suitable model for bottom slope as a function of wave and current climate must be considered. In our work we are interested

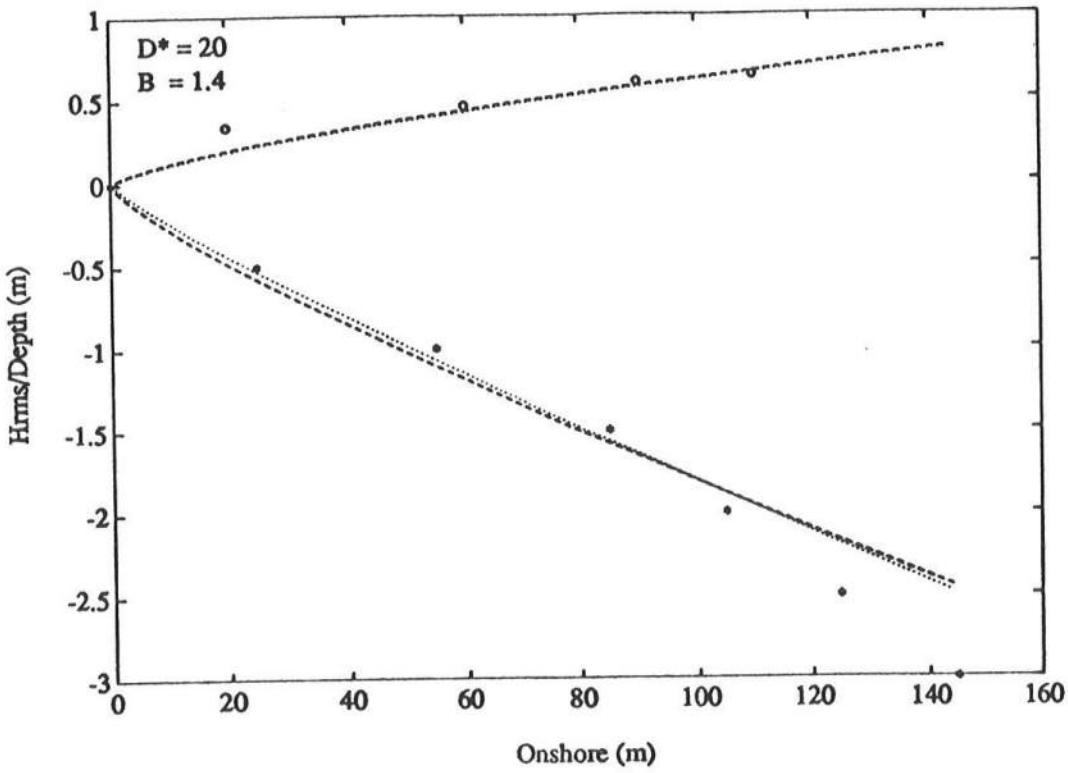


**Figure 2.1:** Equilibrium beach profile solutions for *simple* (dashed) and *complete* (dotted) dissipation models compared to wave and profile data (solid) (Torrey Pines CA., November 18, 1978), (with permission of Dalrymple and Kaihatu).

in the energetics-based sediment transport formulations of Bagnold (1963, 1966), Bowen (1980), Bailard and Inman (1981) and Bailard (1981) to obtain such formulations for bottom slope.

### 2.2.1 The Energetics Sediment Transport Models

Historically, the energetics sediment transport models of Bagnold (1963, 1966) have been used as suitable descriptions of fluid-sediment interactions. Bagnold's original formulation dealt strictly with two-dimensional stream flow where the unidirectional downstream flow and gravity work in parallel to transport sediment. This energetics model is based on the argument that sediment is transported in two distinct modes, bedload and suspended load, where each mode of sediment transport results from different mechanisms and thus requires different percentages of the total power of the stream. The bedload transport is maintained through grain-to-grain interactions under the force of the bottom flow, while the suspended load transport is maintained via turbulent diffusion throughout the water column. Two efficiency factors $\epsilon_b$ and $\epsilon_s$ for bedload and suspended load, respectively, are measures of the amount of total flow power required by each mode of sediment transport and have been calibrated through experimental measurements.

Bagnold's total load instantaneous sediment transport for unidirectional flow can be written as

$$i_x = c_D \rho \left[ \frac{\varepsilon_b u^3}{\tan\phi - \frac{u \tan\beta}{|u|}} + \frac{\varepsilon_s u^3 |u|}{w - u \tan\beta} \right] \tag{2.21}$$

where $i_x$ is the cross-shore immersed weight sediment transport weight, $u$ is the representative velocity component, $c_D$ is a drag coefficient, $w$ is the settling velocity of sand, $\rho$ is the fluid density, $\tan\phi$ is the angle of internal friction of sand, and $\tan\beta$ is the bottom slope.

Bagnold (1963) developed an energetics model for oscillatory flow to investigate nearshore sediment transport. The result is a model based on the argument that the wave-induced oscillatory motion suspends the sediment and maintains the sediment suspension, but does not produce net transport of the sediment. A mean current or a higher order flow component superimposed on oscillatory current will produce a net transport of sediment in the direction of the current. Bagnold's final formulation of instantaneous total load sediment transport under oscillatory flows is

$$i_\theta = K' \omega \frac{u_\theta}{u_m} \tag{2.22}$$

where $i_\theta$ is the time-averaged immersed weight transport rate in an arbitrary direction, $u_\theta$ is the steady current in the $\theta$-direction from shore normal, $\omega$ is the local time-averaged rate of energy dissipation (not to be confused with the angular frequency of the wave field), $u_m$, is the magnitude of the wave orbital velocity, and $K'$ is a dimensionless constant.

Bailard and Inman (1981) and Bailard (1981) recognized that Bagnold's formulation for oscillatory flow does not include a bottom slope term or a time-average sediment transport rate. Bailard and Inman reformulated this problem for bedload using Bagnold's energetics sediment transport formulation for unidirectional flow and accounted for the time-varying flow over a sloping bottom. Bailard furthered this study to include suspended load sediment transport, and combined his findings with those of Bailard and Inman, yielding a model for total load sediment transport in the presence of time-varying oscillatory flow over a sloping bottom. Assuming a normally incident wave climate and considering only onshore-offshore transport, Bailard's total load model is

$$i_x(t) = c_f \rho \left[ \frac{\varepsilon_b}{\tan\phi} \left[ u(t) \left| u(t) \right|^2 - \frac{\tan\beta}{\tan\phi} \left| u(t) \right|^3 \right] + \frac{\varepsilon_s}{w} \left[ u(t) \left| u(t) \right|^3 - \frac{\varepsilon_s}{w} \tan\beta \left| u(t) \right|^5 \right] \right] \tag{2.23}$$

where $i_x(t) = i_B + i_S$ is the time-varying total cross-shore immersed weight sediment transport weight, $i_B$ begin the bedload component and $i_S$ the suspended load component, $\varepsilon_b$ and $\varepsilon_s$ are efficiency factors as in Bagnold's formulation, $c_f$ is the drag coefficient for the bed, $w$ is the settling velocity of sand, $\tan\phi$ is the angle of internal friction of sand, and $\tan\beta$ is the bottom slope. The velocity terms $u(t)|u(t)|^n$ and $|u(t)|^n$ are the odd and even velocity moments, respectively, and are the mechanisms relating the flow field to the transport of sediment. The first term in the right-hand-side is the contribution from bedload transport, and the second term describes the contribution from suspended load transport. It is this formula of time-varying cross-shore sediment transport under oscillatory flows that provides the basis for the modelling of equilibrium conditions of the nearshore region.

### 2.2.2 No-Net Transport Condition

The equations for bottom slope are arrived at via a *no-net* sediment transport condition. Unlike the *null-point* hypothesis addressed by Ippen and Eagleson (1955), Eagleson and Dean (1961), and Eagleson, Glenne and Dracup (1963), where the null-point is based on a stable grain size distribution across the equilibrium profile, the no-net transport condition is a time-averaged balance between the bedload and suspended load contributions across the equilibrium profile. In essence, the total net transport must be zero at a given horizontal location, but net transport can be represented through the bedload and suspended load components.

Equations 2.21 and 2.23 are the basis for the total load equilibrium beach slope solutions by Bowen (1980) and Bailard (1981), respectively. Imposing a no-net sediment transport condition across the entire profile and solving for the bottom slope, analytical expressions for the beach slope are shown to represent trends apparent in nature. This approach was first used by Bowen, who presented equilibrium solutions to the suspended load, bedload, and total load formulations of Bagnold's unidirectional sediment transport model, where the flow is defined as positive onshore. Later and Bailard applied the

method of Bowen to his generalized form of Bagnold's stream flow model and presented a qualitative comparison to the results of Bowen.

Bowen argued that the existence of a beach is due to a balance between onshore forcing of the incident wave field balanced by the effects of gravity in the downslope or offshore direction. Specifically, the onshore forcing from the flow field is a combination the orbital velocities from linear wave motion and a perturbation from a higher order wave component, causing time-averaged onshore flow, or an imposed mean current, such a bottom drift velocities. Ideally, it is this mean onshore flow which opposes the downslope forces of gravity to create a beach. Without the forcing of the shoreward directed flow field, gravity would bring a beach to an equilibrium shape or a slope equal to the angle of internal friction of the sediment, which is approximately 33° from the horizontal for sand.

Bowen applied this argument by adopting Bagnold's unidirectional sediment transport model (eqn. 2.21) as a basis for sediment transport representation and where forcing effects of a flow field are related to the forcing of gravity. The slope term in this model is represented by $\tan\beta$. To describe the flow field, Bowen assumes the flow to be a combination of two components, $u = \overline{u} + \tilde{u}$, where $\tilde{u} \gg \overline{u}$. The larger component $\tilde{u}$ is the fundamental component of the flow modelled by the orbital flow under a linear wave. The smaller component $\overline{u}$ may be the result of flows induced by a steady current superimposed on the orbital flow, flow induced by the presence of higher harmonics in the wave form, or the effects of wave forms not bound to the fundamental wave form (*i.e.*, nearshore infragravity waves). Of these, Bowen addressed the first two as flows that can be modelled and attributed to the tendency for onshore sediment transport from the incident wave field. The steady current was chosen as the steady-streaming velocities found by the conduction solution of Longuet-Higgins (1953), where the mean drift in the boundary layer of a second order wave is in the direction of wave propagation. The higher order harmonic, bound to the linear wave, forms a vertically asymmetric wave form where the short, intense forward flows are under the crest and longer, less intense,

offshore flows are under the trough, resulting in a net onshore movement of sediment.

It is straightforward to model these flows individually; however, the total flow moments (*i.e.*, $u^n\,|u|$), seen in eqn. 2.21 and 2.23, are combinations of the individual flows. In order to represent the total flow moments in a form where the individual flow mechanisms can be modelled, the moments must be expanded in terms of a small quantity $\overline{u}$. Bowen argues that under the assumption that $\tilde{u} \gg \overline{u}$ and applying a binomial expansion, terms of the form $u^n\,|u|$ can be approximated as

$$u^n\,|u| = \tilde{u}^n\,|\tilde{u}| + (n+1)\overline{u}\;\tilde{u}^{n-1}\,|\tilde{u}| + \frac{n(n+1)}{2}\overline{u}^2\;\tilde{u}^{(n-2)}\,|\tilde{u}| + \ldots \tag{2.24}$$

where now the total flow moments are expressed in terms of the fundamental and secondary flows.

As a simple first approximation, Bowen chose to represent the oscillatory flow field containing a higher order nonlinear harmonic with Stokes second order wave solution,

$$\tilde{u} = u_m \cos\sigma t + \frac{3}{4}\frac{u_m^2}{C\sinh^2(kh)}\cos 2\sigma t \tag{2.25}$$

and the mean current with Longuet-Higgins' streaming velocity,

$$\overline{u} = \frac{u_m^2}{C} \tag{2.26}$$

The combination of these flows provide a net onshore flow across the nearshore region.

Requiring the system to steady, Bowen time-averaged the flows over several wave periods and imposed the no-net sediment transport condition,

$$\langle i_x \rangle = 0, \tag{2.27}$$

to obtain the total load bottom slope model

$$\tan\beta = \left\{\left(\frac{\epsilon_b}{\tan\phi}\right)\left[\left(\frac{27\pi}{64\sinh^2(kh)}\right)\left(\frac{u_m}{C}\right)+\left(\frac{9\pi}{8}\right)\left(\frac{u_m}{C}\right)\right]+ \left(\frac{u_m}{w}\right)\epsilon_s\left[\left(\frac{9}{5\sinh^2(kh)}\right)\left(\frac{u_m}{C}\right)+4\left(\frac{u_m}{C}\right)\right]\right\}\left\{\frac{\epsilon_b}{\tan^2\phi}+\frac{4}{5}\left(\frac{u_m}{w}\right)^2\epsilon_s\right\}^{-1} \tag{2.28}$$

This model is a function of wave amplitude, wave period, and sediment fall velocity. Changes in bottom slope due to variations of these variables are shown graphically in figure 2.2.

Bowen pointed out the qualitative advantages of this model in that beach slope increases as fall velocity increases, as depth decreases, and as wave period increases. All of these characteristics of the nearshore beach slope are generally observed in nature. It must be noted that Bowen does not use this model explicitly to express changes in bottom bathymetry as a function of changes in the wave field.

Bailard also used this approach with his cross-shore total load sediment transport model but had less success in representing realistic beach slope magnitudes. Only a qualitative order of magnitude comparison to Bowen's results was made where trends in the models response to changes in wave field and sediment characteristics are recognized. Bailard's resulting expression,

$$\tan\beta = \left\{\left(\frac{\epsilon_b}{\tan\phi}\right)\left[\left(\frac{27\pi}{64\sinh^2(kh)}\right)\left(\frac{u_m}{C}\right)+\left(\frac{9\pi}{8}\right)\left(\frac{u_m}{C}\right)\right]+ \left(\frac{u_m}{w}\right)\epsilon_s\left[\left(\frac{9}{5\sinh^2(kh)}\right)\left(\frac{u_m}{C}\right)+4\left(\frac{u_m}{C}\right)\right]\right\}\left\{\frac{\epsilon_b}{\tan^2\phi}+\frac{4}{5}\left(\frac{u_m}{w}\right)^2\epsilon_s^2\right\}^{-1} \tag{2.29}$$

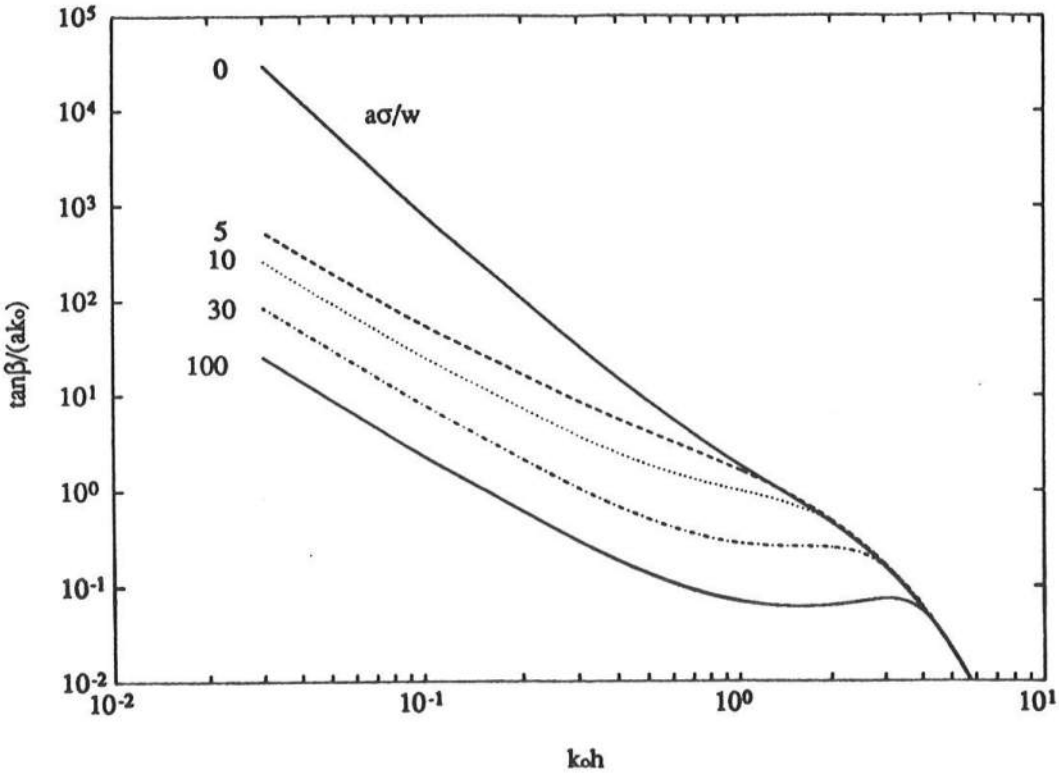


**Figure 2.2:** Normalized beach slope $\beta/ak_o$ as a function of the nondimensional depth $k_o h$ for various values of the suspension parameter $a\sigma/w$, (Bowen 1980).

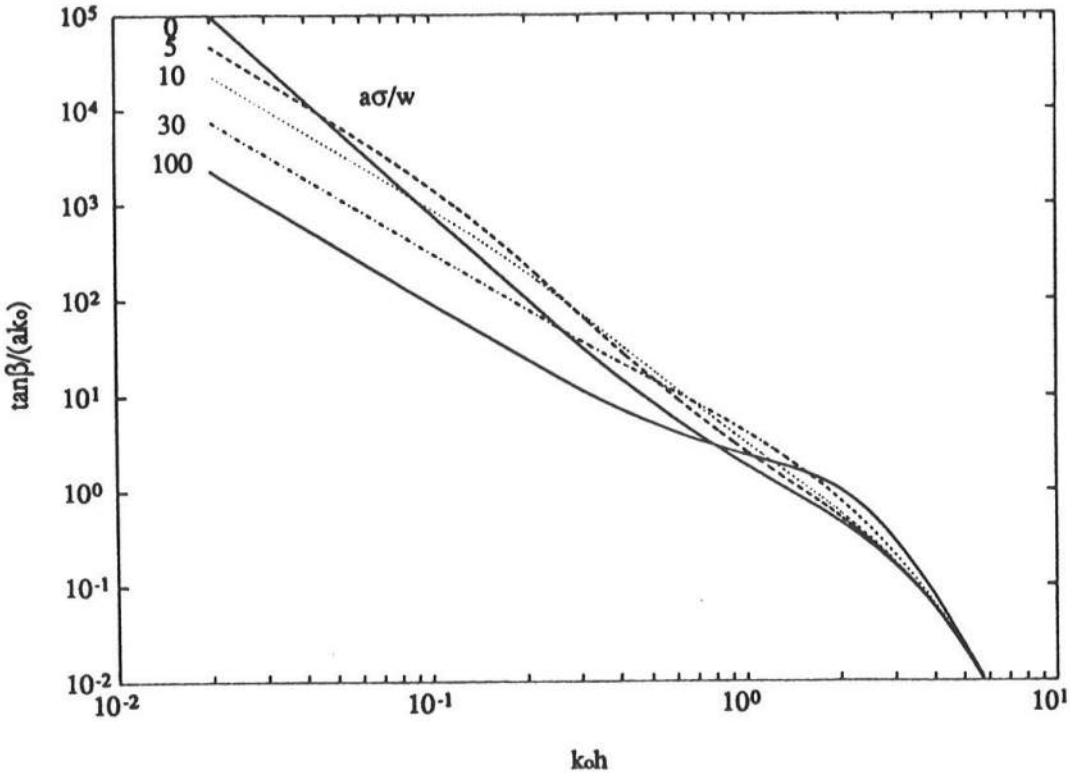


**Figure 2.3:** Normalized beach slope $\beta/ak_o$ as a function of the nondimensional depth $k_oh$ for various values of the suspension parameter $a\sigma/w$, (Bailard 1981).

is expressed graphically in figure (2.3). It can be seen through a comparison of figures (2.2) and (2.3) that the two models respond identically for pure bed load conditions but quickly differ as suspended sediment is added to the system. This response is attributed to the additional $\epsilon_s$ term in the denominator of Bailard's expression.

These kinematic models present the beach slope in terms of nondimensional parameters that can be used to relate general trends of the beach slope to changes in relative water depth $k_oh$ and suspension parameter $a\sigma/w$. Unfortunately, these models are not solved explicitly for the shape of the beach. Bailard points out that the extreme slopes obtained in shallow water from these models may be the result of the inappropriate use of Stokes theory in shallow water and until a better flow model is developed, including more accurate shallow water wave representations, solving for beach shape

may be problematic.

To conclude, the results from the dynamic approach have been shown to give reasonable and usable representations for the beach shape explicitly. However, the assumptions and approximations used to derive these models and the quantification of $D_*$ leads to a search for a more complete and accurate description of the nearshore bathymetry. The kinematic approach presents a possible alternative for describing the equilibrium shape of a beach profile and offers enormous flexibility in that any sediment transport model based on nearshore processes and accurate wave and current descriptions can be applied through numerical methods. The most critical aspect of these models is obtaining wave and current models that can model the actual flow fields present in nature. In this study, the accurate stream function theory of Dean (1965) will replace the Stokes second order approximation as a model for the short wave climate, and the undertow model of Stive and De Vriend (1987) will provide a representation of the steady cross-shore flow. A wave height decay model for a random wave field will be intergrated simultaneously with the bottom slope model to provide the solutions to wave height, mean water level, and bottom depth for a state of no-net sediment transport across an equilibrium beach shape.

# Chapter 3

## GOVERNING EQUATIONS AND MODEL FORMULATION

The method in this thesis is described by Dean and Dalrymple (1992) as a kinematic approach to the solution of an equilibrium beach profile. The kinematic approach is applied to define the balance between the modes of sediment transport, via a no-net motion requirement along the profile, providing a bottom slope relationship dependent on variations in the wave and current climate. Specifically, an equilibrium beach profile can be modelled kinematically by establishing a relationship between the change in wave height across a surf zone and, thus, the current field and the response of the bottom slope, balancing the system to maintain no-net sediment motion.

The model proposed here will address the use of a generalized bottom slope formulation as a means to describe the shape of the nearshore bathymetry in an equilibrium state. The no-net sediment transport argument of Bowen (1980) and Bailard (1981) will be applied to Bailard's (1982) instantaneous, energetics cross-shore sediment transport equation resulting in a generalized expression for the bottom slope. The bottom slope equation will be re-expressed in terms of the nearshore velocity moments following the method of R&S, resulting in a generalized bottom slope equation expressed explicitly in terms of a steady current component, central odd velocity moments and central even velocity moments in the cross-shore direction. Following the definition of R&S, the central odd velocity moments are the time-averaged terms of the form $\langle \tilde{u}\,|\tilde{u}|^n \rangle$ and the central even moments are terms of the form $\langle |\tilde{u}|^n \rangle$, arising from the expansion of the total velocity moments in terms of time-varying $\tilde{u}$ and steady current $\overline{u}$ contributions. A method similar to that of R&S, who isolated longshore bar generating flows, will be

used to model the velocity moments in an attempt to produce a longshore bar formation in the equilibrium beach profile.

The energy decay model adopted will be applied for a random wave field where extensive work has been conducted in the calibration of the wave height distribution and velocity flow moments across the surf zone (*e.g.*, Bailard (1982), Guza and Thornton (1985), Battjes and Stive (1984), Stive (1986), and R&S). The wave energy dissipation in a random wave field will follow the work of Battjes and Janssen (1978) and Battjes and Stive (1985) to be consistent with the decay model used by Stive (1986) and R&S, where specific calibration of the total flow moments in a random wave field has been made.

Specifically, the basic formulation of this model consists of three first order linear differential equations: the bottom slope equation, the energy flux equation, and the momentum equation. This system of equations is coupled through wave energy, mean water surface elevation, and bottom depth and must be solved with an iterative scheme, or by simultaneous integration of all three equations. An attractive characteristic of this system is that it is an initial value problem and solutions to these equations are found with a standard $O(\Delta x)^4$ Runge-Kutta ordinary differential equation solver, where all three equations are solved simultaneously. Given this system of equations, solutions for water depth, wave height, mean water surface elevation, are provided as function of $x$, positive in the onshore direction. This will also provide solutions for the velocity moments and their respective components as a function of cross-shore distance. A definition sketch of the proposed model solutions is seen in figure 3.1.

In the following chapter, the equations for the generalized equilibrium beach profile model, referred to hereafter as the GEBP model, will be developed in a detailed discussion of the bottom slope equation and energy decay model.

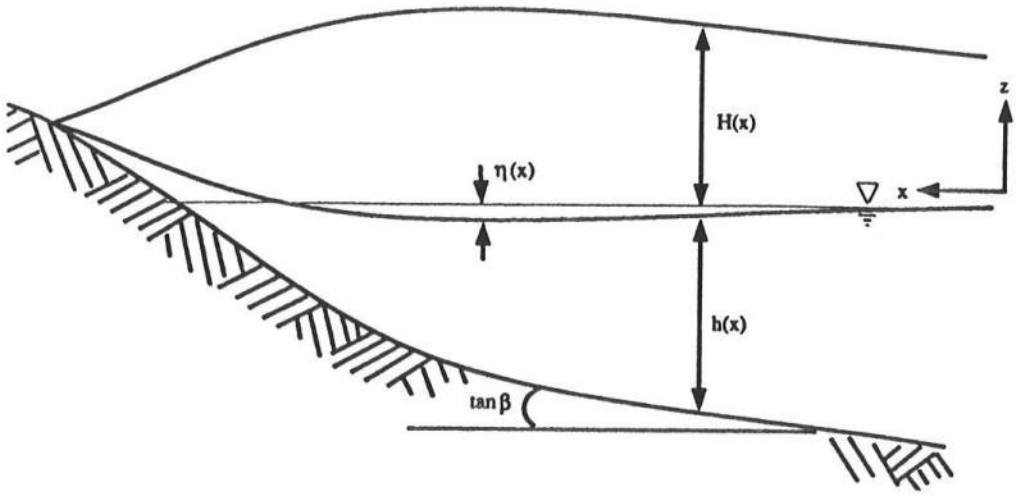


Figure 3.1: Definition sketch of proposed model solutions and sign convention.

## 3.1 Bottom Slope Equation

For the depth solution, the bottom slope model of Bailard (1981) is used as a basis for the development a more elaborate slope model by considering more complete wave and current current models. The new model will be formulated to correct problems with the simplified representations of wave and current models used in Bailard's model. Specifically, the use of Stokes second order solution in shallow water for the nonlinear wave component may lead to erroneous results for beach slope in the shallower areas of the surf zone; therefore, the Stream Function theory of Dean (1965) will be applied to ensure valid nonlinear wave solutions for a vertically symmetric wave form in any depth across the entire surf zone. Further, using the bottom drift velocity as the representative mean current may be suitable outside the surf zone, but we are interested in solutions across the entire nearshore region; therefore, the undertow solution of Stive and de Vriend (1987) will be used as the steady current model across the entire nearshore region, providing onshore flows outside the surf zone and offshore flows inside the surf zone.

### 3.1.1 Bailard's Analytical Model

Bailard (1981) addresses the equilibrium solutions of his total load sediment transport formulation by imposing the no-net sediment transport condition and defining the nonlinear nearshore wave field with Stokes second order solution and the steady current with Longuet-Higgins' (1953) steady streaming solution. In his analysis, Bailard only presents solutions for bottom slope and does not solve for the profile shape due to unrealistically steep values for bottom slope in shallow water. Bailard speculates the steep values may be the result of the suspended load efficiency factor $\epsilon_s^2$ in the denominator of the slope equation and the use of Stokes second order solutions well into the surf zone, where this wave theory is known to provide physically invalid results. Without addressing the physics of the sediment transport formulation, $\epsilon_s^2$ must remain in the model; however, substitutions can be made for the wave and current models representing the velocity moments. Using Bailard's model as the fundamental sediment transport formulation for the equilibrium slope, we will present Bailard's analytical solution for the equilibrium beach slope equation and point out terms that can be replaced with more accurate wave and current models.

To begin, Bailard's instantaneous, time-averaged total load sediment transport equation for flows in an arbitrary direction is

$$\left\langle \vec{i}_t \right\rangle = c_f \rho \left[ \frac{\varepsilon_b}{\tan\phi} \left[ \left\langle \vec{u} |\vec{u}|^2 \right\rangle - \frac{\tan\beta}{\tan\phi} \left\langle |\vec{u}|^3 \right\rangle \right] + \frac{\varepsilon_s}{w} \left[ \left\langle \vec{u} |\vec{u}|^3 \right\rangle - \frac{\varepsilon_s}{w} \tan\beta \left\langle |\vec{u}|^5 \right\rangle \right] \right] \quad (3.1)$$

where $\left\langle \vec{i}_t \right\rangle$ is the total, time-averaged immersed weight sediment transport, $\vec{u}_t$ is the instantaneous velocity vector, $\left\langle \vec{u} |\vec{u}|^2 \right\rangle$ and $\left\langle \vec{u} |\vec{u}|^3 \right\rangle$ are the total, time-averaged odd velocity moments, $\left\langle |\vec{u}|^3 \right\rangle$ and $\left\langle |\vec{u}|^5 \right\rangle$ are the total, time-averaged even velocity moments, $\varepsilon_b$ and $\varepsilon_s$ are efficiency factors describing the ability of the flow to transport bed load and suspended load, respectively, $c_f$ is the drag coefficient for the bed, $w$ is the settling velocity of sand, $\tan\phi$ is the angle of internal friction of sand, and $\tan\beta$ is the bottom

slope. The time-average will be over a wave period; but in the case of random waves, which will be addressed later, the time average is over the wave groups. Therefore, the time average is defined as

$$\left\langle \vec{i}_t \right\rangle = \frac{1}{nT} \int_t^{t+nT} \left( \vec{i}_t \right) dt, \tag{3.2}$$

where $T$ is the wave period and $n$ is the number of wave periods required for the averaging.

To express eqn. (3.1) in terms of arbitrarily directed velocity components, it is necessary to define the instantaneous velocity vector $\vec{u}_t$ in the onshore direction $x$ and longshore direction $y$ as

$$\vec{u}_t = (\tilde{u}\cos\alpha + \overline{u}\cos\theta)\,\hat{i} + (\tilde{u}\sin\alpha + \overline{u}\sin\theta)\,\hat{j}, \tag{3.3}$$

where $\tilde{u}$ is the time-varying velocity component, $\overline{u}$ is the steady current component, $\alpha$ and $\theta$ are the angles of the time-varying velocity and the steady current, respectively, related to shore normal direction (figure 3.2).

In order to make use of this expression in eqn. 3.1, Bailard approximates the total flow moments with a binomial expansion assuming $\tilde{u} \gg \overline{u}$ and $(\overline{u}/\langle|\tilde{u}|\rangle) \ll 1$. Nondimensionalizing with the amplitude of the orbital wave velocity $u_m$, Bailard arrives at two sediment transport expressions, one cross-shore and the other longshore, each being functions of cross-shore and longshore velocities. With interest in the cross-shore direction only, the cross-shore sediment transport component from the expansion is presented as

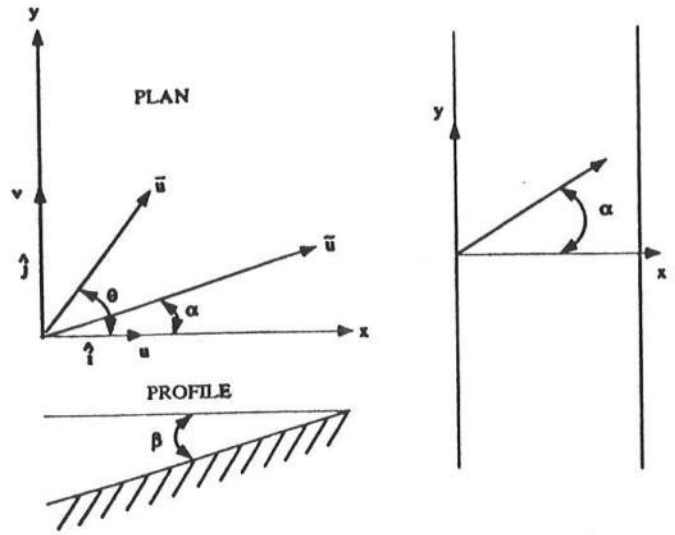


**Figure 3.2:** Schematic of orientation and defined direction of time-varying velocity vector, steady current vector and bottom slope.

$$\langle i_x \rangle = c_f \rho u_m^3 \left( \left[ \psi_1 \cos\alpha + \delta_u^3 + \delta_u \left( \frac{1}{2} + \cos^2\alpha + \delta_v^2 \right) + \right.\right.$$
$$\left.\left. \delta_v \sin\alpha \cos\alpha - \frac{\tan\beta}{\tan\phi} (u3)^* \right] \right)$$
$$+ c_f \rho u_m^3 \left( \frac{\varepsilon_s u_m}{w} \left[ \psi_2 \cos\alpha + \delta_u (u3)^* \right] - \left( \frac{\varepsilon_s u_m}{w} \right)^2 \tan\beta \, (u5)^* \right), \qquad (3.4)$$

where

$$\delta_u = \frac{\overline{u}}{u_m} \cos\theta, \qquad (3.5)$$

$$\delta_v = \frac{\overline{u}}{u_m} \sin\theta, \qquad (3.6)$$

$\psi_1$ and $\psi_2$ are the nondimensionalized odd velocity moments defined as

$$\psi_1 = \frac{\langle \tilde{u}^3 \rangle}{u_m^3} \tag{3.7}$$

$$\psi_2 = \frac{\langle \tilde{u} \, |\vec{u}|^3 \rangle}{u_m^4} \tag{3.8}$$

The odd velocity moments are zero for purely oscillatory flow and only contribute to sediment transport when higher order flow effects are present, such as those associated with nonlinear wave forms.

The even velocity moments are expressed as the integrals,

$$(u3)^* = \frac{1}{T} \int_0^T \left( \delta^2 + 2\delta \cos(\theta - \alpha) \cos \sigma t + \cos^2 \sigma t \right)^{3/2} \tag{3.9}$$

$$(u5)^* = \frac{1}{T} \int_0^T \left( \delta^2 + 2\delta \cos(\theta - \alpha) \cos \sigma t + \cos^2 \sigma t \right)^{5/2} \tag{3.10}$$

which are the lowest order even moments from the expansion and are nonzero for oscillatory flows. Therefore, to a first order approximation and assuming weak cross-shore currents, these moments can be modelled with the time varying velocity approximation,

$$\tilde{u} = u_m \cos \sigma t + u_{2m} \cos 2\sigma t + ... \tag{3.11}$$

where $u_m \gg u_{2m} \gg ....$ Substituting this approximation and integrating in time leads to the following values for the even moments, which essentially are the first order linear values for the even moments,

$$\langle |\tilde{u}|^3 \rangle = \frac{4u_m^3}{3\pi} \tag{3.12}$$

$$\langle |\tilde{u}|^5 \rangle = \frac{16u_m^5}{15\pi} \tag{3.13}$$

Assuming the beach to be in longshore equilibrium, where no changes in the longshore sediment transport occur, and imposing the no-net sediment transport condition, eqn. 3.4 can be reexpressed as the bottom slope equation

$$\tan\beta = \left[\frac{\varepsilon_b}{\tan\phi}\left(\psi_1\cos\alpha + \delta_u^3 + \delta_u\left(\frac{1}{2}+\cos^2\alpha+\delta_v^2\right)+\delta_v\sin\alpha\cos\alpha\right)+ \frac{u_m\varepsilon_s}{w}\left(\psi_2+(u3)^*\delta_u\right)\right]\left[(u3)^*\frac{\varepsilon_b}{\tan^2\phi}+(u5)^*\varepsilon_s^2\left(\frac{u_m}{w}\right)^2\right]^{-1} \tag{3.14}$$

where $\theta = 0$ and $\alpha = 0$. Substituting the above defined expressions and values for the odd and even velocity moments, respectively, the expression for bottom slope is finally

$$\tan\beta = \left[\frac{\varepsilon_b}{\tan\phi}\left(\psi_1+\frac{3}{2}\left(\frac{\overline{u}}{u_m}\right)\right)+\frac{u_m\varepsilon_s}{w}\left(\psi_2+\frac{4}{3\pi}\left(\frac{\overline{u}}{u_m}\right)\right)\right] \left[\frac{4}{3\pi}\frac{\varepsilon_b}{\tan^2\phi}+\frac{16}{15\pi}\varepsilon_s^2\left(\frac{u_m}{w}\right)^2\right]^{-1} \tag{3.15}$$

where $\psi_1$, $\psi_2$ and $\overline{u}$ remain unevaluated.

To evaluate the odd moments, $\psi_1$ and $\psi_2$ and the mean current $\overline{u}$, Bailard assumes Stokes second order solution (eqn. 2.25) and Longuet-Higgins' (1953) streaming velocity model (eqn. 2.26), respectively, to explicitly evaluate the model in terms of wave parameters. It is noted that eqn. 3.14 is still intractable due to the appearance of $\psi_2$, which is still represented in terms of the total of the time-varying velocity vector $\vec{u}_t$. For this reason, $\psi_2$ requires further expansion before individual flow contributions can be applied to this term. After some manipulation, the resulting expression is presented in Section 2.2.2 as eqn. 2.29.

To this end, we use this approach to obtain a more generalized expression for the bottom slope where models for the steady current, and the central odd and even velocity moments can be chosen from more complete theories. Therefore, in the following

section, the expansion of the flow moments will follow the work of Stive (1986) and R&S, resulting in a generalized expression for bottom slope.

### 3.1.2 Generalized Solution

For the study of equilibrium beach profiles, only the cross-shore sediment transport is of interest in developing a slope formulation. Since the development of Bailard's cross-shore sediment transport model, work by Stive and Battjes (1984), Stive (1986), de Vriend and Stive (1987), and R&S has been conducted which utilizes this sediment transport model as a physical basis for time-dependent sediment transport in the nearshore region caused time-averaged flows in a random wave field. However, after long term calculations of the sediment transport under a constant wave climate, an equilibrium solution describing the stable cross-shore shape of the nearshore bathymetry has not been obtained. Therefore, with interest in an equilibrium solution to these models, we adopt these wave and current models as the driving mechanisms of nearshore sediment transport and force an equilibrium solution by applying the no-net transport condition directly to Bailard's transport model. Thus, from the start, the problem is assumed to be two-dimensional in $x$ and $z$. The instantaneous cross-shore total load sediment transport model of Bailard (eqn. 3.1) is used where the instantaneous total flow vector is defined as

$$\vec{u}_t = (\tilde{u} + \overline{u})\,\hat{i} \tag{3.16}$$

where $\tilde{u}$ is the time-varying velocity component, $\overline{u}$ is the steady current component, and $\hat{i}$ is the onshore unit vector.

The time-averaged, instantaneous, total cross-shore sediment transport equation is presented again for completeness in this derivation. The cross-shore approximation of

this equation is governed by the assumption of the instantaneous velocity vector (eqn. 3.16).

$$\left\langle \vec{i}_x \right\rangle = c_f \rho \left[ \frac{\varepsilon_b}{\tan\phi} \left[ \left\langle \vec{u} \left| \vec{u} \right|^2 \right\rangle - \frac{\tan\beta}{\tan\phi} \left\langle \left| \vec{u} \right|^3 \right\rangle \right] + \frac{\varepsilon_s}{w} \left[ \left\langle \vec{u} \left| \vec{u} \right|^3 \right\rangle - \frac{\varepsilon_s}{w} \tan\beta \left\langle \left| \vec{u} \right|^5 \right\rangle \right] \right] \quad (3.17)$$

where $\tan\beta$ is the bottom slope and $\left\langle \vec{u} \left| \vec{u} \right|^2 \right\rangle$, $\left\langle \vec{u} \left| \vec{u} \right|^3 \right\rangle$, $\left\langle \left| \vec{u} \right|^3 \right\rangle$, $\left\langle \left| \vec{u} \right|^5 \right\rangle$ are the total velocity moments in the cross-shore direction.

As before, to obtain the equilibrium bottom slope model, the no-net motion condition

$$\left\langle \vec{i}_x \right\rangle = 0 \quad (3.18)$$

is applied and after grouping the terms and solving for bottom slope, we arrive at

$$\tan\beta = \left[ \frac{\varepsilon_b}{\tan\phi} \left\langle \vec{u} \left| \vec{u} \right|^2 \right\rangle + \frac{\varepsilon_s}{w} \left\langle \vec{u} \left| \vec{u} \right|^3 \right\rangle \right] \left[ \frac{\varepsilon_b}{\tan^2\phi} \left\langle \left| \vec{u} \right|^3 \right\rangle + \left( \frac{\varepsilon_s}{w} \right)^2 \left\langle \left| \vec{u} \right|^5 \right\rangle \right]^{-1} \quad (3.19)$$

This form of the slope model is different from Bailard's in that the flow moments have not been nondimensionalized with the fundamental velocity, $u_m$, and no simplification of the flow moments has yet been made. This result is quantitatively the same as Bailard's for the case of Stokes second order solution and bottom stream velocities; however, it is not necessary to nondimensionalize this expression for application of the proposed moments.

To express the velocity moments in terms of the steady current and central odd and central even velocity moments (eqn. 3.16) is substituted into the total velocity moment expressions which are approximated with a binomial expansion. Assuming

$\tilde{u} \gg \overline{u}$, which is basically stating that the mean return flow is several orders of magnitude smaller than the flow induced by the wave groups, the expanded flow moments are

$$\left\langle \vec{u}\,|\vec{u}|^2 \right\rangle = \left\langle \tilde{u}\,|\tilde{u}|^2 \right\rangle + 3\overline{u}\left\langle |\tilde{u}|^2 \right\rangle + 3\overline{u}^2\left\langle |\tilde{u}| \right\rangle + \overline{u}^3 \tag{3.20}$$

$$\left\langle \vec{u}\,|\vec{u}|^3 \right\rangle = \left\langle \tilde{u}\,|\tilde{u}|^3 \right\rangle + 4\overline{u}\left\langle |\tilde{u}|^3 \right\rangle + 6\overline{u}^2\left\langle \tilde{u}\,|\tilde{u}| \right\rangle + 4\overline{u}^3\left\langle |\tilde{u}| \right\rangle + \overline{u}^4 \tag{3.21}$$

$$\left\langle |\vec{u}|^3 \right\rangle = \left\langle |\tilde{u}|^3 \right\rangle + 3\overline{u}\left\langle \tilde{u}\,|\tilde{u}| \right\rangle + 3\overline{u}^2\left\langle |\tilde{u}| \right\rangle + \overline{u}^3 \tag{3.22}$$

$$\left\langle |\vec{u}|^5 \right\rangle = \left\langle |\tilde{u}|^5 \right\rangle + 5\overline{u}\left\langle \tilde{u}\,|\tilde{u}|^3 \right\rangle + 10\overline{u}^2\left\langle |\tilde{u}|^3 \right\rangle + 10\overline{u}^3\left\langle \tilde{u}\,|\tilde{u}| \right\rangle + \overline{u}^4\left\langle |\tilde{u}| \right\rangle + \overline{u}^5 \tag{3.23}$$

**and to the lowest order approximation,**

$$\left\langle \vec{u}\,|\vec{u}|^2 \right\rangle = \left\langle \tilde{u}\,|\tilde{u}|^2 \right\rangle + 3\overline{u}\left\langle |\tilde{u}|^2 \right\rangle \tag{3.24}$$

$$\left\langle \vec{u}\,|\vec{u}|^3 \right\rangle = \left\langle \tilde{u}\,|\tilde{u}|^3 \right\rangle + 4\overline{u}\left\langle |\tilde{u}|^3 \right\rangle \tag{3.25}$$

$$\left\langle |\vec{u}|^3 \right\rangle = \left\langle |\tilde{u}|^3 \right\rangle \tag{3.26}$$

$$\left\langle |\vec{u}|^5 \right\rangle = \left\langle |\tilde{u}|^5 \right\rangle \tag{3.27}$$

Only the first terms of the total even moments are retained by the argument that wave asymmetry does not strongly effect these terms. This point will be addressed in detail in Chapter 4.

These expressions are substituted directly into eqn. 3.19, resulting in the approximate expression for bottom slope

$$\tan\beta = \left[\frac{\varepsilon_b}{\tan\phi}\left(\left\langle\tilde{u}\,|\tilde{u}|^2\right\rangle + 3\overline{u}\left\langle|\tilde{u}|^2\right\rangle\right) + \frac{\varepsilon_s}{w}\left(\left\langle\tilde{u}\,|\tilde{u}|^3\right\rangle + 4\overline{u}\left\langle|\tilde{u}|^3\right\rangle\right)\right] \left[\frac{\varepsilon_b}{\tan^2\phi}\left\langle|\tilde{u}|^3\right\rangle + \left(\frac{\varepsilon_s}{w}\right)^2\left\langle|\tilde{u}|^5\right\rangle\right]^{-1} \tag{3.28}$$

This is the final form of the bottom slope equation explicit in terms of the steady current and the time-varying central odd and even moments. Given models for each of these individual components, various bottom slope equations can be obtained depending on the combinations of wave and current models used and assumptions made in the wave field representations. From this bottom slope expression, the central odd moments $\left\langle\tilde{u}\,|\tilde{u}|^2\right\rangle$ and $\left\langle\tilde{u}\,|\tilde{u}|^3\right\rangle$, can be approximated with Stokes second order, the central even moments, $\left\langle|\tilde{u}|^3\right\rangle$ and $\left\langle|\tilde{u}|^5\right\rangle$ with linear approximations, and the steady current with the bottom streaming solution (eqn. 2.26) and recover the bottom slope expression of Bailard (eqn. 2.29).

The generalized bottom slope equation is extremely flexible in that any available nearshore wave or current theory can be used to model the velocity moments. The models chosen for use in the GEBP will be presented and discussed in Chapter 4.

## 3.2 Wave Energy Decay Model

### 3.2.1 Random Wave Field

Formulation of the equilibrium beach profile model requires a wave height model which responds directly to local changes in bottom bathymetry across the surf zone. Battjes and Janssen (1978) presented a method for describing the change in root-mean-squared wave height, $H_{\text{rms}}$, across the surf zone due to the dissipation of a random wave field. They related the change in energy flux to a dissipation term based on the rate of

dissipation of a single monochromatic wave, modelled after the dissipation in a hydraulic jump, and the probability that a particular wave will be breaking at a given $x$ location. To better understand this model, Battjes and Stive (1985) conducted further verification and calibration against tank experiments and present guidelines for estimating the two free parameters $\gamma$ and $\alpha$ given the incident wave field. To extend the work of Battjes and Janssen to field application, Thornton and Guza (1983) reformulated the random dissipation by considering the transformation of the wave height probability density function across the surf zone as well as a change in wave height. Further recognizing that the wave field inside the surf zone can be described as a narrow-banded Gaussian distribution, Thornton and Guza presented two forms of the dissipation in a natural surf zone, one simple and one complete, where the simple form provides an explicit analytical solution for wave height across a plane beach. These models were established by calibrating the distribution of wave heights across the surf zone to measured field data at Torrey Pines, California.

For completeness, the use of both of these breaking models should be attempted; however, to be consistent with the work of R&S, where tank calibration of the velocity moments has been made, we have chosen to the breaking model of Battjes and Janssen. It may be argued that for comparisons to field data, the breaking model of Thornton and Guza should be used.

#### 3.2.1.1 The Energy Equation

Wave height variation across a changing bathymetry is determined by the conservation of energy flux, where energy flux is the rate of energy propagation in the wave form. Where no energy is dissipated, the energy flux remains constant but allows the wave height and wave length can increase and decrease with changes in depth in shallow water. This is the effect known as shoaling. However, in the nearshore region where the waves have shoaled to a critical or unstable height, energy is dissipated from the system in the form of wave breaking. After the wave has broken, all the energy is not

lost instantaneously, but rather, the wave continues to travel across the surf zone as a dissipative bore. The reduction of wave energy will continue until a stable height is reached by the propagating broken wave or all the wave energy is dissipated.

To formulate the change in wave energy and thus wave height across the surf zone, neglecting bottom friction and other losses, the change in energy flux is equated to the dissipation of wave energy due to wave breaking. Thus the energy balance takes the form

$$\frac{\partial EC_g}{\partial x} + D = 0, \tag{3.29}$$

where $EC_g$ is the linear onshore energy flux per unit width, $D$ is the dissipation per unit width, and $E$ is the linear wave energy,

$$E = \frac{1}{8}\rho g H^2, \tag{3.30}$$

and $C_g$ is the group speed of the linear wave form,

$$C_g = \frac{2\pi f}{k}\left[\frac{1}{2} + \frac{kh}{\sinh(2kh)}\right] \tag{3.31}$$

This form of the energy balance establishes a relationship between the potential for the wave field to shoal and slow down with decreasing depth and the need for the waves to break as the stable wave height is exceeded. The establishment and calibration of the dissipation caused by wave breaking is critical in describing the change in wave height across the surf zone.

#### 3.2.1.2 Random Wave Energy Dissipation

The wave field has been established to be random and thus a dissipation term for the change in the characteristics of the random wave height across the surf zone is required. Battjes and Janssen (1978) present a model for the change in the $H_{rms}$ wave height across a mildly sloping bottom, arguing that not all waves break at the same location. At a given location, wave breaking will occur only for the waves exceeding a maximum wave height criteria, $H_{max}$, where those waves exceeding the critical height are represented through the function,

$$H_{max} = \frac{0.88}{k} \tanh\left(\frac{\gamma k h}{0.88}\right) \tag{3.32}$$

Again, the local wave number, $k$, is determined using linear dispersive monochromatic theory and the spectral peak frequency, $f_p$. The maximum height is determined following the Miche-type criterion for periodic waves. The term $\gamma$ is an adjustable calibration parameter allowing for the effects of bottom slope and incident wave steepness that can change the breaking characteristics of the wave field.

Across the surf zone in a random wave field, only a fraction of the waves are breaking at any given location. Typically, further offshore the fraction is small and most waves pass the point unbroken. However, as the depth decreases, most notably at locations closer to the shoreline, the fraction of waves breaking increases until the water depth approaches zero where all waves are breaking or broken. Battjes and Janssen model the fraction of breaking or broken waves based on the argument that the wave height distribution is Rayleigh-type and the probability of exceedance for a given wave compared to the maximum wave height, $H_{max}$, at a given location. Following this hypothesis, they arrive at the following expression for the percent of waves breaking, $Q_b$,

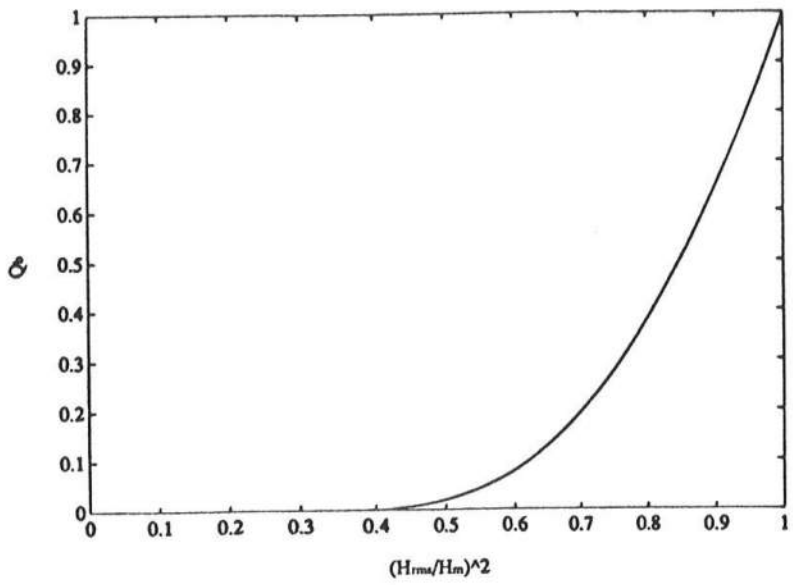


**Figure 3.3:** Percent Breaking Waves vs. $(H_{\rm rms}/H_{\rm max})^2$.

$$\frac{1-Q_b}{\ln Q_b} = -\left(\frac{H_{\rm rms}}{H_{\rm max}}\right)^2 \tag{3.33}$$

This expression must be solved by iteration for the local value of $Q_b$, given the $H_{\rm rms}$ wave height found by integration of the energy equation, and $H_{\rm max}$. The function is seen, figure (3.3), to vary between zero and one for combinations of $(H_{\rm rms})/(H_{\rm max})$.

The dissipation term for the fraction of breaking and broken waves is fundamentally based of the dissipation in a propagating bore, such as a moving hydraulic jump. However, for a random wave field, given the values for local maximum wave height and the measure of the breaking fraction of the wave field, $Q_b$, the expression for time-averaged dissipation of wave energy per unit area is

$$D = -\frac{1}{4}\alpha Q_b f_p \rho g H_{\rm max}^2 \tag{3.34}$$

where $\alpha$ is taken to be 1 in the calibration of Battjes and Stive (1985).

Battjes and Stive also present a calibration of $\gamma$ which is found to be a function of the incident wave steepness. The expression for $\gamma$ is

$$\gamma = 0.5 + 0.4 \tanh(33\, s_o) \tag{3.35}$$

where the deep water wave steepness $s_o$ is

$$s_o = \frac{2\pi H_{\text{rmso}} f_p}{g}, \tag{3.36}$$

where $H_{\text{rmso}}$ is the deep water root-mean-squared wave height.

The change in wave energy flux due to $D$ is coupled to changes in depth through $Q_b$ and the intensity of wave breaking is governed by the changes in depth which makes this model attractive for variable depth beaches such as those with bar fields.

#### 3.2.1.3 Shallow Water Asymptote for Random Wave Energy Dissipation

In our model, particular interest is in the shallow water asymptote of the energy decay model and the dissipation limit in the shallow water region. Considering the shallow water asymptote of $H_{\text{max}}$,

$$H_{\text{max}} = \gamma h \tag{3.37}$$

and taking the derivative of this expression in $x$, the change in the maximum wave height is found to linearly varying with changes in bottom slope as

$$\frac{\partial H_{\text{max}}}{\partial x} = \gamma \frac{\partial h}{\partial x} \tag{3.38}$$

In this region where all the waves are breaking or broken, $H_{rms} = H_{max}$ and $Q_b = 1$. After substitution of these relationships into the energy balance (eqn. 3.29), and some manipulation, the change in energy where all waves are breaking or broken is

$$\frac{\partial E}{\partial x} = \frac{2\gamma E}{H_{rms}} \frac{\partial h}{\partial x} \tag{3.39}$$

This expression linearly relates the change in wave energy to bottom slope through the local values of $\gamma$, $E$ and $H_{rms}$. This is a somewhat *ad hoc* approach, but it is an alternative to stopping the integration once $Q_b = 1$, as used by Battjes and Janssen. This result will be shown to be useful in the equilibrium beach profile solutions in regions of extreme beach slope, where the assumption of a mildly sloping bottom is violated.

#### 3.2.1.4 Momentum Equation

For completeness, the momentum balance used by Battjes and Janssen (1978) is adopted for further calibration of the wave heights and velocity moments on a plane beach. To begin, the total water depth is defined as,

$$h = d + \overline{\eta} \tag{3.40}$$

The momentum balance is governed by the relationship between the radiation stress $S_{xx}$ and changes in the mean water surface elevation $\overline{\eta}$. Radiation stress was first conceptualized by Longuet-Higgins and Stewart (1962) and is defined as the flux of excess momentum caused by the presence of the wave. A force balance on the water column between the vertical pressure gradient and the radiation stress yields the following mathematical relationship:

$$\frac{\partial S_{xx}}{\partial x} + \rho g h \frac{\partial \overline{\eta}}{\partial x} = 0 \tag{3.41}$$

To the first order the radiation stress in the cross-shore direction is

$$S_{xx} = \left(\frac{1}{2} + \frac{2kh}{\sinh(2kh)}\right) E \tag{3.42}$$

Inclusion of this equation provides more accurate results for wave height near the shoreline where there is an increase in water depth due to the excess of mass flux from wave breaking.

## 3.3 Model Summary

In this chapter the governing equations for the evaluation of the total depth $h$ and $H_{\text{rms}}$ wave height across a profile where there is no-net sediment transport have been presented. The generalized bottom slope equation does not require predefined wave or current models for the evaluation of the total velocity moments. In the following chapter, the models for the components of the total velocity moments will be presented as the driving wave and current models for the sediment transport. The wave energy decay model is chosen to be the time-averaged random dissipation model of Battjes and Janssen (1978) following the work of R&S where the nearshore shore total velocity moments have been modelled and measured. In Appendix A, a detailed general description of the equations and algorithm used in this model is presented. The explicit expressions for the derivatives required by the Runge-Kutta scheme are describe in the logical order necessary for a solution to these equations. To this end, the reader is referred to Appendix A for the explicit description of the model's equations.

# Chapter 4

# MODELLING CROSS-SHORE FLOWS

This chapter will introduce the wave and current models used to evaluate the steady current component, the central odd, and central even velocity moments, defined in Section 3.2.1, required by the total load cross-shore sediment transport formulation of Bailard (1982). The flow models will be calibrated according to the data of R&S for the case of a plane 1 on 40 beach and assumed to be valid in the solution for the equilibrium beach profile. First, an introduction to the experiments of R&S, where the cross-shore variation of the wave height, mean water surface elevation, and the total velocity moments are measured, will be presented. Next, solutions to the wave energy decay model of Battjes and Janssen (1978), calibrated according to Battjes and Stive (1985), will made for the case of the 1:40 plane beach. From the known wave height and mean water surface elevation, the total velocity moments can be calculated. Following the assumptions and basic procedure of R&S, the analytical and numerical solutions for the undertow, odd central moments, and the central even moments, with slight modifications to the models for the central odd and central even moments, will be presented. It is noted that the measured values of the velocity moments may not be accurately represented across a profile in no-net transport equilibrium, but this calibration is accepted as a means to establish an accurate representation of the flow mechanisms in the nearshore region.

## 4.1 Experimental Procedure and Results

R&S conducted experiments to measure the wave height, mean water surface elevation, and current field across the surf zone of two idealized beach profiles. The experiments allowed for the calibration of their proposed cross-shore sediment transport model and established the magnitude of the individual mechanisms for cross-shore sediment transport. Their goal was to isolate and measure specific flow contributions to the cross-shore sediment transport, specifically the breaking-induced turbulent flow, wave-induced asymmetric oscillatory flow, momentum decay-induced return flow, and wave grouping-induced long-wave flow.

The experiments were conducted at Delft Hydraulics with a flume 55 meters in length, 1 meter wide, and 1 meter deep. Two beach geometries were chosen, one plane and one barred, to simulate two distinctive nearshore bathymetric features present in nature and to determine the near-bottom current characteristics across such profiles. Because the calibration is based on the data presented by R&S, where only data for the total velocity moments over the plane beach are presented, the discussion will address this case only.

The plane beach was set initially to 1 on 40 and the depth of closure to the flat bottom was 0.59 meters deep. Measurements for the wave height variation and mean water level was taken across the surf zone using conductivity-type wave gages where effects of the aerated breaking waves were found to have little effect on the free surface measurements. The near-bottom horizontal velocities were measured at 5 cm above the bottom using an acoustic sediment transport meter and provided measurements within the accuracy of $\pm$ 1 cm/sec.

The random wave conditions were selected using a Jonswap-spectrum where the peakedness factor was assigned a value of 3.3 to simulate a normal storm wave climate. This was selected to enhance the wave and current fields ability to produce excessive offshore transport and thus create a longshore bar. The plane beach test was conducted

Table 4.1: Incident Wave Climate for Initially Plane 1:40 Beach (Roelvink and Stive 1989)

| $H_{rmsd}$ $(m)$ | $T_p$ $(sec)$ | $h_d$ $(m)$ | $s_o$ |
|---|---|---|---|
| 0.123 | 2.00 | 0.59 | 0.021 |

for 12 hours with a constant incident wave field, but the bottom, composed of 100 $\mu$m sediment, deformed throughout the experiment. The fall velocity $w$ of the sediment is taken to be 0.01 (m/s).

The wave conditions selected have a relatively steep offshore wave steepness, $s_o$, as seen in table 4.1. This will prove to be an extreme erosional condition when using the GEBP. The wave height in table 4.1 is the input wave height at the wave paddle for the given depth $h_d$. This input and the resulting measurements of the $H_{\rm rms}$ wave height variation and the total velocity moments will be used for comparison in the following sections to verify the analytical and numerical representations of the cross-shore wave and flow models.

## 4.2 Calibration of the Breaking Model

To demonstrate the implementation of the wave height model over a mildly sloping plane beach, the results for the $H_{\rm rms}$ wave height and mean water surface elevation, $\overline{\eta}$, as presented by R&S are reproduced. This specific example is chosen to be consistent with their model and data measurements throughout this discussion.

The wave energy decay model follows directly from Battjes and Stive (1985) where calibration involves the selection of the free parameters $\alpha$ and $\gamma$. As has been recommended by Battjes and Stive, the value of $\alpha$ is set to 1 enabling the calibration

to be based on a single free parameter. With $\alpha = 1$, $\gamma$ is obtained from the proposed relationship of Battjes and Stive (eqn. 3.35). This relationship is based on changes in the numerical wave field representation, compared to data, in response to changes in the incident wave steepness. Therefore, given the incident wave climate, $\gamma$ is found directly from eqn. 3.35. The incident wave field characteristics presented in table 4.1 result in $\gamma = 0.73$. Using a standard fourth order Runge-Kutta scheme, the energy balance (eqn 3.29) and momentum balance (eqn 3.41) are integrated simultaneously to obtain values for $H_{rms}$ and $\overline{\eta}$ across the surf zone.

It must be pointed out that eqn. 3.33, the percent of breaking waves, is solved at each $x$ location. It is this expression that couples the energy dissipation to changes in depth and thus is the mechanism which adjusts the intensity of breaking as the numerical solution propagates across the domain.

Our results agree well with those presented by R&S. For a comparison, solutions for $H_{rms}$ and $\overline{\eta}$ as a function of $x$ directed from offshore to onshore are presented in figure 3.1. Accepting these results as accurate representations of the wave field variations across the surf zone, we progress to modelling the current fields driven by wave height and water depth.

## 4.3 Nearshore Wave and Current Fields

An accurate representation of the combined, time-averaged surf zone flows required by Bailard's (1982) total load sediment transport equation is presented by R&S. R&S argued that surf zone flows can be recognized as breaking-induced turbulent flow, wave-induced asymmetric oscillatory flow, momentum decay-induced return flow, and wave grouping-induced long-wave flow. Each of these flows can be modelled individually via respective formulations. It was shown in Chapter 3, with a mean flow $\overline{u}$ much smaller than a time-varying oscillatory flow $\tilde{u}$, and a binomial expansion, that the total flow moments can be expressed explicitly as combinations of a steady current, central odd,

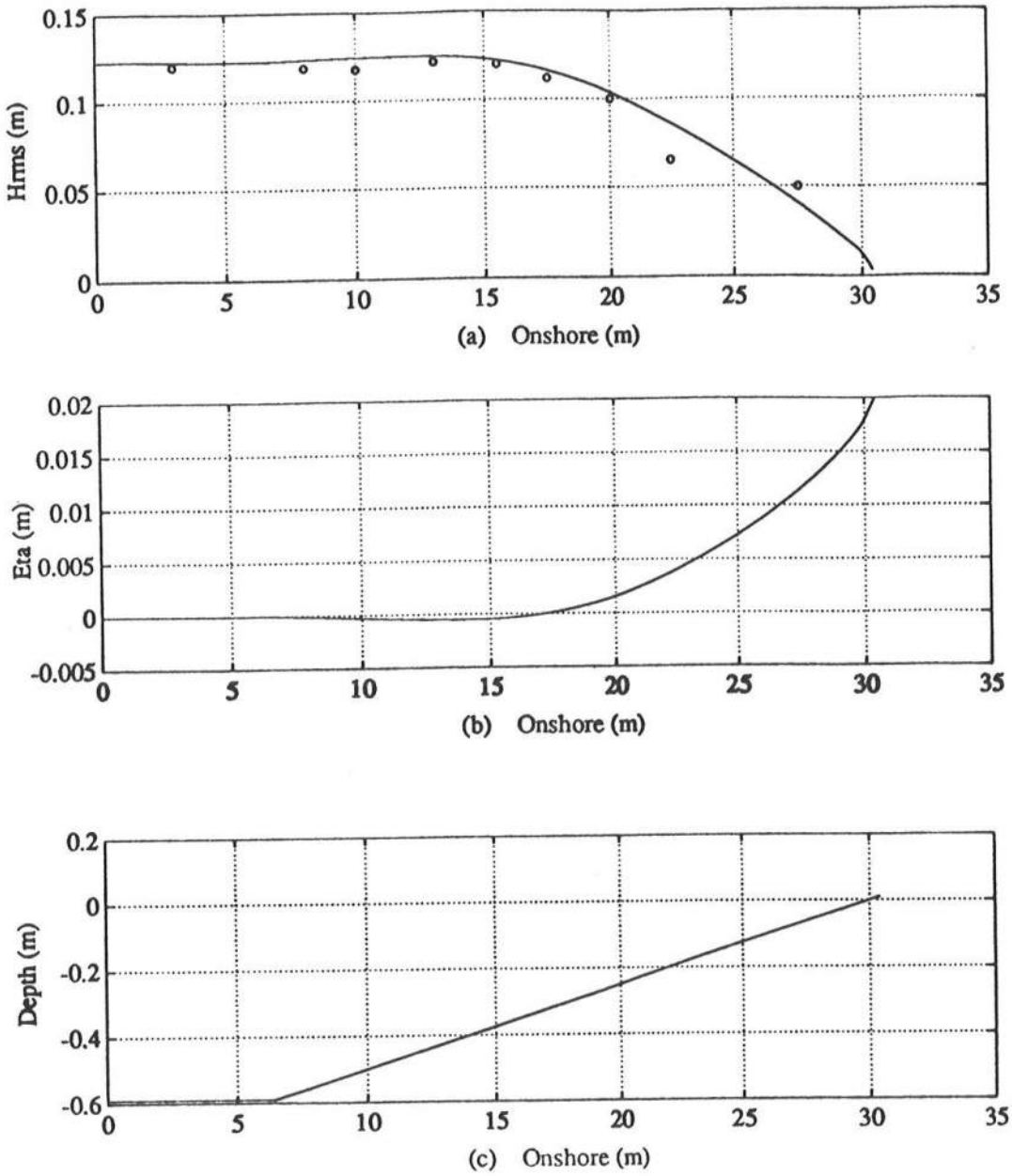


**Figure 4.1:** Results from Breaking Model Over 1:40 Plane Beach (a) $H_{\text{rms}}$ (meters), (b) $\overline{\eta}$ (meters), (c) $d$ (meters).

velocity moments and central even velocity moments. In this study, for simplicity, the turbulent flow induced by breaking, which is modelled by R&S to improve the location of the maximum intensity of the undertow will be neglected. Further, only short wave contributions to the total odd moments will be considered and contributions from the grouping-induced long-wave flow will be neglected.

### 4.3.1 Steady Current Component - Undertow Solution

It is well established that the dominant mean flow within the surf zone in the cross-shore direction is the momentum decay-induced undertow, or return flow established due to the excessive shoreward directed mass flux above trough level induced by wave breaking. This mechanism was first addressed by Dyhr-Nielsen and Sorensen (1970) who recognized the imbalance between the vertically non-uniform wave momentum flux and the vertically uniform pressure gradient in the presence of wave breaking. The problem has been addressed for the case of monochromatic waves by Dally (1980), Börekci (1982), Svendsen (1984), Stive and Wind (1986), Svendsen and Hansen (1988), and Svendsen, Schaffer and Hansen (1987). For the case of random waves, the problem was first attempted by Stive and Battjes (1984), which led to further studies by de Vriend and Stive (1987), Stive and de Vriend (1987), and R&S.

The model of Stive and de Vriend (1987), which includes the matching solution of Svendsen *et al.* for the bottom boundary layer, is presented in a usable final form and is the model used by R&S in their bar generating cross-shore sediment transport. Following this work, the model of Stive and de Vriend is accepted as a suitable analytical representation of the near-bottom mean return flow. To this end, the solution from this model is established as the dominant cross-shore steady current in the nearshore region in the presence of random waves and define it as the mean flow component $\overline{u}$ in our final bottom slope equation. For completeness, the governing equations, resulting analytical expressions, and respective calibration is discussed in Appendix B. For purposes here, only the resulting analytical expression will be presented.

The expression for the undertow comes directly from the solution presented in Appendix B and is

$$\overline{u} = \frac{\tau_b}{\rho \nu_{tb}} \delta + \frac{\alpha}{2\nu_{tb}} \delta^2 + u_s(z_l) \tag{4.1}$$

where $\overline{u}$ is the steady current, $\tau_b$ is the bottom shear stress, $\alpha$ is the driving force, $\delta$ is the thickness of the bottom boundary layer, and $u_s(z_l)$ is the bottom streaming velocity. The depth to the bottom is $z_b$.

To utilize this result, the location of the patching level, $z_l$, where the middle and bottom layers are interfaced, is defined as

$$z_l = z_b - \delta, \tag{4.2}$$

where the thickness of the bottom boundary layer, $\delta$, is the thickness of wave induced laminar boundary layer

$$\delta_w = \left(\frac{2\nu_{tb}}{\omega}\right)^{\frac{1}{2}} \tag{4.3}$$

where $\nu_{tb}$ is the turbulent viscosity defined in Appendix B and $\omega$ is the angular frequency of the wave field. This specification provides the best results between our reproduction of this model and the results presented by Stive and de Vriend.

This result provides a complete model for the momentum decay induced return flow for random wave breaking where the wave height, water depth, and energy dissipation $D$, are required to determine the mean flow. An important aspect of the solution is that when wave breaking is minimal, dissipation $D$ being small, the streaming velocity $u_s(z_l)$ provides onshore flow at our chosen $z = z_l$ location for near-bottom flow. However, as wave breaking increases, the disspation induced return flow overcomes the drift

velocity and the mean flow becomes offshore. This transition from onshore to offshore mean flow will prove to produce longshore bars in the equilibrium beach profile.

The contributions of a change in the direction of the bottom velocity to bar formation is a concept first presented by Dyhr-Nielsen and Sorensen (1970), who qualitatively described the presence of longshore bars as the result of the change in direction of the bottom shear stress from onshore to offshore as the waves begin to break. Dally (1987) supported this hypothesis from findings of experiments conducted which exaggerated two possible mechanisms thought to be responsible for the establishment and movement of longshore bars. The two mechanisms were surf beat generated from random wave field induced wave groups and breaking induced mean return flow. Dally concluded that the dominant mechanism in the establishment of the longshore bar is the breaking induced mean return flow. The hypothesis of Dyhr-Nielsen and Sorensen and the observations of Dally are important in describing the results obtained with the GEBP.

The undertow model is calibrated with the data provided by R&S using the results from the wave energy decay model and the final form of the near-bottom return flow. Figure 4.2 shows the results for the undertow across the 1:40 plane slope where the starting depth restricts the model's ability to produce onshore flow due to substantial wave energy dissipation at the starting location.

### 4.3.2 Central Odd Flow Moments

From expansion of the total time-averaged flow moments, the terms $\left\langle \tilde{u}\,|\tilde{u}|^2 \right\rangle$ and $\left\langle \tilde{u}\,|\tilde{u}|^3 \right\rangle$ are found to contribute to the total odd moments. As a first approximation, the group-induced long wave flows are assumed to be negligible and the time-averaged central odd moments are represented with only the short wave flows under nonlinear wave forms as

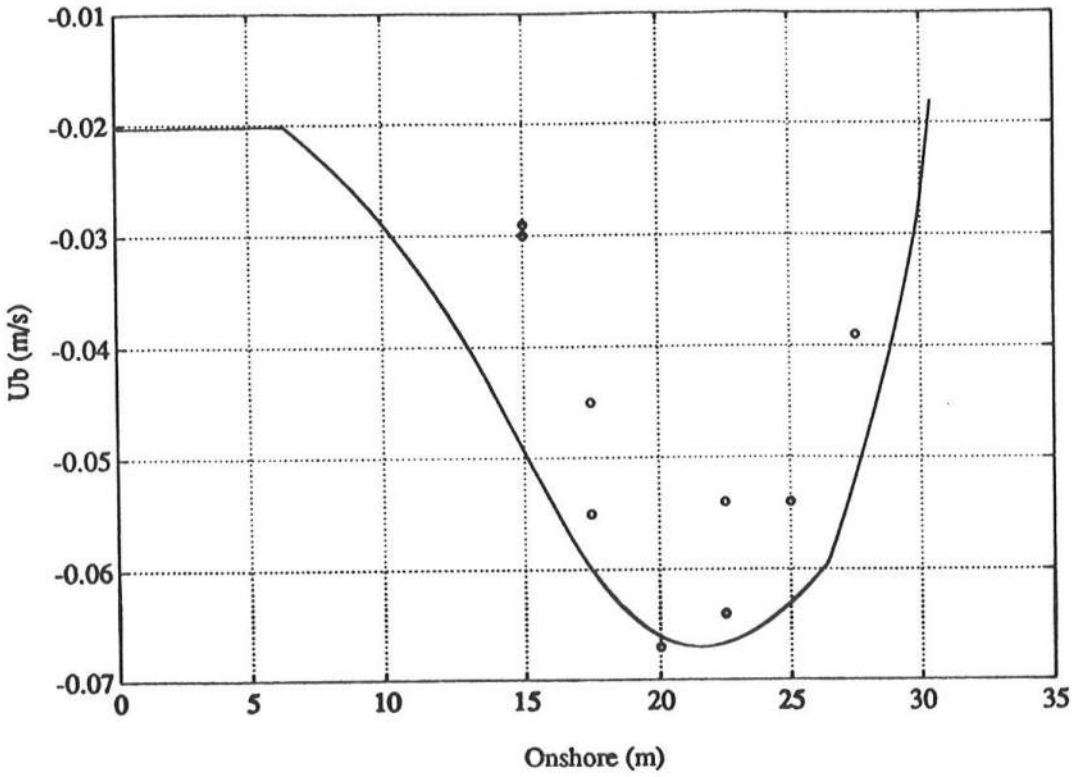


**Figure 4.2:** Undertow Solution (Stive and de Vriend 1987) (computed = *solid*) vs. Measured Data (Roelvink and Stive 1989) for 1:40 Plane Beach.

$$\left\langle \tilde{u}\,|\tilde{u}|^2 \right\rangle = \left\langle u_s\,|u_s|^2 \right\rangle \tag{4.4}$$

$$\left\langle \tilde{u}\,|\tilde{u}|^3 \right\rangle = \left\langle u_s\,|u_s|^3 \right\rangle \tag{4.5}$$

where $u_s$ is the bottom-velocity of a given wave form.

With these definitions, the central odd moments are zero for symmetric flows such as

$$u_s = u_m \cos \sigma t \tag{4.6}$$

and thus require a higher order wave representation to produce nonzero values. As shown in Chapter 2, Bailard (1981) represents the nonlinear wave field with the Stokes second order solution. This approach is effective in describing the central odd velocity moments outside the surf zone, but as shallow water is approached, the Stokes solution becomes invalid in representing the free surface variations and thus the time-varying bottom velocity. Recognizing this, the Dean's Stream Function theory solution is selected to ensure valid representations of vertically symmetric waves forms in any depth across the surf zone. The routine developed by Dalrymple (1974) has been adopted as a means to determine the stream function solution of any set of conditions. Six components are required for stream function convergence to optimize computer time and to insure accurate representation of the wave field. Stream Function theory provides the harmonic amplitudes for the stream function, $\Psi$, describing the fluid motion. The derivative of $\Psi$ in $z$,

$$u_{bn} = -\frac{\partial \Psi}{\partial z}|_{z=0}, \tag{4.7}$$

provides the bottom velocity under the wave form for each stream function harmonic. From this, a time series for the bottom velocity over a wave period can be constructed as

$$u_s = \sum_{n=1}^{6} u_{bn} \cos(n\omega_p t) \tag{4.8}$$

where $u_{bn}$ is the amplitude of the velocity for each of the 6 components.

Following R&S, the breaking and unbroken waves are assumed to be uncorrelated and vertically symmetric wave form solutions are acceptable representations of unbroken waves in the inner surf zone. Following this approximation, the contributions to the odd moments from the unbroken waves are represented by considering the fraction of waves breaking $Q_b$ and relate the difference from all waves as

$$\left\langle \tilde{u}\,|\tilde{u}|^2 \right\rangle = (1 - Q_b)\left\langle u_s\,|u_s|^2 \right\rangle \tag{4.9}$$

$$\left\langle \tilde{u}\,|\tilde{u}|^3 \right\rangle = (1 - Q_b)\left\langle u_s\,|u_s|^3 \right\rangle \tag{4.10}$$

These expressions represent the unbroken short wave contributions to the central odd velocity moments.

Solving for the time series necessary to compute the time averaged odd moments, the method by Dalrymple requires the wave height, wave period and water depth at a given location. The monochromatic equivalent wave height needed by Stream Function theory is approximated with the $H_{rms}$ wave height from the breaking model. The energy in a nonlinear wave form can differ greatly from a linear wave across the surf zone, especially in very shallow water where the wave is very peaked. Thus, this increase in wave energy is accounted for through an effective wave height for the Stream Function

convergence. To do this, the nondimensional total energy equivalents tabulated by Dean (1974) are adopted, which account for the percentage difference in energy in a linear wave of given height to that energy due to the nonlinear effects in a wave of the same height. The values presented by Dean (1974) are tabulated in table 4.2. Using a standard two dimensional cubic spline routine, Press *et al.* (1986), the nondimensional total energy equivalent is found and used to adjust the representative wave height accordingly.

Table 4.2: Dimensionless Total Average Energy, $\Phi$

| $h/L_o$ | $H/H_b$ | | | |
|---|---|---|---|---|
| | 0.250 | 0.500 | 0.750 | 1.000 |
| 0.002 | 0.424 | 0.308 | 0.249 | 0.213 |
| 0.005 | 0.605 | 0.446 | 0.344 | 0.263 |
| 0.010 | 0.755 | 0.580 | 0.455 | 0.342 |
| 0.020 | 0.880 | 0.722 | 0.577 | 0.467 |
| 0.050 | 0.966 | 0.873 | 0.733 | 0.527 |
| 0.100 | 0.988 | 0.939 | 0.830 | 0.618 |
| 0.200 | 0.995 | 0.966 | 0.887 | 0.686 |
| 0.500 | 0.988 | 0.979 | 0.928 | 0.750 |
| 1.000 | 0.988 | 0.979 | 0.932 | 0.811 |
| 2.000 | 0.988 | 0.979 | 0.933 | 0.836 |

Defining the energy in the wave form with the linear representation

$$E = \frac{1}{8}\rho g H_{rms}^2 \tag{4.11}$$

and determining the scaling $\Phi$ from linear to actual energy from table 4.2, the effective wave energy is calculated as

$$E' = \Phi E \tag{4.12}$$

where $\Phi$ = dimensionless total average energy for a given $h/L_o$ and $H/H_b$. Given this expression, the effective wave height for use in the Stream Function solution can be

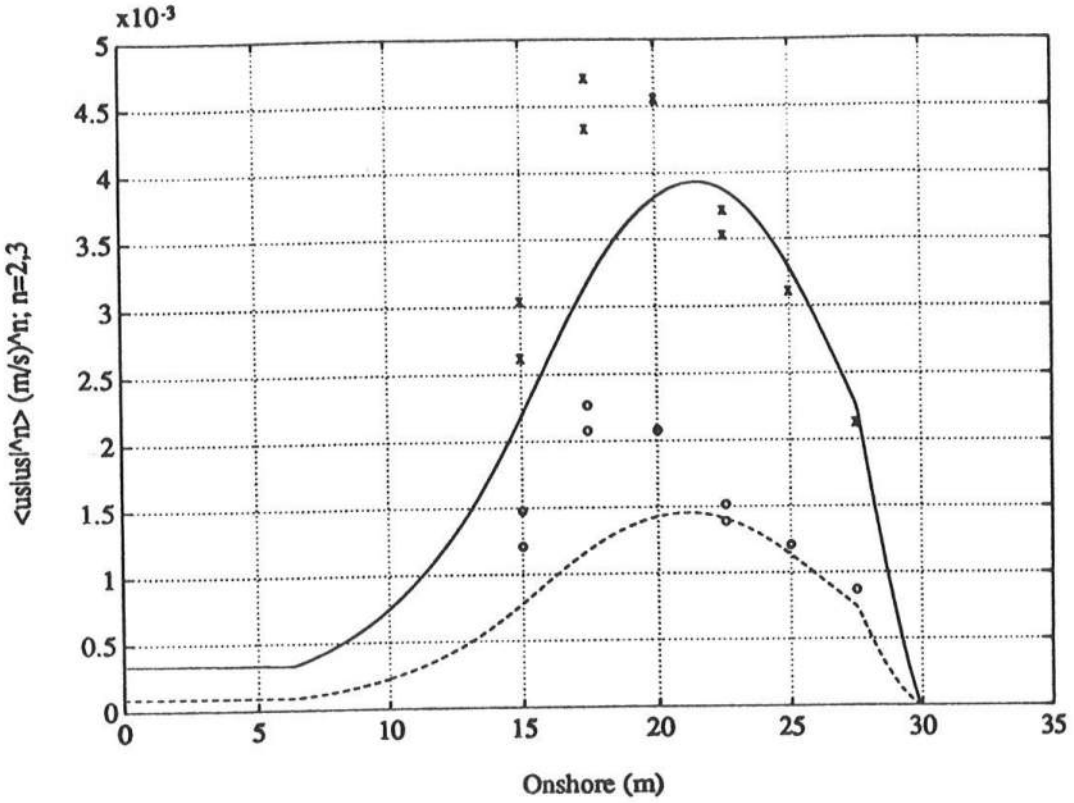


**Figure 4.3:** Central Odd Moments (Dean's Stream Function theory) vs. Measured Data (Roelvink and Stive 1989) for 1:40 Plane Beach: $\langle u_s|u_s|^2\rangle$ (computed = *solid* - measured = *x*), $\langle u_s|u_s|^3\rangle$ (computed = *dashed* - measured = *o*)

determined as

$$H'_{\text{rms}} = \left[\frac{8E'}{\rho g}\right]^{\frac{1}{2}} \tag{4.13}$$

which will in effect be converging on actual wave energy rather than wave height.

Again, applying the results from the wave energy decay model, solutions for the central odd moments across the 1:40 plane slope are seen in figure (4.3).

As an additional comment, it is well established, Flick (1978), that waves in the inner surf zone are not vertically symmetric and achieve a phase relationship between successive wave components of $\pi/2$, where the wave form is unsymmetric in the vertical

and horizontal. This wave form has been termed the "saw-toothed" shaped wave. An analytical method for describing the moments for "saw-toothed" wave forms is not available, thus the assumption of a vertically symmetric wave form across the surf zone is accepted as an approximation.

### 4.3.3 Central Even Flow Moments

The central even moments $\langle|\tilde{u}|^n\rangle$ are nonzero for symmetric wave forms and thus do not require the high order nonlinear wave solutions to produce contributions to the mean flows in the surf zone. Guza and Thornton (1985) address the accurate representation of the even velocity moments for a linear Gaussian random wave field. For a linear monochromatic wave field, Bowen (1980) and Bailard (1981), as well as Guza and Thornton, estimate the time-averaged low order even velocity moment as

$$\left\langle|\tilde{u}|^2\right\rangle = 0.5u_m^2 \tag{4.14}$$

$$\left\langle|\tilde{u}|^3\right\rangle = 1.20\left\langle|\tilde{u}|^2\right\rangle^{3/2} \tag{4.15}$$

$$\left\langle|\tilde{u}|^5\right\rangle = 1.92\left\langle|\tilde{u}|^2\right\rangle^{5/2} \tag{4.16}$$

where

$$u_m = \frac{H_{\text{rms}}\sigma}{2\sinh kh} \tag{4.17}$$

These expressions are the same as those presented for the even moments in Section 3.1.1.2.

For the case of a random wave field, Guza and Thornton argued that a simple linear representation of the wave field is not sufficient to describe the even moments and suggest as a first approximation representing the wave field using a Gaussian description of the wave heights in the surf zone of a linear random sea. They recognized that a Gaussian distribution is not a complete representation of the wave field in the surf zone, but argue that for the lower order moments the Gaussian distribution is acceptable.

The lowest order even velocity moments are

$$\left\langle |\tilde{u}|^2 \right\rangle = 0.5 u_m^2 \tag{4.18}$$

$$\left\langle |\tilde{u}|^3 \right\rangle = 1.58 \left\langle |\tilde{u}|^2 \right\rangle^{3/2} \tag{4.19}$$

$$\left\langle |\tilde{u}|^5 \right\rangle = 6.38 \left\langle |\tilde{u}|^2 \right\rangle^{5/2} \tag{4.20}$$

where they equated the variance in a monochromatic wave train to the variance in a linear Gaussian wave field and presented the lowest order moments as scaled quantities of the variance. It is shown that accounting for the Gaussian nature of the random wave field, the even moments are larger than those found with the monochromatic representation. This difference is noted by Guza and Thornton to be the result of infrequent large velocities in the Gaussian distribution which contribute to the even moments. The effect of this mechanism is seen to have a greater effect as the order of the moments increase. The results for these expressions are presented as functions of $x$ over the 1:40 plane beach, (figure 4.1c), in figure 4.4.

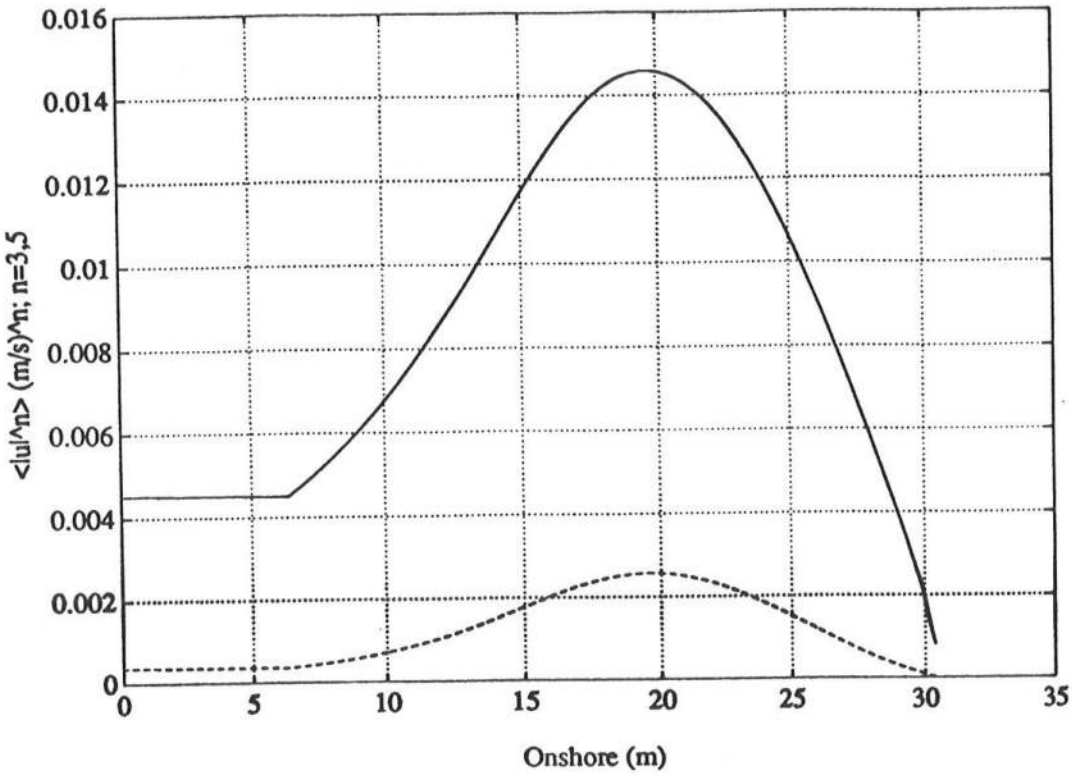


**Figure 4.4:** Central Even Moments (Gaussian Model) for 1:40 Plane Beach: $\langle |u_s|^3 \rangle$ (computed = *solid*, $\langle |u_s|^5 \rangle$ (computed = *dashed*)

### 4.3.4 Total Velocity Moments

The total flow moments, described in Section 3.1.2 as the combinations of the undertow, central odd velocity moments, and the central even velocity moments, are

$$\left\langle \vec{u}\,|\vec{u}|^2 \right\rangle = \left\langle \tilde{u}\,|\tilde{u}|^2 \right\rangle + 3\overline{u}\left\langle |\tilde{u}|^2 \right\rangle \tag{4.21}$$

$$\left\langle \vec{u}\,|\vec{u}|^3 \right\rangle = \left\langle \tilde{u}\,|\tilde{u}|^3 \right\rangle + 4\overline{u}\left\langle |\tilde{u}|^3 \right\rangle \tag{4.22}$$

$$\left\langle |\vec{u}|^3 \right\rangle = \left\langle |\tilde{u}|^3 \right\rangle \tag{4.23}$$

$$\left\langle |\vec{u}|^5 \right\rangle = \left\langle |\tilde{u}|^5 \right\rangle \tag{4.24}$$

Substituting the resulting expressions for the even moments and recalling the results from the undertow and central even moments, the total velocity moments are expressed as

$$\left\langle \vec{u}\,|\vec{u}|^2 \right\rangle = \left\langle \tilde{u}\,|\tilde{u}|^2 \right\rangle + 1.5\overline{u}u_m \tag{4.25}$$

$$\left\langle \vec{u}\,|\vec{u}|^3 \right\rangle = \left\langle \tilde{u}\,|\tilde{u}|^3 \right\rangle + 6\overline{u}u_m^3 \tag{4.26}$$

$$\left\langle |\vec{u}|^3 \right\rangle = 0.75u_m^3 \tag{4.27}$$

$$\left\langle |\vec{u}|^5 \right\rangle = 3.19u_m^5 \tag{4.28}$$

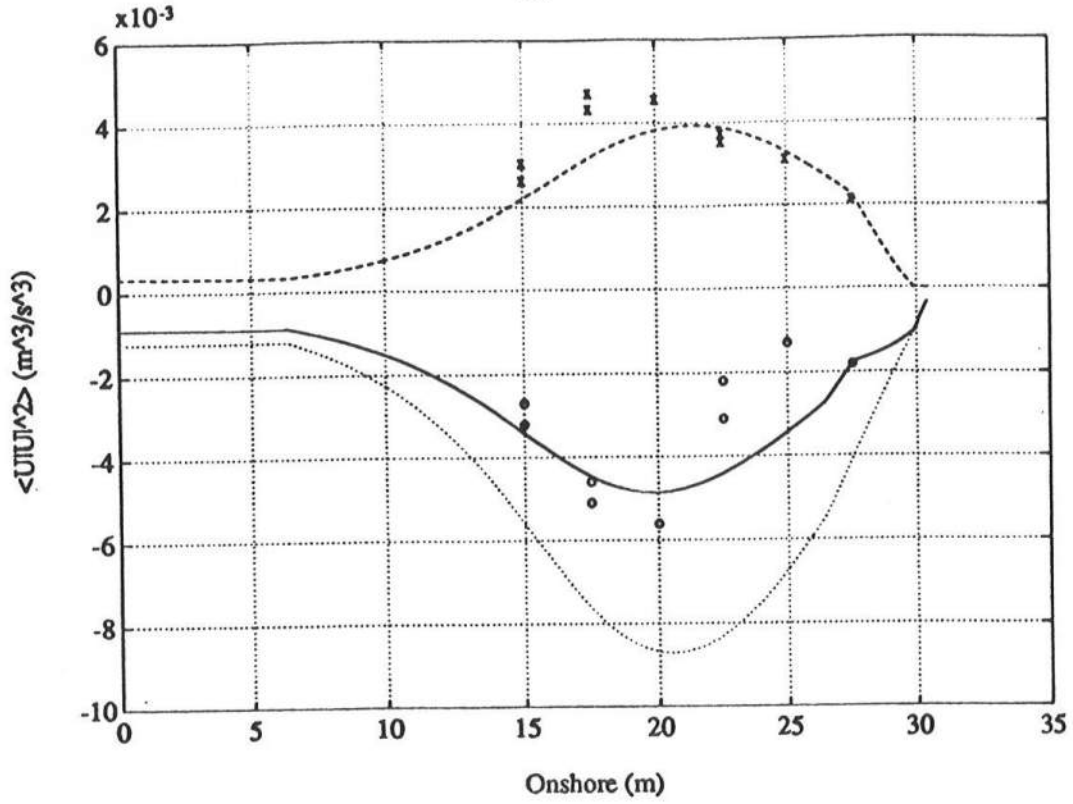


**Figure 4.5:** Total Velocity Moment $\left\langle \vec{u}|\vec{u}|^2 \right\rangle$ vs. Measured Data (Roelvink and Stive 1989) for 1:40 Plane Beach: (computed = *solid* - measured = *o*).

For completeness, the values for the total odd velocity moments from eqn. 4.25 and eqn. 4.26 are determined as functions of $x$ over the 1:40 plane slope and shown in figure 4.5 and figure 4.6, respectively.

To conclude, the purpose of this chapter was to develop the flow fields necessary to compute the total time-averaged velocity moments across a 1:40 plane slope and compare the results and data of R&S. This exercise provides a method for calibration of the flow moment models to be used in the GEBP model where the bottom is not known *a priori*. To this end, the calibration of the velocity moment across a plane beach is assumed to provide sufficient and approximate representations to the velocity moments across the depths found with the no-net sediment transport condition.

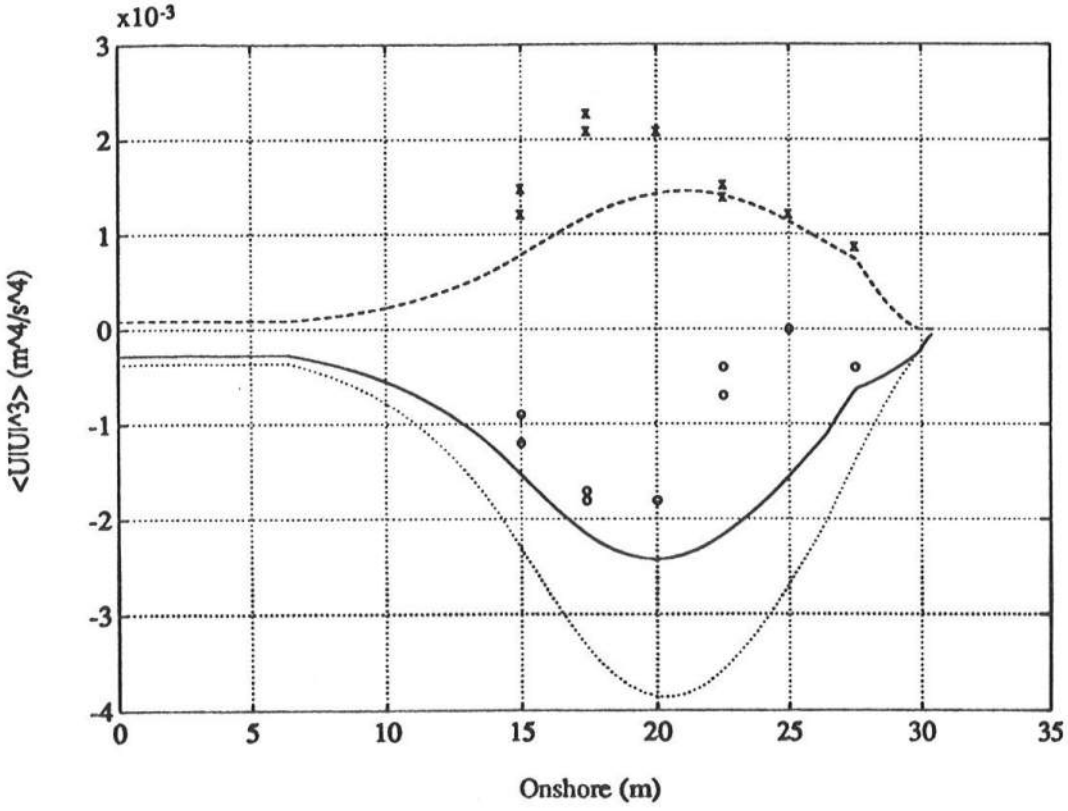


**Figure 4.6:** Total Velocity Moment $\left\langle \vec{u}\,|\vec{u}|^3 \right\rangle$ vs. Measured Data (Roelvink and Stive 1989) for 1:40 Plane Beach: (computed = *solid* - measured = *o*).

# Chapter 5

# RESULTS AND DATA COMPARISON

In this chapter, we will present results obtained with the generalized equilibrium beach profile model, GEBP, as presented in Appendix A. Since the selection of deep-water wave conditions and initial starting depth are critical to accurate execution of the model, a methodology for selection of suitable offshore starting conditions is established. A solution to the model given an arbitrary set of initial conditions is presented to emphasize the mechanisms required to establish a longshore bar in an equilibrium beach profile. The sensitivity to offshore wave conditions is addressed to characterize trends of the model in response to changes in wave climate. The GEBP model is based on the proposed flow moment models of R&S and is calibrated to their measured data over a plane beach. Thus, input from R&S will be used in the GEBP model to determine if an equilibrium solution exists for their input parameters. Finally, comparison to data from the U.S. Army Corps of Engineers - Field Research Facility is made in an attempt to relate the model to field conditions.

## 5.1 Selection of Input

The model requires wave height, mean water surface elevation, and depth as input for the integration of the three governing equations. The offshore incident wave conditions are established as a datum for the $H_{\text{rmso}}$ wave height and wave period, $T_p$. The mean water surface displacement, $\overline{\eta}$, is taken to be zero far offshore from the surf zone. The selection of the input depth, $d$, is arbitrary as long as wave breaking has

not been initiated. It is satisfactory to chose a depth just outside the region where the largest waves will begin to break. Given the deep water incident wave conditions, linear theory is used to shoal the waves to a starting depth. (It is noted that this may not be an accurate representation for shoaling the $H_{rms}$ wave height, due to the probabilistic nature of the representative wave height, but for our purposes we accept this approximation well in to the shoaling region before wave breaking begins). The conservation of energy flux argument is applied and, assuming the $H_{rms}$ wave height to be a representative monochromatic wave height, the wave height at any depth relative to the offshore wave conditions is found by the linear shoaling expression,

$$H_{rmsd} = K_s H_{rmso} = \sqrt{\frac{C_{go}}{C_{gd}}} H_{rmso} \tag{5.1}$$

where $K_s$ is the linear shoaling coefficient, $H_{rmsd}$ is the equivalent $H_{rms}$ wave height at the starting depth, $H_{rmso}$ is the deep water $H_{rms}$ wave height, and $C_{gd}$ and $C_{go}$ are the linear group speeds at the starting depth and deep water, respectively. The use of the linear shoaling saves computational time in that the same results will be found numerically from the energy balance equation where dissipation is negligible.

For the bottom slope equation, we adopt Bailard's (1981) calibration of the bedload and suspended load sediment transport efficiency factors as $\epsilon_b = 0.025$ and $\epsilon_s = 0.01$, respectively. The internal angle of friction sand, $\tan\phi$, is taken as 0.63, the fluid density, $\rho$, is 1000 $(kg/m^3)$ and the gravitational acceleration, $g$, is 9.81 $(m/s^2)$.

## 5.2 Generalized Equilibrium Beach Profile Model (GEBP)

The GEBP model is unique in the fact that the undertow model provides an onshore directed steady current outside the breaking region which is reversed as breaking begins and dissipation increases. In the following section, the results for the GEBP model will be discussed to identify the mechanisms responsible for a change in slope

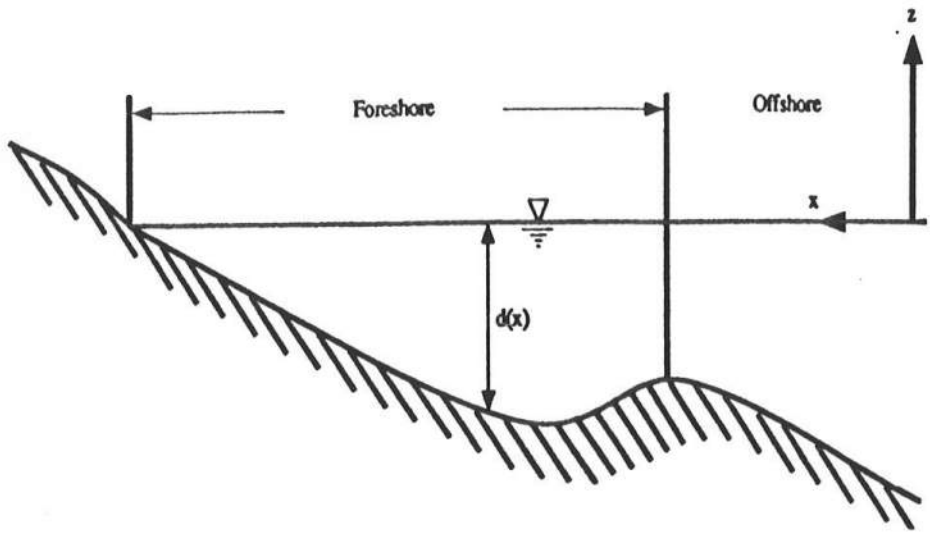


**Figure 5.1:** Definition Sketch for the GEBP Model Solution.

across the equilibrium beach profile. A set of input conditions has been selected which demonstrate a solution and emphasize the mechanisms responsible for a change in bottom slope.

### 5.2.1 Solution Characteristics

Solutions for the GEBP model are difficult to compare directly to measured laboratory data due to the lack of equilibrium profile experiments carried out with random waves. Therefore, no attempt will be made to quantitatively compare the results to data, and we will only make qualitative observations of the solutions. The resulting values for the velocity moments may be hypothesized as the values of these terms necessary for an equilibrium beach profile to exist. In this discussion, the *offshore* location is the portion of the solution offshore of the break in slope. The area between the break in slope and the shoreline is referred to as the *foreshore*. See the definition sketch in figure 5.1.

Input conditions for a relatively mild offshore wave steepness are selected for this discussion. These are based on average values recorded at the U.S. Army Corps

of Engineers Field Research Facility (CERC-FRF) in 1981, Miller *et al.* (1985). For this discussion, we modify the average values from the FRF measurements to obtain a solution that provides the best descriptive results for this discussion. The deep water $H_{rms}$ wave height, $H_{rmso}$, is taken to be 1.0 $m$, the peak period, $T_p$ is 10.0 $sec$ and the starting depth, $h_d$, is 20 $m$ and the sediment fall velocity, $w$, is approximated to be 0.03 $(m/s)$. (It is noted, that these values are well within the standard deviation of the averaged values and do represent occasional wave conditions at the FRF.)

In general, the GEBP model provides equilibrium solutions for the $H_{rms}$ wave height, the mean water level, $\overline{\eta}$, and the water depth, $d$. The equilibrium solutions are the result of the balance of the total velocity moments in the bottom slope equation (eqn. 3.28) necessary to maintain the no-net sediment transport condition. The total velocity moments are combinations of the wave-asymmetry-dependent central odd moments, $\langle\tilde{u}|\tilde{u}|^2\rangle$ and $\langle\tilde{u}|\tilde{u}|^2\rangle$, the wave field variance-dependent central even moments, $\langle|\tilde{u}|^3\rangle$ and $\langle|\tilde{u}|^5\rangle$, and the steady current, $\overline{u}$, across the nearshore region. These components vary in magnitude across the nearshore region which lend to variations in the bottom slope across the equilibrium beach.

The system of equations is strongly coupled through the $H_{rms}$ wave height, the mean water level, $\overline{\eta}$, and the water depth, $d$, and solutions depend on the response of the individual components of the total flow moments to changes in total depth and wave height. Therefore, as will be presented in the following discussion, the central moments and the steady current provide physically descriptive solutions for the respective flow field components, but variations in the relative magnitude of these terms are the results of the balance within the system to establish the no-net sediment transport condition. The solution for each of these equations and flow components will be discussed for the present input conditions.

Figure 5.2a shows the results for the $H_{rms}$ wave height across the equilibrium beach profile, where $x$ is positive onshore. As the waves shoal, the wave height first

increases in size, up to where most of the waves begin to break, and then the wave height decreases to zero where the mean water level is zero. Figure 5.2b shows the solution for the mean water surface, $\overline{\eta}$, across the equilibrium solution, where set-down is most pronounced as the waves shoal to their maximum height and set-up increases as wave breaking intensifies.

Figure 5.2c shows the equilibrium beach profile as a function of onshore distance. The point of interest is the change in slope in the equilibrium solution between $x = 200\ m$ and $x = 250\ m$ where the slope changes from a steep offshore slope before breaking to a milder foreshore slope after breaking has initiated. This is the result of a change in the direction from onshore to offshore of the steady current, $\overline{u}$, as wave breaking dissipation increases with the decrease in depth. In figure 5.3, the resulting mean flow across the surf zone changes direction at approximately $x = 200\ m$. As seen in eqn. 3.28, a change in the steady current, $\overline{u}$, is directly related to the bottom slope equation through the total odd velocity moments, and a decrease in magnitude or change in sign of $\overline{u}$ results in a decrease in bottom slope. Strictly speaking, the bottom slope is influenced by a balance of forces between the flow field and gravity. In the offshore region, the flow forcing is predominantly in the onshore direction where the mean wave-induced current and asymmetric flows are onshore. The combination of onshore flows works against the flattening effects of gravity to produce a steep bottom slope. As wave breaking begins and the mean return flow is established, the onshore flow forcing is reduced as the result of the offshore directed mean current opposing the asymmetric onshore flows and the slope becomes milder.

The switch in the direction of the mean flow is a result of the inclusion of the conduction solution streaming velocity in the bottom boundary layer. Where there is little breaking offshore, the streaming velocity is substantial enough to maintain onshore near-bottom mean flow. As the probability of wave breaking increases and the percent of waves breaking, $Q_b$, increases, (figure 5.4), the wave breaking induced dissipation establishes a mean return flow that changes the steady current from the onshore to the

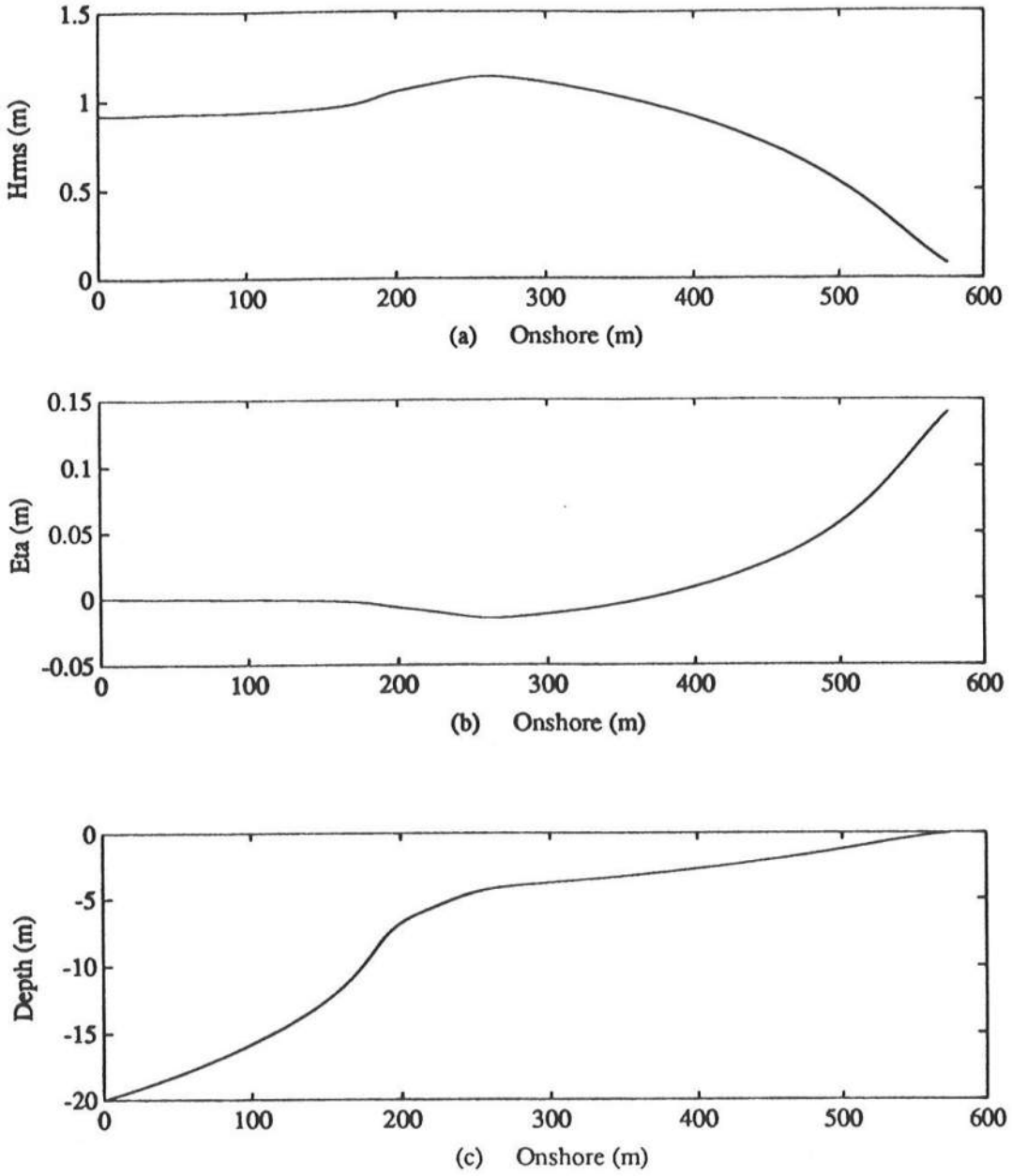


**Figure 5.2:** Equilibrium Beach Profile (a) $H_{\text{rms}}$, (b) $\overline{\eta}$, (c) $d$.

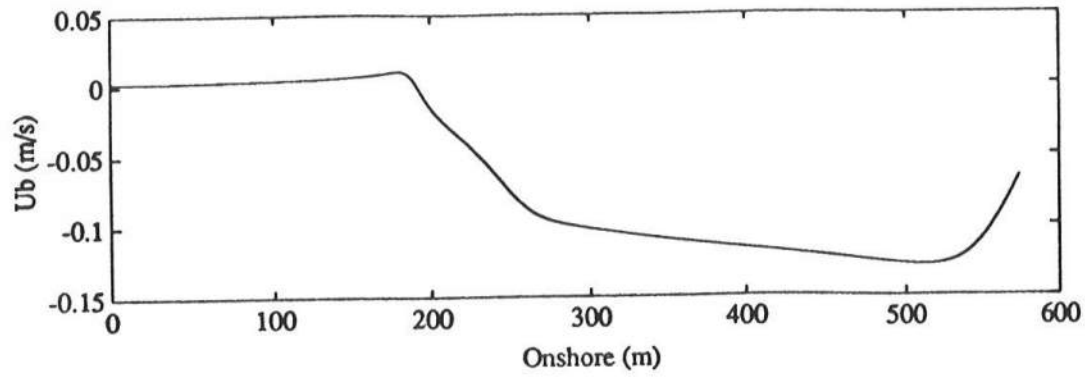


**Figure 5.3:** Steady Current, $\overline{u}$, Across an Equilibrium Beach Profile.

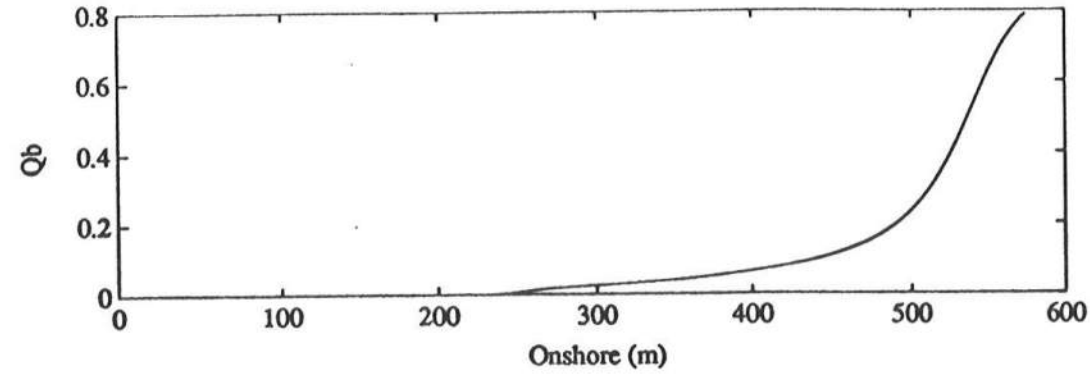


**Figure 5.4:** Percent Breaking Waves, $Q_b$, Across an Equilibrium Beach Profile.

offshore direction. The resulting change in slope due to the change in direction of the steady current, $\overline{u}$, can be defined as a longshore bar following the hypothesis of Dyhr-Neislen and Sorensen (1970), where a change in the direction of the bottom shear stress contributes to bar formation.

Figure 5.5a shows the total odd moments across the equilibrium profile. In the equilibrium state, the magnitude of the total odd moments, $\langle u|u|^2 \rangle$ and $\langle u|u|^3 \rangle$ in eqn. 3.28 is forced by the relative magnitude of the central moments and the steady current. As seen in figure 5.5a, the total odd moments are predominately positive across the entire surf zone. This is a result of the net balance of the flow forcing in the onshore direction. The balance is established through the combinations of the central odd and

even moments and the steady current where net onshore flows are required to balance the system and maintain a negative sloping bottom, reducing the depth from offshore to onshore.

As in the case of the plane slope, discussed in Section 4.3.3, the even moments (figure 5.5b) are positive for all values of wave height and water depth and contribute to the intensity of the net onshore flow. The magnitudes of the even moments are a function of local value of wave height, water depth, and wave period.

Figure 5.6 shows the central odd moments, which are the result of the asymmetric onshore flow of the nonlinear wave form in the nearshore region to maintain positive values across the entire surf zone. A qualitative comparison to figure 4.3, where the measured values of R&S for the central odd moments are presented, demonstrates the GEBP models ability to establish physically valid results for these terms across the equilibrium profile. However, the relative magnitudes of these terms in the GEBP model are governed by the balancing of the equilibrium solution between the suspended load and bedload and do not result in a order of magnitude difference between $\langle \tilde{u}|\tilde{u}|^2 \rangle$ and $\langle \tilde{u}|\tilde{u}|^3 \rangle$ as measured by R&S.

As an example of the balance between the suspended load and the bedload modes of transport, which is the governing condition in this system, the values for the bottom slope and total moments are back substituted into eqn. 3.17 and solved for the total load sediment transport across the surf zone. Figure 5.7 demonstrates the balance between the two modes of transport and provides a means to demonstrate the magnitude of the total velocity moments required to satisfy the no-net sediment transport condition across the surf zone. The change in direction between the bedload and suspended load components results from the response of the total velocity moments to the restriction of the no-net transport condition. When compared to figures 5.5a and 5.5b, the changes in direction of the sediment transport modes are related to abrupt changes of magnitude in the total velocity moments. However, the solution is not dependent on the specific

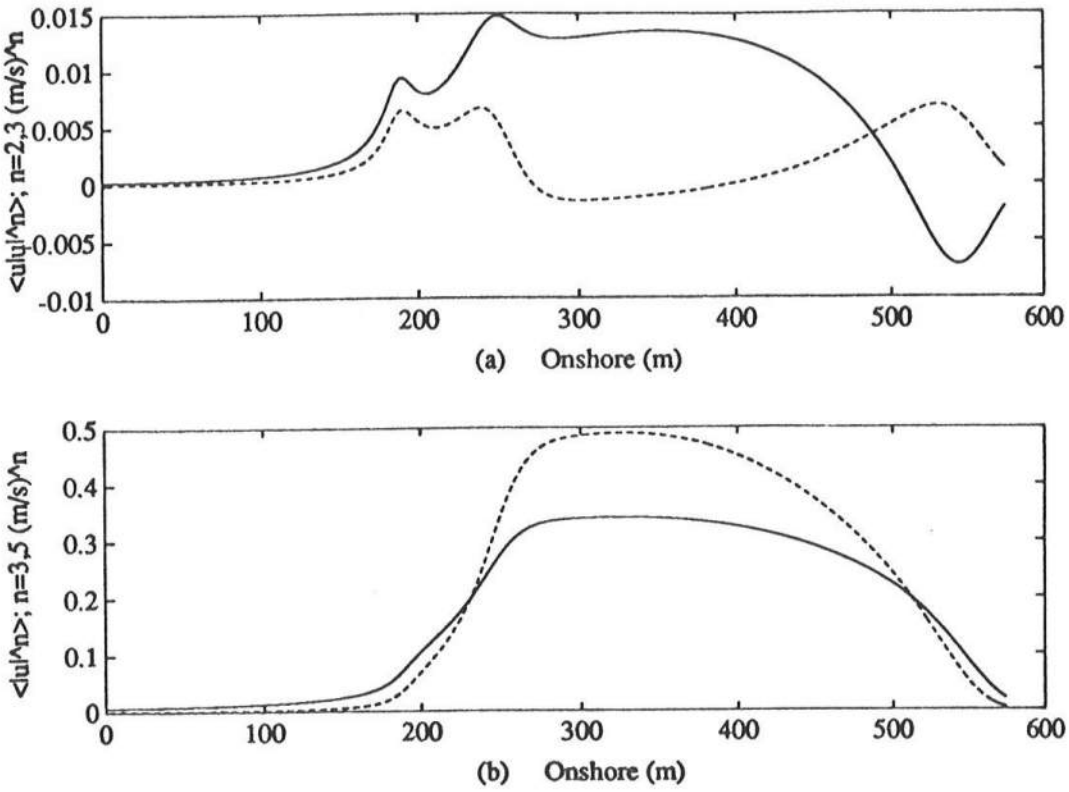


**Figure 5.5:** Total Moments Across an Equilibrium Beach Profile (a) Odd: $\langle u|u|^2 \rangle$ (solid), $\langle u|u|^3 \rangle$ (dashed), (b) Even: $\langle |u|^3 \rangle$ (solid), $\langle |u|^5 \rangle$ (dashed).

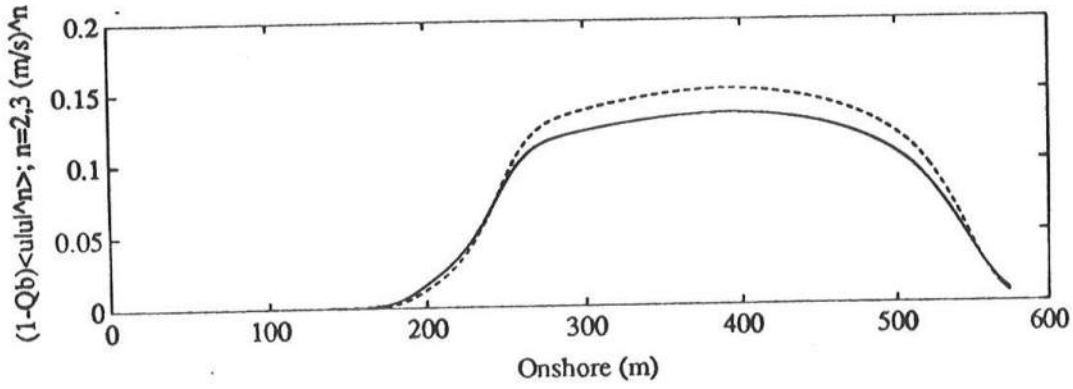


**Figure 5.6:** Central Odd Moments Across an Equilibrium Beach Profile: $\langle \tilde{u}|\tilde{u}|^2 \rangle$ (solid), $\langle \tilde{u}|\tilde{u}|^3 \rangle$ (dashed).

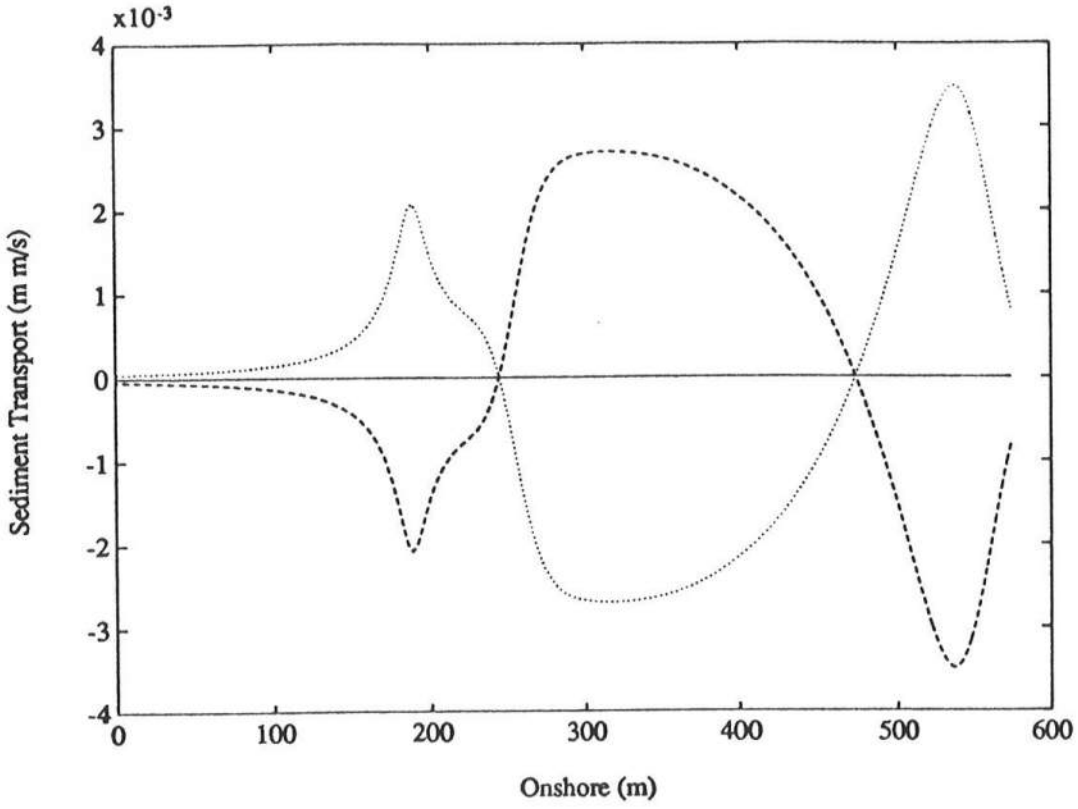


**Figure 5.7:** Sediment Balance Between the Bedload and Suspended Load: Total Load $Q_x$ (solid), Suspended Load $Q_{xb}$ (dashed), Bedload $Q_{xs}$ (dotted).

direction of each mode of transport as long as the balance between the modes results in no-net transport.

It has been shown that the bottom slope responds to changes in the wave height and, thus, total velocity moments to maintain the no-net sediment transport balance. For the present case, the combination of the total odd moments is positive across the entire surf zone. This result contradicts the values for the odd moments measured by R&S (figure 4.5), in that the results from their model provide negative total odd moments across the entire surf zone. This difference may be the result of the extreme erosional conditions imposed in their experiment, which produce strong offshore flows, and an equilibrium may not be obtained for their input conditions. This point will be addressed in a later section.

Additionally, the solutions obtained with this model are strictly dependent on the input. Because the scheme is a forward difference scheme, the solution at the previous $x$ location contributes to the solution at the next successive $x$ location.

### 5.2.2 Sensitivity Analysis

To understand the response of the model to changes in wave climate and sediment characteristics, a sensitivity analysis to variations in these wave parameters is made. Values for the $H_{\text{rms}}$ wave height, wave period, $T_p$, and sediment fall velocity, $w$, will be adjusted individually to determine relationships between these input parameters and the GEBP model solutions.

Additionally, beach response has been characterized by nondimensional relationships that relate combinations of wave and sediment characteristics to changes in the nearshore bathymetry. Specifically, Dean (1973) related the wave height, wave period, and sediment fall velocity with the nondimensional parameter,

$$D_o = \frac{H}{wT}, \tag{5.2}$$

known as the Dean number. Large wave periods (small Dean Number) lead to accretional beach conditions, and short period waves produce erosional conditions characterized by a breakpoint bar. Dalrymple (1992) developed the dimensionless profile parameter,

$$P = \frac{gH^2}{w^3T}, \tag{5.3}$$

based on large scale tank tests, which has been shown to predict the erosional and accretionary conditions for values above and below $P \sim 10{,}400$, respectively. These two nondimensional parameters and the deep water wave steepness, $s_o$, (steeper waves

**Table 5.1:** Input - GEBP Model Sensitivity Analysis

| $CaseNo.$ | $H_{rmso}$ $(m)$ | $T_p$ $(sec)$ | $s_o$ | $\gamma$ | $h_d$ $(m)$ | $w$ $(m/s)$ | $D_o$ | $P$ |
|---|---|---|---|---|---|---|---|---|
| 1 | 0.123 | 3.25 | 0.00746 | 0.596 | 3.00 | 0.01 | 3.78 | 45670 |
| 2 | 0.133 | 3.50 | 0.00695 | 0.590 | 3.00 | 0.01 | 3.80 | 49580 |
| 3 | 0.123 | 3.50 | 0.00643 | 0.584 | 3.00 | 0.01 | 3.51 | 42400 |
| 4 | 0.113 | 3.50 | 0.00591 | 0.577 | 3.00 | 0.01 | 3.22 | 35790 |
| 5 | 0.123 | 3.75 | 0.00561 | 0.573 | 3.00 | 0.01 | 3.28 | 39580 |
| 6 | 0.123 | 3.50 | 0.00643 | 0.584 | 3.00 | 0.005 | 7.02 | 339000 |
| 7 | 0.123 | 3.50 | 0.00643 | 0.584 | 3.00 | 0.015 | 2.34 | 12560 |

erode the beach and milder waves build the beach) have been related to trends in beach shape. Therefore, they will be calculated to determine if the results from the GEBP model exhibit trends predicted with these parameters.

Values selected for the sensitivity analysis (table 5.1) are based on numerous trials to determine the range of validity where the GEBP is most effective. The GEBP works best for mild accretionary wave parameters, where the offshore wave steepness is between $O(10^{-4})$ for accretionary profiles and $O(10^{-2})$ for erosional profiles. The values chosen as input are combinations of $H_{\rm rms}$ wave height, wave period, $T_p$, and sediment fall velocity, $w$, to determine the sensitivity for a broad range of initial conditions. These input conditions are similar to the range of input conditions specified in the work of R&S, used for comparison in the next section. Trends from the variations in wave height, wave period and sediment fall velocity will be presented and compared to the related nondimensional parameters. The values for $\gamma$, which is an adjustable parameter of the time-averaged wave energy dissipation $D$, are given as an indication of variations in the characteristics of the breaking model.

Figure 5.8 shows the relationship between changes in incident offshore wave

height and the location and shape of the longshore bar. For the largest wave height, Case 2, the longshore bar assumes a position farther offshore and in deeper water, compared to the two solutions resulting from the smaller wave heights in Cases 3 and 4. The offshore bar from the larger wave height, Case 2, is in deeper water, as a result of the increased probability of wave breaking at a greater depth for larger wave heights. The increased wave height strengthens the onshore flow from the steady streaming, and the bottom slope increases. As a result, the offshore depth approaches shallow water more quickly than the cases for smaller wave heights. However, as the waves begin to break, the intensity of wave breaking is approximately the same for Case 2, 3 and 4 (figure 5.9), but, because the larger wave, Case 2, requires a greater amount of energy dissipation, the foreshore region becomes broader and the slope milder. Solutions for large waves develop a steep offshore slope and a mild foreshore slope and small waves attribute to a mild offshore slope and a steep foreshore slope.

Figure 5.10 shows the relationship between changes in the peak frequency of the wave field and the location and depth of the longshore bar. The lower frequency wave field, with longer waves, develops a steeper overall solution across the profile. This is the result of a strong dependence of wave asymmetry, and the central odd velocity moments on wave length. Longer waves develop the characteristic vertical asymmetric shape in deeper water than shorter waves, which contributes more strongly to the central odd velocity moments across the nearshore region and results in an increased onshore flow forcing. For the longer period waves, Case 5, the offshore slope is steeper as a result of an increase in the onshore forcing from central odd moments. As the waves begin to break, the relative magnitude between the central odd moments and the combination of the mean return flow and the central even moments result in an increased net onshore forcing, thus creating a steeper foreshore. The relative magnitude between the central odd moments and the combination of the mean return flow and the even moments is defined as the total odd moments, $\langle u|u|^2 \rangle$ and $\langle u|u|^3 \rangle$, Section 3.1.2. As the wave length is shortened, Cases 1 and 3, the total odd moments become smaller compared to those for the longer waves, Case 5 (figures 5.11 and 5.12), and create a stronger net onshore

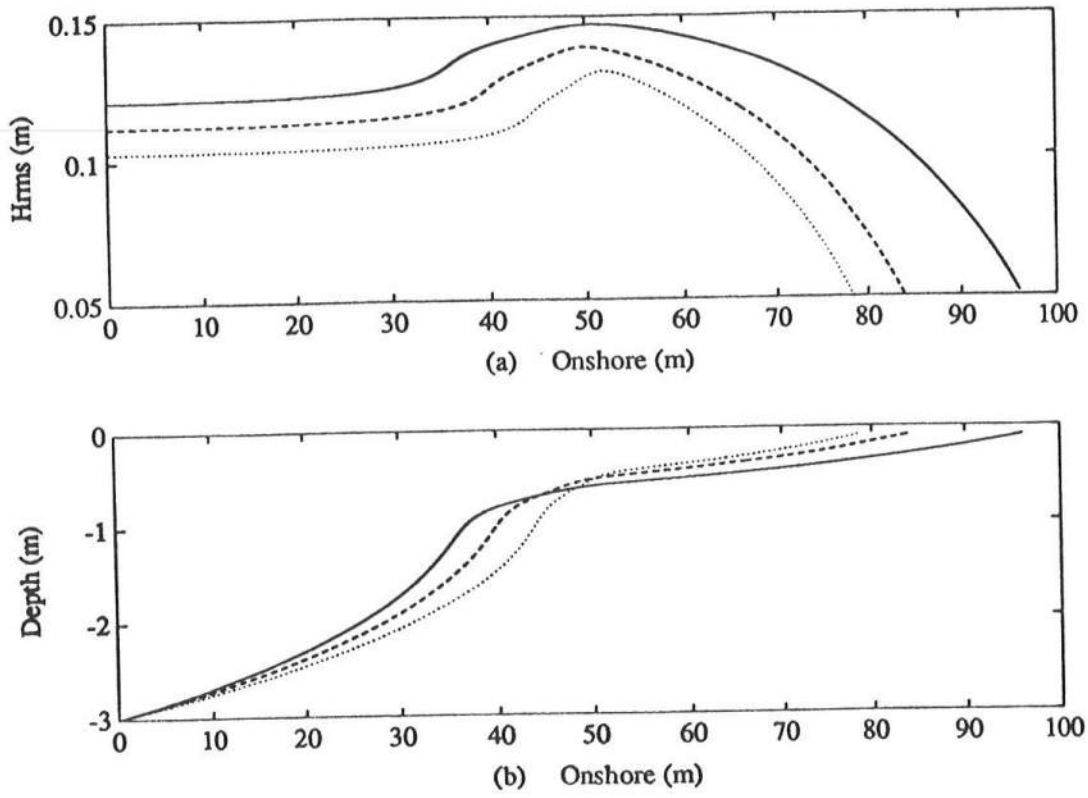


**Figure 5.8:** Sensitivity of GEBP Model to Changes in Offshore Wave Height (a) $H_{\text{rms}}$, (b) $d$: Case 2 (solid), Case 3 (dashed), Case 4 (dotted).

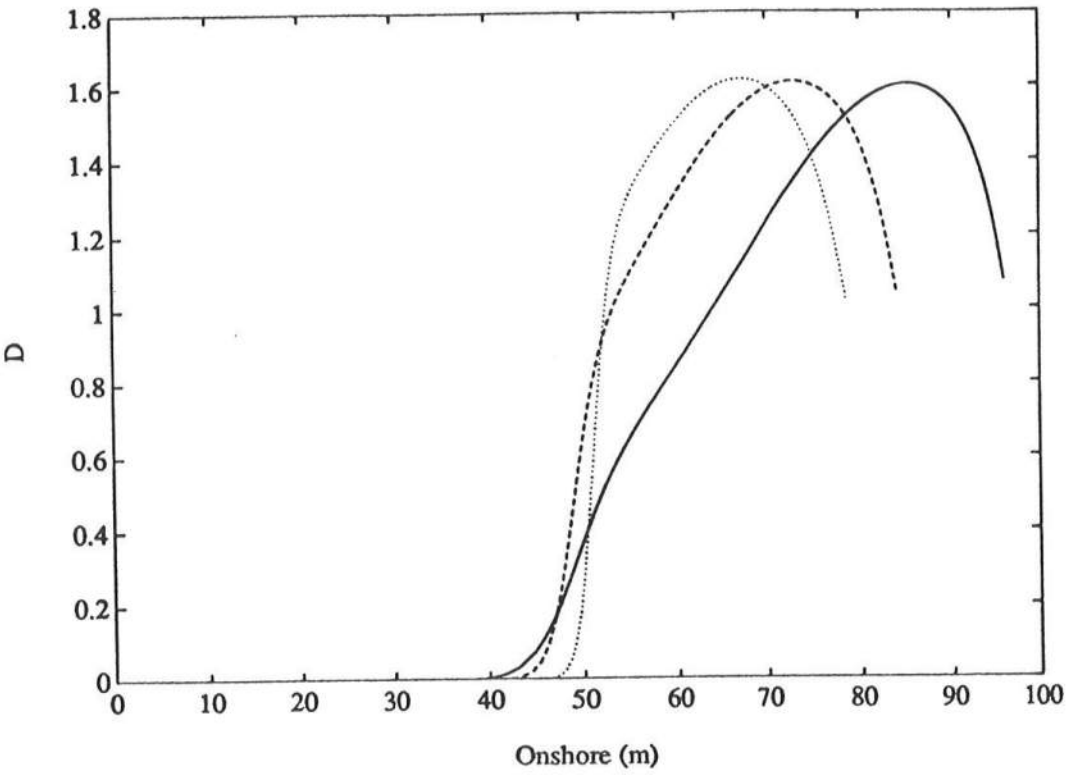


**Figure 5.9:** Sensitivity of Disspation $D$ to Changes to Variations in Offshore Wave Height: Case 2 (solid), Case 3 (dashed), Case 4 (dotted).

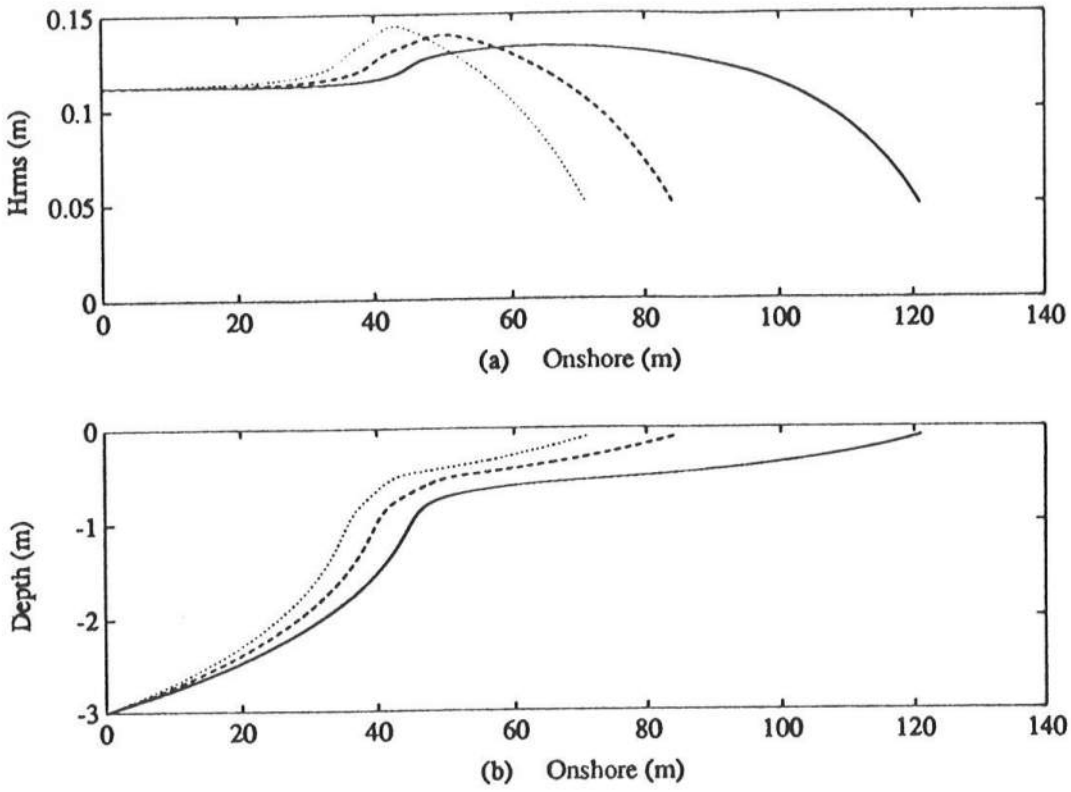


**Figure 5.10:** Sensitivity of GEBP Model to Changes in Peak Frequency (a) $H_{rms}$, (b) $d$: Case 1 (solid), Case 3 (dashed), Case 5 (dotted).

flow, forcing a milder bottom slope across the foreshore. Bar depth is also dependent on wave length. Solutions for the longer period waves, Case 5, establish the bar formation in relatively shallow water, yet the shorter period waves, Cases 1 and 3, which begin breaking at a deeper depth, force the bar to a deeper location. Because of the sensitivity of the central odd moments to wave period, the response of this model is strongly related to variations in wave period.

In a qualitative sense, the trends of the model's response to changes in wave climate have been shown to be strongly related to wave period and to a lesser degree to wave height. Additionally, figure 5.13 shows the model's response to changes in sediment fall velocity. Variations in sediment fall velocity do not greatly change the results of the GEBP model. For variations in wave height and wave period, when significant changes

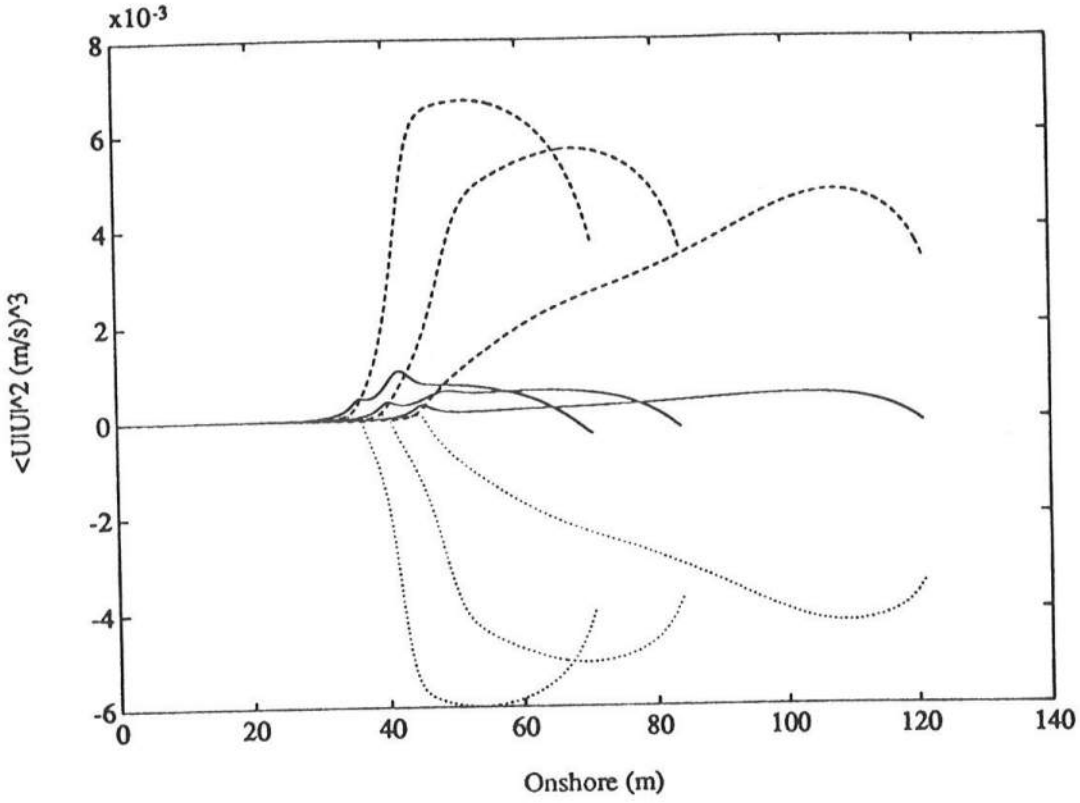


**Figure 5.11:** Sensitivity of Total Odd Moments to Changes in Peak Frequency: Total Odd Moment (solid), Central Odd Moments (dashed), Mean Return Flow (dotted): Case 1 (right), Case 3 (middle), Case 5 (left).

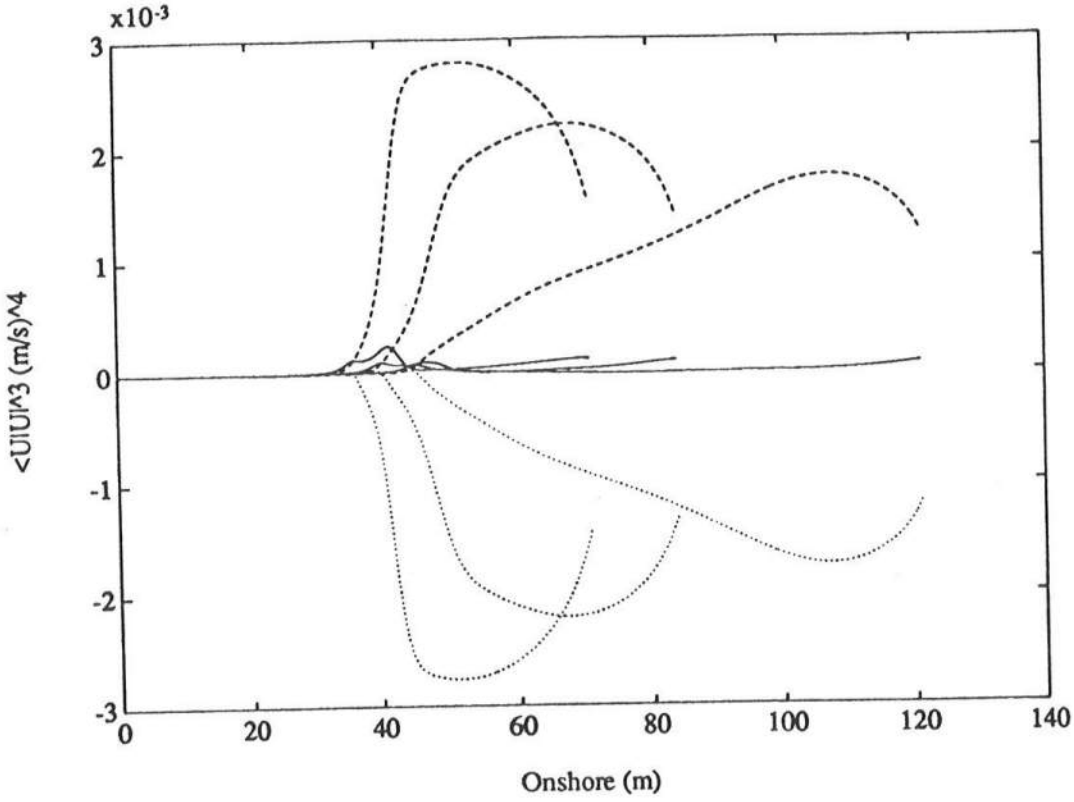


**Figure 5.12:** Sensitivity of Total Odd Moments to Changes in Peak Frequency: Total Odd Moment (solid), Central Odd Moments (dashed), Mean Return Flow (dotted): Case 1 (right), Case 3 (middle), Case 5 (left).

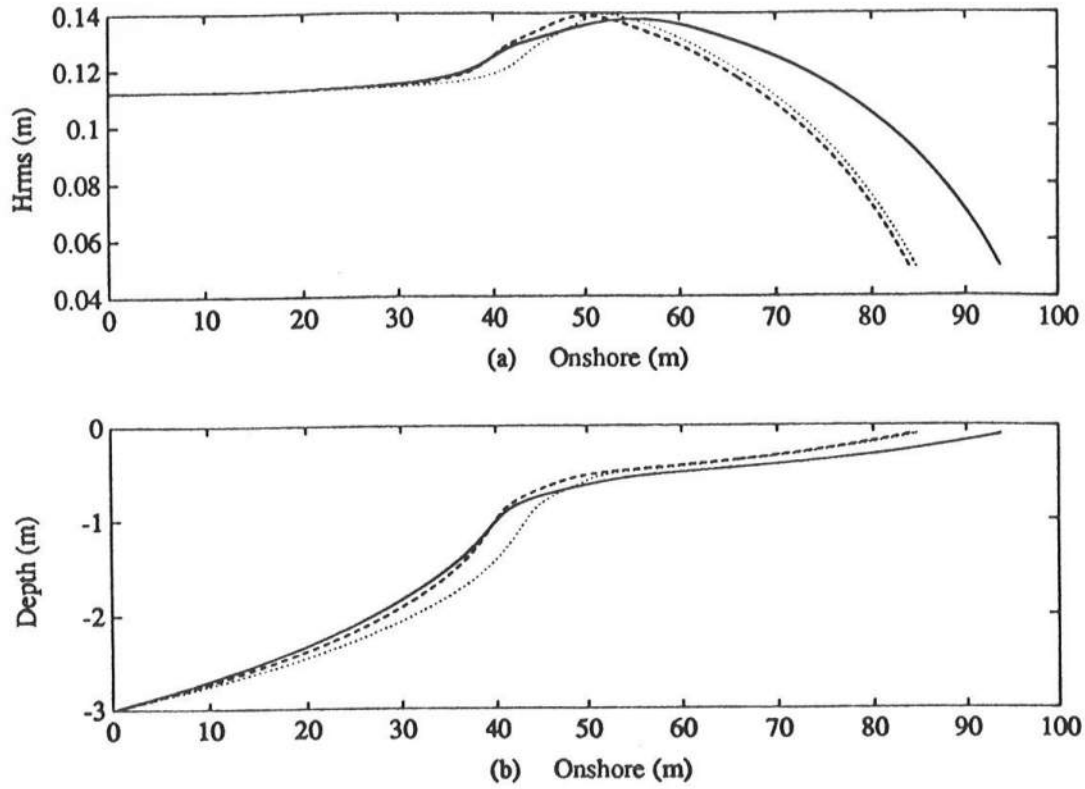


**Figure 5.13:** Sensitivity of GEBP Model to Changes in Sediment Fall Velocity (a) $H_{\text{rms}}$, (b) $d$: Case 6 (solid), Case 3 (dashed), Case 7 (dotted).

in the GEBP model solutions are recognized, the Dean number and P-parameter do not greatly differ. However, as indicated by large variations in the Dean Number and P-parameter, Cases 3, 6 and 7, the change in beach profile shape is expected to be significant. This demonstrates the strong dependency of the sediment transport model to wave period and and wave height as compared to the sediment fall velocity.

Relating the values of the Dean number, P-parameter and deep water wave steepness to variations of the solutions for Cases 1-5, it is seen (figure 5.14) that the state of the foreshore slope can be predicted as a function of the deep water wave steepness, where a mild slope corresponds to the erosive conditions of large wave steepness. However, the offshore slope and shape is individually related to variations in wave height and wave period (figure 5.14), and is not predictable from the Dean number, P-parameter

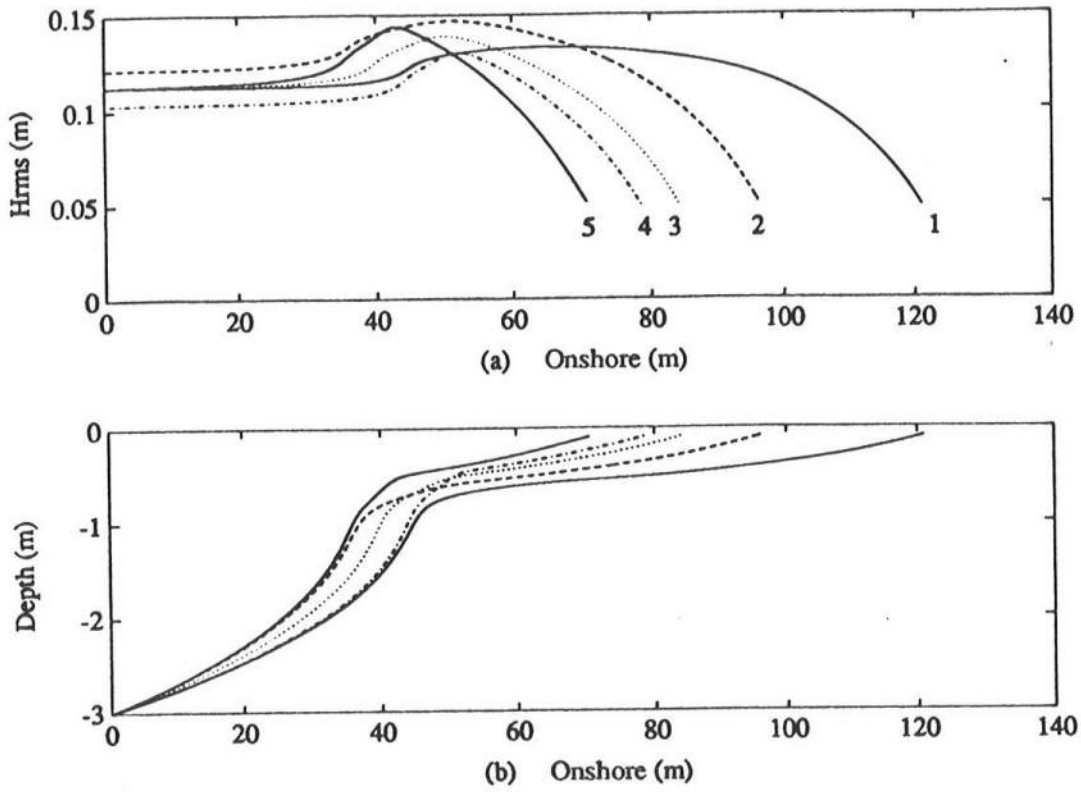


**Figure 5.14:** Sensitivity of GEBP Model to Changes in Offshore Wave Steepness (a) $H_{rms}$, (b) $d$.

and deep water wave steepness. The reason for this is in the response of the central velocity flow moments and the mean current model to changes in wave characteristics. A trend for the shape and location of the offshore bar with variations in deep water wave steepness, Dean number, or P-parameter does not exist as as seen in table 5.1 and figure 5.14. Thus, as the GEBP model is defined, solutions are unique for specific combinations Dean number, P-parameter and deep water wave steepness, but variations in solutions cannot be predicted with variations in in these parameters. Only changes in foreshore slope may by characterized by variations in deep water wave steepness.

The results from this sensitivity analysis agree with the observations of Dally (1987). Dally recognized that longer period waves, and thus milder wave steepness, produced bar formations in shallow water and thus closer to the shoreline, and the

shorter period waves move the location of the bar to deeper water and further offshore.

## 5.3 Comparison to Roelvink and Stive (1989)

To validate the model against actual wave conditions and beach profile data, comparisons to the results of R&S will be addressed. Because the GEBP is based on the flow moments proposed and calibrated by the work of R&S, an attempt will be made to determine why their model never reached an equilibrium condition.

As stated in Chapter 4, R&S intended to simulate strongly erosive conditions with emphasis on generating longshore bar formations from an initially plane beach. Thus, the input conditions they used provided a large offshore wave steepness (Case 1, table 4.1). Under these conditions, their experimental profile and numerical model never reached an equilibrium condition.

Implementing the GEBP model under the extreme wave conditions used by R&S does not converge to a physically reasonable solution (figure 5.15). The result can be described as an infinitely wide beach. Our reasoning for this solution draws on the previous argument that as wave steepness increases, the contributions for the odd velocity moments (the dominate onshore forcing mechanism in this model) is reduced to values too small to balance the forcing for the mean return flow and thus an infinite flat beach results. This is a physically unreasonable result, but demonstrates the ability of this type of model to predict the equilibrium beach profile if one were to exist, under storm conditions. However, to emphasize this point and to demonstrate the model's limits to extreme wave steepness, we arbitrarily increase the wave length and thus the contribution from the central odd moments. This is Case 2 of table 5.2, where the value for $s_o$ is 0.0083 is a order of magnitude smaller than the value in the R&S experiments and will be shown to be an approximate upper limit of this model as an input offshore wave steepness. Figure 5.16 shows the solution for these input conditions. The model converged to a solution, but the width of the foreshore region is unrealistically wide.

**Table 5.2:** Input - Roelvink and Stive (1989) Data Comparison

| Case No. | $H_{rmsd}$ $(m)$ | $T_p$ $(sec)$ | $h_d$ $(m)$ | $s_o$ | $\gamma$ |
|---|---|---|---|---|---|
| 1 | 0.123 | 2.00 | 3.00 | 0.0210 | 0.73 |
| 2 | 0.123 | 3.00 | 3.00 | 0.0083 | 0.61 |

This proves two points; (1) this model does not predict equilibrium beach profiles for extreme wave conditions under the inherent assumptions, and (2) physical mechanisms important to changes in the beach profile during storm events are likely not to be included in the model.

This exercise brings to light two interesting questions: (1) For a given set of offshore wave conditions, is there always an equilibrium profile? The GEBP predicts that for an extreme offshore wave steepness, the equilibrium beach solution exists as an infinitely wide foreshore for which the bottom is flat and the waves propagate without dissipation. (2) Is there a value for offshore wave steepness that is the determining quantity of whether or not a beach can establish an equilibrium condition. From this brief investigation, the limit of deep water wave steepness to obtain an equilibrium is $O(10^{-2})$ under the assumptions of this model. We accept the limits of this model in that the physics describing the sediment transport are not accurately quantified across the entire nearshore region and that the model neglects many of the nearshore forcing mechanisms present in the nearshore environment.

## 5.4 Comparison to FRF Data

A beach profile existing in pure equilibrium on a real shoreline may never be observed as defined by the assumptions of the GEBP model. Only in controlled experimental conditions can a beach be subject to constant a wave field for an indefinite

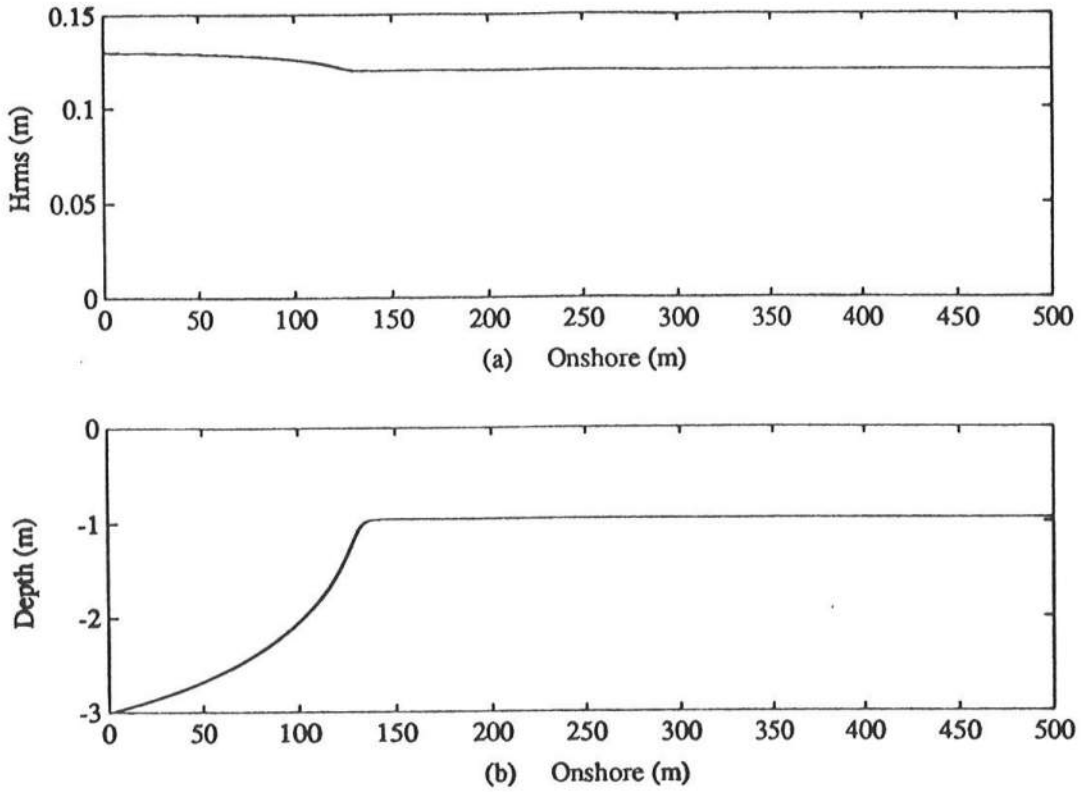


**Figure 5.15:** GEBP solution for *actual* input conditions of Roelvink and Stive (1989), (a) $H_{\text{rms}}$, (b) $d$: Case 1.

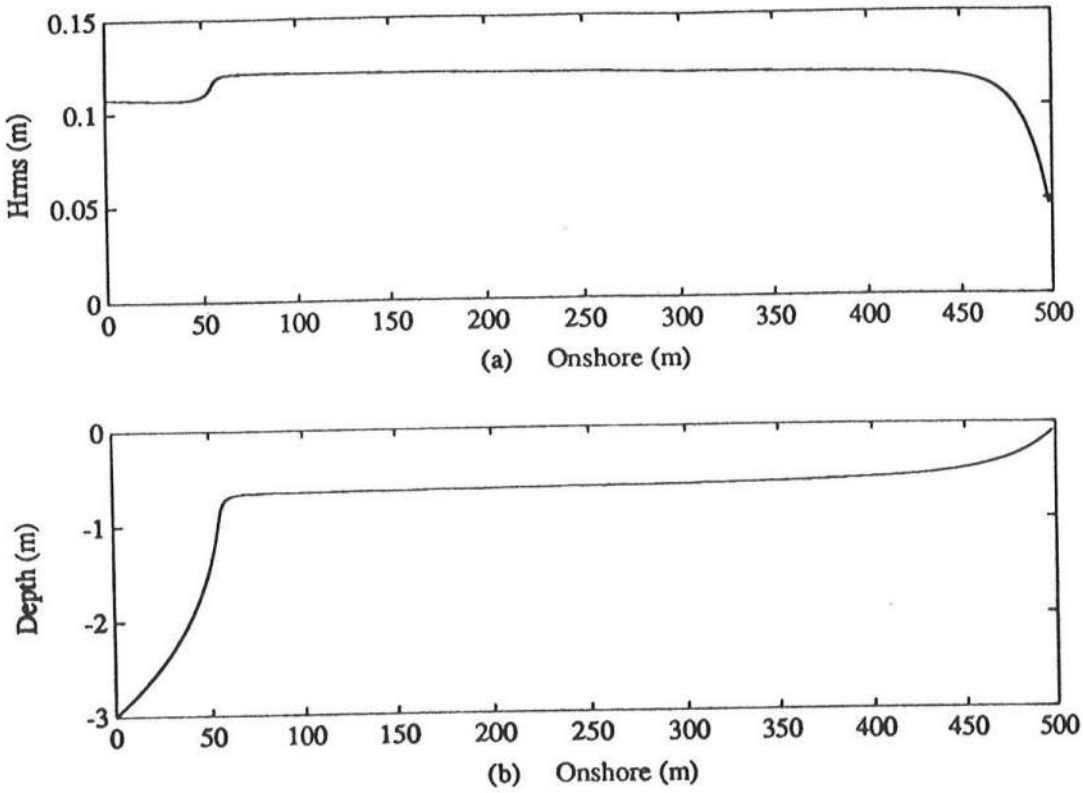


**Figure 5.16:** GEBP solution for *modified* input conditions of Roelvink and Stive (1989), (a) $H_{\text{rms}}$, (b) $d$: Case 2.

period of time. However, a profile averaged over a long period of time, may be assumed to exhibit the features of an equilibrium profile. To this end, we use data from the Corps of Engineers Field Research Facility, which provides accurate measurements of the time varying wave conditions and nearshore bathymetry. We have chosen the data collected at the facility during the years 1981 to 1984, Howd and Birkemeier (1987), as our representative sample. Measurements along profile line 58 have been selected to represent the nearshore variations at the FRF.

To analyze the average shape of profile line 58, the Empirical Orthogonal Eigenfunction method (EOF) of Winant *et al.* (1978) is applied, which describes the time dependent profile change with a measure of the mean squared variance of the cross-shore depth. This method describes variations in the data with combinations of orthogonal eigenfunctions, where the the first eigenfunction represents the largest amount of variation in the data and the remaining variation is describe with the successive eigenfunctions. The largest amount of variance, approximately 98%, resulting from the time dependent profile measurements, is represented with first eigenfunction which has been defined as the *mean* beach function. Ninety-one profiles measured between 1981 and 1984 are use in the analysis. Profiles that are not measured to the depth of closure or are taken during extreme storm events are remove as not to bias the data to a larger than average longshore bar.

The average profile from the data set is of particular interest due to the presence of a longshore bar at $x = 400\ (m)$. Assuming this to be the equilibrium beach profile and adopting the mean nearshore wave height and peak wave period during the four years, the equilibrium beach profile will be calculated.

The wave characteristics at the FRF, which are measured at the end of the research pier in 4 meters of water, are tabulated as average values. Therefore, as a result of the GEBP requiring the $H_{\text{rms}}$ wave height, the wave field is assumed to be represented by a Rayleigh distribution and the statistical relationship between the mean

**Table 5.3:** Wave Data - CERC-FRF (1981): Case 1 (measured); Case 2 (adjusted)

| | $H_{mean}$ $(m)$ | *Std.Dev.* $H_{mean}$ $(m)$ | $T_p$ $(sec)$ | *Std.Dev.* $T_p$ $(sec)$ | $H_{rmso}$ $(m)$ | $T_p$ $(sec)$ | $s_o$ |
|---|---|---|---|---|---|---|---|
| Case 1 | 0.9 | 0.6 | 8.7 | 2.9 | 1.02 | 8.7 | 0.0079 |
| Case 2 | | | | | 1.02 | 10.0 | 0.0056 |

wave height, $H_{mean}$ and the $H_{rms}$ is

$$H_{rms} = 1.128 H_{mean} \tag{5.4}$$

The peak wave period is taken as the reported value at the FRF, the sediment fall velocity is estimated to be 0.03 $(m/s)$ and the initial depth is 20 $m$. The offshore wave conditions are determined from the measure values at 4 meters following the linear shoaling approach presented earlier in this chapter. The wave parameters are presented in table 5.3 along with the adjusted wave period that provide a better fit to the data. Figure 5.17 shows the representation of the GEBP, given the measured values at the FRF, superimposed onto the first eigenfunction from profile line 58. The agreement is unsatisfactory in a quantitative sense, but trends in the shape of the cross shore are represented in a qualitative sense as indicated by a deep offshore bar in the data and a broad foreshore region.

Optimizing the sediment transport efficiency factors, $\epsilon_b$ and $\epsilon_s$, by a best fit procedure across the profile may provide suitable results in replicating barred equilibrium beach profiles. However, due to the complexity of the GEBP model and the computational time required for solution, the problem becomes increasingly difficult. To this end, adjustment of the offshore wave parameters within the range of the standard deviation of the measurements is accepted for a qualitative comparison to the data. A

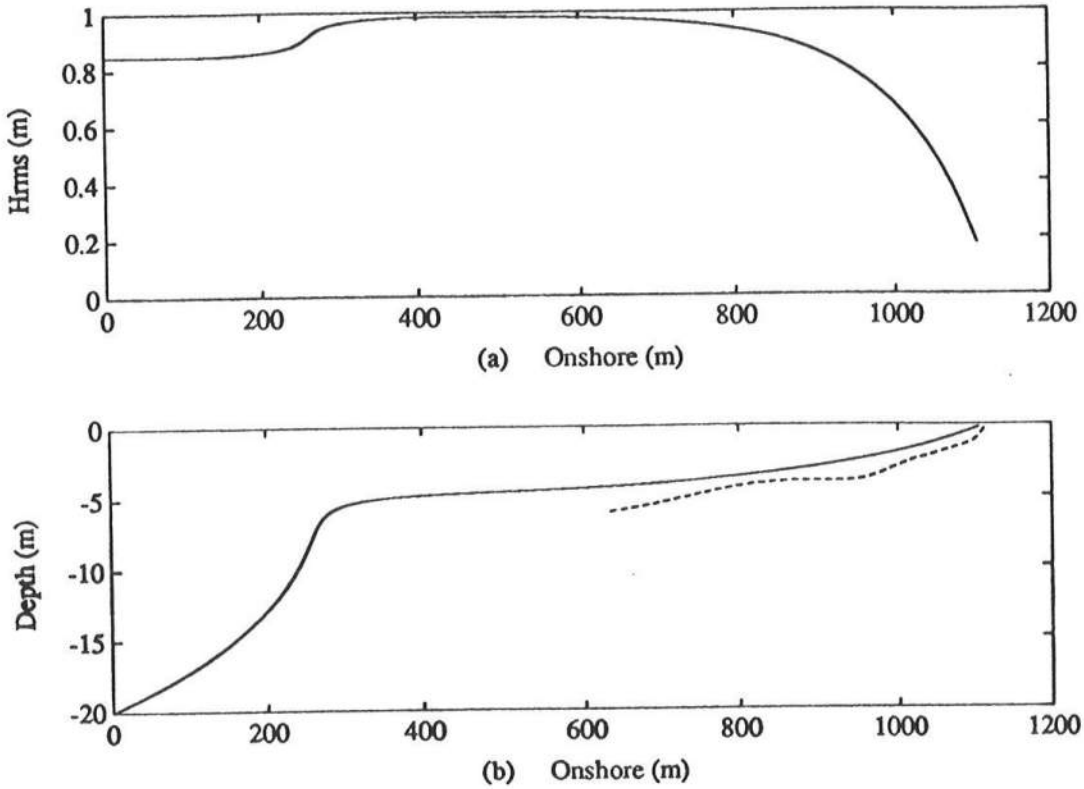


**Figure 5.17:** GEBP (solid) and First Eigenfunction (dashed) FRF (1981-1984): Case 1.

beach profiles. However, due to the complexity of the GEBP model and the computational time required for solution, the problem becomes increasingly difficult. To this end, adjustment of the offshore wave parameters within the range of the standard deviation of the measurements is accepted for a qualitative comparison to the data. A methodology for adjusting the offshore waves conditions to match the nearshore beach profile data is not established and may not be useful in terms of developing a better quantitative estimation of the profiles. However, the wave height and wave period will be adjusted to determine in a approximate representation of the data is obtainable with reasonable variations of the wave parameters.

Figure (5.18) presents the results for the first eigenfunction as the representative profile where the results from the GEBP model from the adjusted wave parameters are superimposed. The agreement is qualitatively promising in that the location and depth of the outer longshore bar is predicted reasonably well as well as the approximate average slope of the for shore region. The depth and location of the outer bar is location and depth that would be influence by waves present during extreme storm events and not by the average wave conditions. Thus the adjusted values do not seem to be unreasonable for the prediction of the outer bar.

A problem with the GEBP model is the predicted extreme offshore bottom slope that is not found in the FRF field data. As seen in the earlier discussions, this is a feature of the model that is not unique to this set of input conditions, but, rather, is consistent for all case of the model that have been examined. Possible sources for this feature could be that Bailard's sediment transport model is not valid in the offshore region where bottom ripples and low suspended load concentrations exist. Further, the strong onshore flow, which has been shown to steepen the beach slope, established by the GEBP model outside the surf zone, may be an overestimation of the actual onshore flow that exists over the offshore region of an equilibrium beach profile.

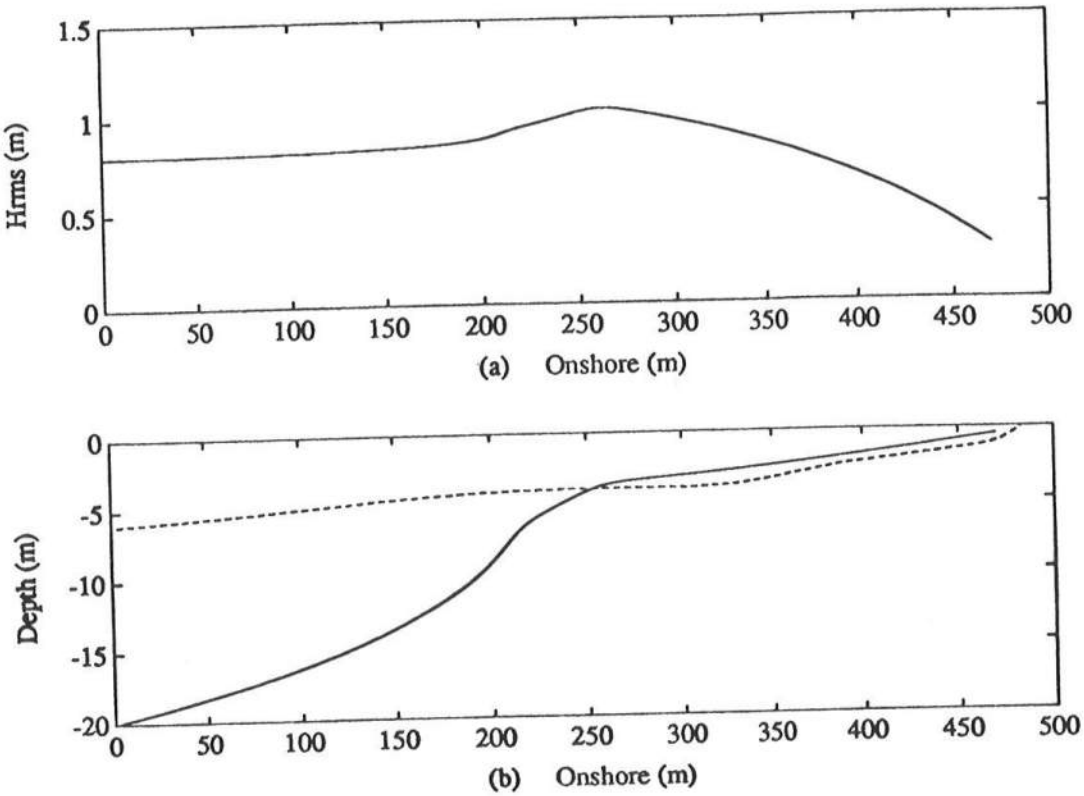


**Figure 5.18:** GEBP (solid) and First Eigenfunction (dashed) FRF (1981-1984): Case 2.

# Chapter 6

# CONCLUSIONS

Establishing a quantitative method for accurately describing the equilibrium state of a beach profile is a necessary tool for coastal engineers in developing accurate general descriptions of the nearshore bathymetry. Certain models may quantify the stable cross-shore shape, but these models require empirical calibration of at least one adjustable parameter to account for the many uncertainties in the problem. Additionally, although longshore bars exist in many measured beach profiles assumed to be in an equilibrium state, the existing quantitative models fail to describe this feature. This thesis considers the physics of the nearshore region in more detail by utilizing well established models that quantify the mechanics of the nearshore wave, current, and sediment transport characteristics.

The approach in this thesis adopts the energy and momentum equations and a bottom slope equation, which is established by imposing a no-net sediment transport condition on Bailard's (1982) instantaneous energetics cross-shore sediment transport formulation, as the governing equations of the nearshore environment. Bailard's sediment transport equation has been used to model satisfactorily time dependent cross-shore sediment transport processes when models for the nearshore hydrodynamics are applied for time-averaged near-bottom flows, R&S. However, an equilibrium solution has not been obtained with such models.

Adopting the proposed models of R&S for the nearshore hydrodynamics, which are approximate representations of the velocity moment terms required by Bailard's

sediment transport equation, an equilibrium beach profile solution is achieved that is dependent on the flow variations across the nearshore region. Assuming the wave field to be a linear Gaussian process and the wave heights to be represented by the Rayleigh distribution, the asymmetric flow contributions from unbroken wave field are modelled with vertically symmetric waves according to Dean's Stream Function theory (1965). The random variation of the wave field is modelled following the even moment approximations of Guza and Thornton (1985), and the steady current resulting from the steady streaming under nonlinear waves and the momentum decay induced return flow are modelled following Stive and De Vriend (1987).

The model establishes an offshore break point bar at a location that agrees qualitatively with the observations of Dally (1987) and R&S, who experimentally developed longshore bars with an emphasised undertow mechanism. The establishment of the longshore bar is directly related to the change in direction of the steady current from onshore flow offshore of the bar to offshore flow shoreward of the bar. However, the model is sensitive to the value of offshore wave steepness and produces an infinite beach solution for extreme values of offshore wave steepness. The infinite beach solution may result from an imbalance of the flow forcing terms that establish excessive net offshore flows when wave steepness exceeds $O(10^{-1})$. For cases of relatively mild offshore wave conditions, the model produces the qualitative trends of longshore bar response to variations in offshore wave climate. For constant wave length and varying wave height, the longshore bar is established farther offshore and in deeper water for large wave heights, while smaller wave heights create nearshore, shallow water bars. For example, constant wave height and variations in period, the longer period waves create a nearshore bar and the shorter period waves move the bar offshore. These trends support observations in laboratory experiments (*i.e.*, Dally 1987, Kraus and Larson 1988). Trends in the solutions are not related the Dean number, P-parameter, or deep water wave steepness across entire profile, but, rather, to individual variations in wave height and wave period. However, the variation in steepness of the foreshore is related to variations in the offshore wave steepness, where steeper waves create a milder foreshore slope. The

apparent poor response to prediction outside the bar location could be the result of the bottom slope model's response to variations in wave height and wave period under the no-net sediment transport condition.

The system of equations has been difficult to model due to the strong sensitivity of the solutions to offshore wave steepness. For extreme wave steepness, the infinite beach solution is obtained, where low wave steepness provides for excessively steep offshore solutions. Further, because the system is established as an initial value problem, each successive step is dependent on the previous one to maintain the no-net sediment transport condition, and the system lacks flexibility in predicting detail descriptions of the nearshore bathymetry, such as a trough on the shore side of the bar.

Despite the inherent problems associated with this model, a more descriptive method to model equilibrium beach profiles has been developed. By considering the spatially varying sediment transport characteristics of the nearshore region and by developing better models to represent the waves and currents, a better description of the equilibrium beach profile may be achieved. The results of this model may be improved with calibration of the adjustable parameters, $\epsilon_b$ and $\epsilon_s$ in the bottom slope equation, with a fit to measured equilibrium beach profile data.

# BIBLIOGRAPHY


Bagnold, R.A., Mechanics of marine sedimentation; *The Sea*, M.N. Hill, ed.; Interscience, Vol. 3, pp. 507-528, 1963.

Bagnold, R.A., An approach to the sediment transport problem from general physics, *U. S. Geol. Surv. Prof. Pap., 422-I*, 1966.

Bailard, J.A., An energetics total load sediment transport model for a plane sloping beach, *J. Geophys. Res.*, 86, pp. 10,938-10,954, 1981.

Bailard, J.A., Modelling on-offshore sediment transport in the surf zone, in *Proceedings of the 18th International Conference on Coastal Engineering*, pp. 1419-1438, American Society of Civil Engineers, New York, 1982.

Bailard, J.A. and D. L. Inman, An energetics bedload load sediment transport model for a plane sloping beach; Local transport, *J. Geophys. Res.*, 86, pp. 2035-2043, 1981.

Bailard, J.A., Surf zone wave velocity moments, in *Procceedings of Special Conference on Coastal Hydrodynamics*, pp. 328-342, American Society of Civil Engineers, New York, 1987.

Battjes, J.A. and M. J. F. Stive, Calibration and verification of a dissipation model for random breaking waves, *J. Geophys. Res.*, 90, pp. 9159-9167, 1985.

Battjes, J.A. and J.P.F.M. Janssen, Energy loss and set-up due to breaking of random wave, in *Proceedings of the 16th International Conference on Coastal Engineering*, American Society of Civil Engineers, New York, 1978.

Bodge K.R., Representing Equilibrium beach profiles with an exponential expression, *Journal of Coastal Research*, 8(1), pp. 47-55, 1992.

Börecki, O.S., Distribution of wave induced momentum fluxes over depth and application within the surf zone, *Doctoral dissertation*, Department of Civil Engineering, University of Delaware, 1982.

Bowen A.J., Simple models of nearshore sedimentation: beach profiles and longshore bars, in *The Coastline of Canada*, edited by S. B. McCann, pp. 1-11, Geological Survey of Canada, Ottawa, 1980.

Bruun, P., Sea level rise as a cause of shore erosion, *Beach Erosion Board, Tech. Memo. 44*, U.S. Army Corps of Engineers, 1954.

Dally, W.R., Longshore bar formation - Surf beat or undertow?, in *Proceedings of Special Conference on Coastal Sediments*, pp. 71-86, American Society of Civil Engineers, New York, 1987.

Dally, W.R., A numerical model for beach profile evolution, M.Sc. thesis, Department of Civil Engineering, University of Delaware, Newark, 1980.

Dally, W.R., R.G. Dean, and R.A. Dalrymple, Wave height variation across beaches of arbitrary profile, *J. Geophys. Res.*, 90, No. 6, pp. 2035-2043, 1985.

Dalrymple, R.A., Personal communication, 1992.

Dalrymple, R.A., A finite amplitude wave on a linear shear current, *J. Geophys. Res.*, 79, No. 30, pp. 4498-4504, 1974.

Dalrymple, R.A., Prediction of storm/normal beach profiles, *J. of Waterw., Port, Coastal and Ocean Eng., A.S.C.E.*, Vol. 118, No. 2, pp. 193-200, 1992.

Dean, R.G., Stream function representation of nonlinear ocean waves, *J. Geophys. Res.*, 70, No. 18, pp. 4561-4572, 1965.

Dean, R.G., Evaluation and development of water wave theories for engineering application, Vols. 1 and 2, *Special Report 1, U.S. Army, Coastal Engineering Research Center*, Fort Belvoir, Va., 1974.

Dean, R.G., Equilibrium beach profiles: U.S. Atlantic and Gulf Coasts, *Ocean Engineering Report 12, Department Civil Engineering*, University of Delaware, 1977.

Dean, R.G., Equilibrium beach profiles: Characteristics and applications, *Journal of Coastal Research*, 7(1), pp. 53-84, 1991.

Dean, R.G. and R.A. Dalrymple, *Water Wave Mechanics for Engineers and Scientists*, World Scientific, 1991.

Dean, R.G. and R.A. Dalrymple, Unpublished manuscript, 1992.

De Vriend, H.J. and Stive, M.J.F., Quasi-3D modelling of nearshore currents, P.P.G. Dyke (Editor), *JONSMOD '86, Coastal Engineering*, 11, pp. 565-601, 1987.

Dyhr-Neilsen, M. and T. Sorensen, Sand transport phenomena on coasts and bars, in *Proceedings of the* $12^{th}$ *International Conference on Coastal Engineering*, pp. 855-866, American Society of Civil Engineers, New York, 1970.

Eagleson, P.S. and R.G. Dean, Wave-induced motion of bottom sediment particles, *Transactions of the American Society of Civil Engineers*, 129, Part 1, pp. 41, 1961.

Eagleson, P.S., B. Glenne, and J.A. Dracup, Equilibrium characteristics of sand beaches, *J. Hydraul. Div. ASCE*, 89, No. HY1, pp. 35-57, 1963.

Flick, R.E., R.T. Guza and D.L. Inman, Elevation and velocity measurements of laboratory shoaling waves, *J. Geophys. Res.*, 86, No. C5, pp. 4149-4160, 1981.

Howd, P.A. and W.A. Birkemeier, Beach and Nearshore Survey Data: 1981-1984 CERC Field Research Facility, *Technical Report CERC-87-9*, US Army Engineer Waterways Experiment Station, Vicksburg, Miss., 1987.

Ippen, D.L., A study of sediment sorting by waves shoaling on a plane beach, *U.S. Army Corps of Engineers, Beach Erosion Board*, Technical Memo. No. 63, pp. 83, 1955.

Guza, R.T. and E.B. Thornton, Velocity moments in nearshore, *J. of Waterw., Port, Coastal and Ocean Eng., A.S.C.E.*, Vol. 111, No. 2, pp. 235-256, 1985.

Kaihatu, J.M., Random wave height variation over equilibrium beach profiles, *Term Project: CE680*, University of Delaware, 1990.

Kraus, N.C. and M. Larson, Beach profile change measured in the tank for large waves 1956-1957 and 1962, *U.S. Army Corps of Engineers Coastal Engineering Research Center, Tech. Rpt. CERC-88-6*, Vicksburg, 1988.

Kriebel, D.L., Personal communication, 1992.

Larson, M., Quantification of beach profile change, Ph.D. Dissertation, *Report 1008, Department Water Resources Engineering*, University of Lund, Sweden, 1988.

Larson, M. and Kraus, N.C., SBEACH: Numerical model for simulating storm-induced beach change, *Report 1, U.S. Army Corps of Engineers Coastal Engineering Research Center, Tech. Rpt. CERC-89-9*, Vicksburg, 1989.

Longuet-Higgins, M.S., Mass transport in water waves, *Philos. Trans. R. Soc. London, Ser. A, 245*, pp. 535-581, 1953.

Miller, C.H., W.E. Grogg, Jr., J.R. Rottier, M.W. Leffler and C.R. Townsend, III, Annual data summary for 1981 CERC Field Research Facility, *Technical Report CERC-85-3*, US Army Engineer Waterways Experiment Station, Vicksburg, Miss., 1985.

Press, W.H., B.P. Flannery, S.A. Teukolsky and Veeterling, W.T., *Numerical Recipes*, Cambridge University Press, New York, 1986.

Roelvink, J.A. and M.J.F. Stive, Bar-generating cross-shore flow mechanisms on a beach, *J. Geophys. Res.*, 94, No. C4, pp. 4785-4800, 1989.

Stive, M.J.F., A model for cross-shore sediment transport, in *Procceedings of the 20$^{th}$ International Conference on Coastal Engineering*, pp. 1550-1564, American Society of Civil Engineers, New York, 1986.

Stive, M.J.F. and J.A. Battjes, A model for offshore sediment transport, in *Procceedings of the 19th International Conference on Coastal Engineering*, pp. 1420-1436, American Society of Civil Engineers, New York, 1984.

Stive, M.J.F. and H.J. De Vriend, Quasi-3D nearshore current modelling: Wave-induced secondary currents, in *Proceedings of Special Conference on Coastal Hydrodynamics*, pp. 356-370, American Society of Civil Engineers, New York, 1987.

Stive, M.J.F. and H.G. Wind, Cross-shore mean flow in the surf zone, *Coastal Engineering*, 10, pp. 325-340, 1986.

Svendsen, I.A., Mass flux and undertow in a surf zone, *Coastal Engineering*, 8, pp. 347-365, 1984.

Svendsen, I. A. and J. B. Hansen, Cross-shore currents in surf zone modelling, *Coastal Engineering*, 12, pp. 23-42, 1988.

Svendsen, I.A., H.A. Schaffer, and J.B. Hansen, The interaction between the undertow and the boundary layer flow on a beach, *J. Geophys. Res.*, 92, pp. 11,845-11,856, 1987.

Thornton, E.B. and R.T. Guza, Transformation of wave height distribution, *J. Geophys. Res.*, 88, C10, pp. 5925-5938, 1983.

Winant, C.D., D.L. Inman and C.E. Nordstrom, Description of seasonal beach changes using empirical eigenfunctions, *J. Geophys. Res.*, 80, pp. 1979-1986, 1975.

# Appendix A

## EXPLICIT DERIVATIVES FOR RUNGE-KUTTA METHOD

In this appendix, the explicit derivative expressions for wave energy, $E$, mean water surface elevation, $\overline{\eta}$, depth, $d$, and the associated derivatives for the analytical expression of linear wave number, $k$, linear wave speed, $C$, and linear wave group speed, $C_g$, are presented. The discussion begins by defining the total water depth, $h$, as the combination of the still water depth, $d$, and mean water surface elevation, $\overline{\eta}$.

The general expression for the bottom slope is expressed as

$$\tan\beta = \left[\frac{\varepsilon_b}{\tan\phi}\left(\left\langle \tilde{u}\,|\tilde{u}|^2\right\rangle + 3\overline{u}\left\langle|\tilde{u}|^2\right\rangle\right) + \frac{\varepsilon_s}{w}\left(\left\langle \tilde{u}\,|\tilde{u}|^3\right\rangle + 4\overline{u}\left\langle|\tilde{u}|^3\right\rangle\right)\right] \left[\frac{\varepsilon_b}{\tan^2\phi}\left\langle|\tilde{u}|^3\right\rangle + \left(\frac{\varepsilon_s}{w}\right)^2\left\langle|\tilde{u}|^5\right\rangle\right]^{-1} \tag{A.1}$$

where $\tan\beta = -\partial d/\partial x$. For expressions of the velocity moments, the reader is referred to Chapter 4, for a detailed discussion of these terms. For this discussion, the slope model is accepted as a general form.

The first step in the integration scheme at a given location is to determine flow field characteristics given the $H_{\text{rms}}$ wave height, water depth, $h$, and the wave number, $k$, which is found with the linear dispersion relationship

$$\sigma^2 = gk\tanh kh \tag{A.2}$$

For the random wave case, Battjes and Stive (1985) recommend using the peak frequency of the wave field, $f_p$, as the governing frequency. Thus, the wave number will be the peak wave number, $k_p$.

The energy balance is presented in the form of a conservation of energy flux, $EC_g$, as

$$\frac{\partial EC_g}{\partial x} + D = 0 \tag{A.3}$$

To solve directly for the wave energy, $E$, derivatives in $x$ are taken for all terms that are functions of $x$ which results in the expression

$$\frac{\partial E}{\partial x} = -\frac{1}{C_g}\left(d + E\frac{\partial C_g}{\partial x}\right) \tag{A.4}$$

With the derivative in this form, an explicit solution at each $x$ location can be found for the right hand side given the linear representations of the local wave energy, $E$, group speed, $C_g$, dissipation, $D$, and the gradient of the group speed, $\partial C_g/\partial x$.

The gradient for the group speed is obtained by taking all $x$ derivatives of the linear expression

$$C_g = \frac{2\pi f}{k}\left(\frac{1}{2} + \frac{kh}{\sinh(2kh)}\right) \tag{A.5}$$

which results in

$$\begin{aligned}\frac{\partial C_g}{\partial x} = -\frac{1}{2}\frac{\partial C}{\partial x} + \frac{1}{\sinh(2kh)}&\left(kh\frac{\partial C}{\partial x} + Ch\frac{\partial k}{\partial x} + Ck\left(\frac{\partial d}{\partial x} + \frac{\partial \overline{\eta}}{\partial x}\right)\right) \\ &-2Ckh\coth(2kh)\left(h\frac{\partial k}{\partial x} + k\left(\frac{\partial d}{\partial x} + \frac{\partial \overline{\eta}}{\partial x}\right)\right)\end{aligned} \tag{A.6}$$

This expression can be explicitly evaluated from the known value of the bottom slope, eqn. A.1.

To express the derivative for the change in mean water surface elevation, $\overline{\eta}$, the momentum equation is used as

$$\frac{\partial S_{xx}}{\partial x} + \rho g h \frac{\partial \overline{\eta}}{\partial x} = 0 \tag{A.7}$$

where the term for the radiation stress is directly substituted before the derivatives are taken.

$$S_{xx} = \left(\frac{1}{2} + \frac{2kh}{\sinh(2kh)}\right) E \tag{A.8}$$

Again, the terms with recognized $x$ dependency and all derivatives in $x$ are taken using chain differentiation. The resulting expression is

$$\frac{\partial \overline{\eta}}{\partial x} = \left(\frac{4khE\cosh(2kh)}{\sinh^2(2kh)}\left(h\frac{\partial k}{\partial x} + k\frac{\partial d}{\partial x}\right) - \frac{2}{\sinh(2kh)}\left(kh\frac{\partial E}{\partial x} + hE\frac{\partial k}{\partial x} + kE\frac{\partial d}{\partial x}\right) - \frac{1}{2}\frac{\partial E}{\partial x}\right)\left(\rho g h + \frac{2kE}{\sinh(2kh)} - \frac{4k^2hE\cosh(2kh)}{\sinh^2(2kh)}\right)^{-1} \tag{A.9}$$

where it is recognized that derivatives for bottom slope, wave speed, wave number, and wave group speed are implicit in the right hand side. However, assuming that these variables can be approximated with linear theory, the first order linear expressions from Dean and Dalrymple (1984) are adopted.

For the derivative of the wave number, $k$, the linear dispersion relationship, eqn. A.2, is used where all derivatives in $x$ are taken and solved for $\partial k/\partial x$. This exercise results in the following expression for the change in wave number with changes in depth.

$$\frac{\partial k}{\partial x} = -\left(k^2 \mathrm{sech}^2(kh)\left(\frac{\partial d}{\partial x} + \frac{\partial \overline{\eta}}{\partial x}\right)\right)\left(\tanh(kh) - kh\mathrm{sech}^2(kh)\right)^{-1} \tag{A.10}$$

For the wave speed $C$ the relationship

$$C = \frac{\sigma}{k} \tag{A.11}$$

is used, where $\sigma = 2\pi f$ and is the peak angular frequency of the random wave field. Taking the derivatives in $x$ results in

$$\frac{\partial C}{\partial x} = -\frac{\sigma}{2Ck^2}\frac{\partial k}{\partial x} \tag{A.12}$$

where the gradient for the wave number is known *a priori* from eqn. (A.10).

Through successive substitution and arranging these expressions to ensure each right hand side is explicitly expressed, the equations are simultaneously solved for bottom depth $d$, wave energy, $E$, and mean water level, $\overline{\eta}$, at each $x$ location given local water depth. The subroutine is arranged in the following order, defining the derivatives by the vector $\partial y/\partial x$.

$$\left(\frac{\partial y_1}{\partial x}\right) = \frac{\partial d}{\partial x} \tag{A.13}$$

$$\left(\frac{\partial y_2}{\partial x}\right) = \frac{\partial E}{\partial x} \tag{A.14}$$

$$\left(\frac{\partial y_3}{\partial x}\right) = \frac{\partial \overline{\eta}}{\partial x} \tag{A.15}$$

One potential problem with this scheme is the implicit term, $\partial\overline{\eta}/\partial x$, in the right hand side of these derivatives. However, the term is small in the offshore regions of the domain and can be approximated with the value calculated at the previous $x$ location. In the shallower regions of the domain, where $\partial\overline{\eta}/\partial x$ increases, the size of $\Delta x$ is decreased with a step-size control routine, Press, *et al.* (1986); thus, the value at the previous $x$ location is an adequate representation of the term and iteration is not necessary.

# Appendix B

## DERIVATION OF UNDERTOW MODEL

This appendix presents the derivation of Stive and de Vriend (1987) for the mean return flow across the surf zone, which includes the flow in the bottom boundary layer as proposed by Svendsen *et al.* (1987). Stive and de Vriend (1987) divided the water column into three layers, trough level and above, between the bottom boundary layer and trough level, and the bottom boundary layer. Figure B.1 provides a definition sketch for the three layered problem. The top, or surface, level is not considered in detail, but the information in that domain is represented via an effective shear stress at trough level,

$$\tau_t = \rho \nu_t \frac{\tilde{u}_b^2 k}{C} \sinh(2kh) + \left(\frac{1}{2} + 7\frac{kh}{2\pi}\right)\frac{D}{C} \tag{B.1}$$

where,

$\nu_t$ is the kinematic viscosity

$k$ is the wave number

$C$ is the wave phase speed

$D$ is the mean energy dissipation due to wave breaking

$\tilde{u}_b$ is the near-bottom oscillatory velocity amplitude

and the mass flux, $m$, above trough level

$$m = \left(1 + Q_b \frac{7kh}{2\pi}\right)\frac{E}{C} \tag{B.2}$$

The effective shear stress represents the dissipation of energy from the nonbreaking portion of the wave field through the viscosity term, $\nu_t$, and the breaking wave dissipation due to the momentum decay above trough level through the dissipation term, $D$, as defined in the wave energy decay model. The mass flux above trough level is modified from a monochromatic representation to account for only the mass flux of the breaking wave portion of the wave field, $Q_b$.

The middle layer is modelled with time-averaged horizontal momentum equation

$$\frac{\partial}{\partial z}\left(\rho\nu_t\frac{\partial u(z)}{\partial z}\right) = \frac{\partial}{\partial z}\left(\rho\left(\overline{u}^2 - \overline{w}^2\right)\right) + \frac{\partial}{\partial x}\left(\rho g\overline{\eta}\right), \tag{B.3}$$

which describes the balance between the vertical variation of the flow and the vertically varying stress and pressure forces required to maintain the flow in the domain. The time-averaging is over many waves to include mean flow effects of the turbulent flow and wave flow.

The bottom layer flow also is modelled by the time-averaged horizontal momentum equation

$$\frac{\partial}{\partial z}\left(\rho\nu_t\frac{\partial u(z)}{\partial z}\right) = \frac{\partial}{\partial z}\left(\rho\left(\overline{u}^2 - \overline{w}^2\right)\right) + \frac{\partial}{\partial x}\left(\rho g\overline{\eta}\right) + \frac{\partial}{\partial z}\left(\rho\overline{\tilde{u}\tilde{w}}\right) \tag{B.4}$$

which is in the same form as the momentum layer, but an additional term is produced from the time-averaging due to the turbulent stresses induced by the flow in the turbulent boundary layer. Essentially, due to the turbulent nature of the flow, an additional driving force governs the flow.

The right hand side of the middle layer momentum equation, which represents the driving forces due to the viscous shear stresses and the pressure gradient is redefined as

$$\alpha(x,z) = \frac{\partial}{\partial z}\left(\rho\left(\overline{u}^2 - \overline{w}^2\right)\right) + \frac{\partial}{\partial z}\left(\rho g \overline{\eta}\right) \tag{B.5}$$

and assume $\alpha$ is constant over and varies in $x$, or $\alpha(x)$. Now the equations are

$$\frac{\partial}{\partial z}\left(\rho \nu_t \frac{\partial u(z)}{\partial z}\right) = \alpha(x) \tag{B.6}$$

for the middle layer and

$$\frac{\partial}{\partial z}\left(\rho \nu_t \frac{\partial u(z)}{\partial z}\right) = \alpha(x) + \frac{\partial}{\partial z}\left(\rho \overline{\tilde{u}\tilde{w}}\right) \tag{B.7}$$

for the bottom layer, where the turbulent shear stress term remains undefined.

The system of equations can solved with the application of five conditions: a no-slip condition at the bed, the shear stress condition at trough level (eqn. B.1) the integral mean flow condition to compensate for the net mean flow above trough level,

$$\int_{z_b}^{z_t} u(z)dz = -\frac{m}{\rho} \tag{B.8}$$

and two patching conditions for the velocity and shear stress at the interface of the middle and bottom layers. The patching solution of Svendsen *et al.* (1987) is applied to the bottom layer to account for mean flows induced by the nonbreaking fraction of the wave field.

The final solution requires a measure of the turbulent viscosity in the middle and bottom layer. Due to the turbulent flow in the bottom layer, the turbulent viscosity in that layer is several orders of magnitude smaller that in the middle layer. Expressions adopted by Stive and de Vriend for the turbulent viscosity in the middle and bottom layers are

$$\nu_t = c_f^2 \frac{\tilde{u}_b^2}{\omega} \tag{B.9}$$

for the middle layer where $c_f$ is a bottom friction factor for wave motion and is $O(10^{-2})$, $\omega$ is the angular frequency of the wave field and

$$\nu_{tb} = Mh\left(\frac{D}{\rho}\right)^{\frac{1}{3}} \tag{B.10}$$

for the bottom layer, where $M$ is an empirical constant of $O\,(10^{-2})$m and $D$ is the time-averaged energy dissipation for the waves.

Applying the above conditions, the middle layer flow is solved for by integrating once in $z$ and applying the surface shear stress, $\tau_t$,

$$\nu_t \frac{\partial u}{\partial z} = \frac{\tau_t}{\rho} \tag{B.11}$$

which results in

$$\frac{1}{\nu_t}\frac{\partial u}{\partial z} = \frac{\tau_t}{\rho} + \alpha(z - z_t) \tag{B.12}$$

Again, integrating in $z$ and defining the velocity at the interface between the middle and bottom layers as $u(z_l)$, which is an unknown, the expression for the middle layer becomes

$$u(z)_m = u(z_l) + \frac{\tau_t}{\rho\nu_t}(z - z_l) - \frac{\alpha}{\nu_t}\left(\frac{1}{2}(z_l - z_t)^2 - \frac{1}{2}(z - z_t)^2\right) \tag{B.13}$$

where $u(z_l)$ and $\alpha$ remain unknown.

Next, the time-averaged equation for flow in the bottom layer is solved following the solution of Svendsen *et al.* (1987) for the breaking waves. Integrating once, and defining an arbitrary unknown bottom shear stress, $\tau_b$, the relationship becomes,

$$\frac{1}{\nu_t}\frac{\partial u}{\partial z} = \frac{\tau_t}{\rho} + \alpha(z - z_t) + \overline{\tilde{u}\tilde{w}} \tag{B.14}$$

where $\overline{\tilde{u}\tilde{w}}|_{z_b} = 0$.

Again, integrating in $z$ and applying the condition $u = 0$ at $z = z_b$, the expression for the vertical velocity distribution in the bottom layer is

$$u(z)_b = \frac{\tau_b}{\rho\nu_{tb}}(z - z_b) - \frac{\alpha}{2\nu_{tb}}(z - z_b)^2 + u_s(z_l) \tag{B.15}$$

where nonlinear term

$$\int \overline{\tilde{u}\tilde{w}}\, dz = u_s(z) \tag{B.16}$$

is defined as the steady streaming in the bottom boundary layer.

At this point there are three unknowns, $u(z_l)$, $\tau_b$ and $\alpha$. The velocity at the interface, $u(z_l)$, and the bottom shear stress, $\tau_b$, are found from matching the velocity and shear stress at the interface. For $u(z_l)$, equations B.13 and B.15 are equated and solved for $u(z_l)$, resulting in

$$u(z_l) = \frac{\tau_b}{\rho\nu_{tb}}\delta + \frac{\alpha}{2\nu_{tb}}\delta^2 + u_s(z_l) \tag{B.17}$$

Next, equations B.12 and B.14 are equated and the resulting bottom shear stress, $\tau_b$, is

$$\tau_b = \tau_t - \rho\left(\alpha d_t - \overline{\tilde{u}\tilde{w}}|_{z_l}\right) \tag{B.18}$$

the definitions for $d_t$ and $\delta$ are found in figure (B.1). The value for $\alpha$ is still undefined. However, by applying the only remaining condition, the continuity condition

$$\int_{z_l}^{z_t} u(z)_m \, dz + \int_{z_b}^{z_l} u(z)_b \, dz = -\frac{m}{\rho}, \tag{B.19}$$

integration yields

$$\begin{aligned} &\alpha\left[\frac{1}{3\nu_t}(d_t-\delta)^3+\frac{1}{\nu_{tb}}\left(d_t\delta(d_t-\delta)-\frac{1}{2}\delta^2(d_t-\delta)+\frac{1}{2}\delta^2 d_t-\frac{1}{6}\delta^3\right)\right]= \\ &\frac{\tau_t}{\rho}\left[\frac{1}{2\nu_t}(d_t-\delta)^2+\frac{1}{\nu_{tb}}\delta(d_t-\delta)+\frac{1}{2}\delta^2\right]-\frac{\overline{\tilde{u}\tilde{w}}|_{z_l}}{\nu_{tb}}\left[\delta(d_t-\delta)+\frac{1}{2}\delta^2\right]+ \\ &u_s(z_l)\left[(d_t-\delta)+\frac{1}{2}\delta\right]+\frac{m}{\rho} \end{aligned} \tag{B.20}$$

where $\alpha$ can be found from substituting the previously defined terms and the expressions from the conduction solution.

The Longuet-Higgins' (1953) conduction solution yields the terms $u_s(z_l)$, the streaming velocity, and $\overline{\tilde{u}\tilde{w}}|_{z_l}$, the steady streaming shear stress, which are expressed as

$$u_s(z_l) = \frac{1}{4}\frac{\tilde{u}_b^2}{C}\left[3+e^{-2}-2e^{-1}(3\cos(1))\right] \tag{B.21}$$

and

$$\overline{\tilde{u}\tilde{w}}|_{z_l} = \frac{1}{8}k\tilde{u}_b^2\delta\left[e^{-1}(\sin(1)+\cos(1))-\frac{1}{2}e^{-2}-\frac{1}{2}\right], \tag{B.22}$$

respectively. The term $\tilde{u}_b$ is the maximum bottom velocity of a linear wave.

This formulation provides a complete model for the momentum decay induced return flow for random wave breaking where only the wave height, water depth, and

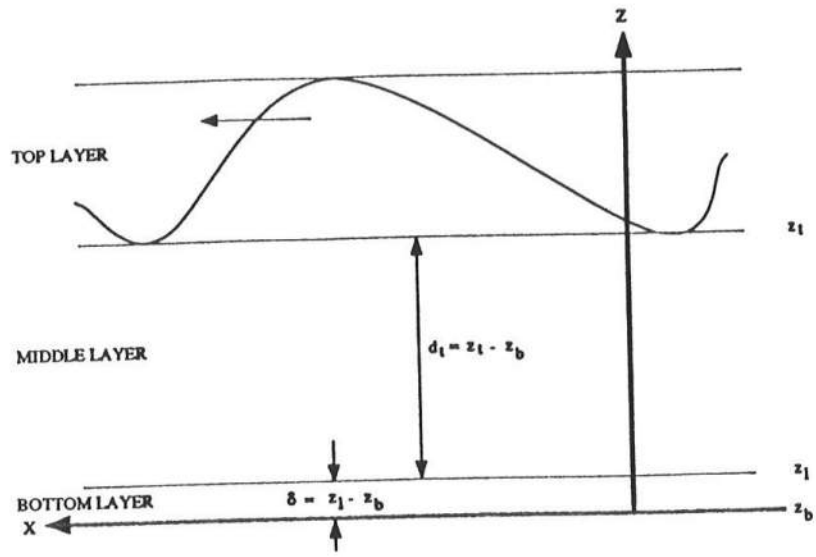


**Figure B.1:** Definition Sketch for Undertow Solution (Stive and de Vriend 1987).

energy dissipation $D$, are required to determine the mean flow. The near-bottom steady current $\overline{u}$ is defined as the velocity at the interface level, $z_l$, defined in eqn. B.17. An important aspect of the solution is that when there is minimal wave breaking, the dissipation $D$ is small, and the conduction solution provides onshore flow at the chosen $z = z_l$ location for near-bottom flow. However, as wave breaking increases, the disspation induced return flow overcomes the drift velocity and the mean flow is offshore. This transition from onshore to offshore mean flow will prove advantageous in producing longshore bars in the equilibrium beach profile.